I. PHOSPHORESCENCE AND THE TRUE LIFETIME OF TRIPLET STATES IN FLUID SOLUTIONS

II. WHY IS CONDENSED OXYGEN BLUE?

Thesis by

Shirley Shieu-lang Cheng Tsai

In Partial Fulfillment of the Requirements

For the Degree of

Doctor of Philosophy

California Institute of Technology

Pasadena, California

1969

(Submitted October 31, 1968)

To My Parents

and My Husband

ACKNOWLEDGMENTS

It is my pleasure to acknowledge Professor G. W. Robinson for much assistance, encouragement and guidance during my stay at Caltech. I should like to acknowledge Professor G. S. Hammond for his encouragement and concern in my first year at Caltech and his constant interest in my work. Financial support of the U. S. Army Research Office-Durham and Caltech is most gratefully acknowledged. I wish to acknowledge Professor W.A. Goddard for the suggestion concerning the approximation of molecular orbitals of $O_2(B\ ^3\Sigma_u^-)$.

Many thanks are due to Dr. S.D. Colson for help and encouragement. Many thanks are also due to Drs. A. Haug, G. Castro, C.-h. Ting, W.E. Palke, D. Hanson, Mr. E. Priestley and Mr. Paul Fehder. Discussion with Mr. D. Burland is highly appreciated. People in the mechanical and the glass-blowing shops are acknowledged for their patience and for doing a fine job with the experimental apparatus. Mr. C. Runyan, Mr. M. Bertolucci, and Miss M. Ory are acknowledged for their reading part of the manuscript.

Finally, I am deeply indebted to Mrs. Jean Charnley and my youngest elder brother. Mrs. Charnley made my $3\frac{1}{4}$ years' stay with her very pleasant and comfortable, so that I could pay full attention to my work.

ABSTRACT

I. PHOSPHORESCENCE AND THE TRUE LIFETIME OF TRIPLET STATES IN FLUID SOLUTIONS

Phosphorescence has been observed in a highly purified fluid solution of naphthalene in 3-methylpentane (3-MP). The phosphorescence lifetime of $C_{10}H_8$ in 3-MP at -45°C was found to be 0.49 ± 0.07 sec, while that of $C_{10}D_8$ under identical conditions is 0.64 ± 0.07 sec. At this temperature 3-MP has the same viscosity (0.65 centipoise) as that of benzene at room temperature. It is believed that even these long lifetimes are dominated by impurity quenching mechanisms. Therefore it seems that the radiationless decay times of the lowest triplet states of simple aromatic hydrocarbons in liquid solutions are sensibly the same as those in the solid phase. A slight dependence of the phosphorescence lifetime on solvent viscosity was observed in the temperature region, -60° to -18°C. This has been attributed to the diffusion-controlled quenching of the triplet state by residual impurity, perhaps oxygen. Bimolecular depopulation of the triplet state was found to be of major importance over a large part of the triplet decay.

The lifetime of triplet $C_{10}H_8$ at room temperature was also measured in highly purified benzene by means of both phosphorescence and triplet-triplet absorption. The lifetime was estimated to be at least ten times shorter than that in 3-MP. This is believed to be due not only to residual impurities in the solvent but also to small amounts

of impurities produced through unavoidable irradiation by the excitation source. In agreement with this idea, lifetime shortening caused by intense flashes of light is readily observed. This latter result suggests that experiments employing flash lamp techniques are not suitable for these kinds of studies.

The theory of radiationless transitions, based on Robinson's theory, is briefly outlined. A simple theoretical model which is derived from Fano's autoionization gives identical result.

ABSTRACT

II. WHY IS CONDENSED OXYGEN BLUE?

The blue color of oxygen is mostly derived from double transitions. This paper presents a theoretical calculation of the intensity of the double transition $(a\ ^1\Delta_g)\ (a\ ^1\Delta_g) \leftarrow (X\ ^3\Sigma_g^-)\ (X\ ^3\Sigma_g^-)$, using a model based on a pair of oxygen molecules at a fixed separation of 3.81 Å. The intensity enhancement is assumed to be derived from the mixing $(a\ ^1\Delta_g)\ (a\ ^1\Delta_g) \sim\sim (X\ ^3\Sigma_g^-)\ (B\ ^3\Sigma_u^-)$ and $(a\ ^1\Delta_g)\ (^1\Delta_u) \sim\sim (X\ ^3\Sigma_g^-)\ (X\ ^3\Sigma_g^-)$. Matrix elements for these interactions are calculated using a π-electron approximation for the pair system. Good molecular wavefunctions are used for all but the perturbing $(B\ ^3\Sigma_u^-)$ state, which is approximated in terms of ground state orbitals. The largest contribution to the matrix elements arises from large intramolecular terms multiplied by intermolecular overlap integrals. The strength of interaction depends not only on the intermolecular separation of the two oxygen molecules, but also as expected on the relative orientation. Matrix elements are calculated for different orientations, and the angular dependence is fit to an anlytical expression. The theory therefore not only predicts an intensity dependence on density but also one on phase at constant density. Agreement between theory and available experimental results is satisfactory considering the nature of the approximation, and indicates the essential validity of the overall approach to this interesting intensity enhancement problem.

TABLE OF CONTENTS

I. PHOSPHORESCENCE AND THE TRUE LIFETIME OF TRIPLET STATES IN FLUID SOLUTIONS

1. INTRODUCTION

Triplet states of organic compounds in fluid solutions play a very important role in many photochemical reactions. Our present knowledge about triplet states of organic compounds in fluid solutions is derived almost entirely from studies of triplet-triplet absorption using flash techniques.[1,2]

The effect of temperature and viscosity on the lifetime of the lowest triplet state of naphthalene has been previously investigated in both solid[3,4] and liquid solutions.[5-7] In the case of the solid, only a very small temperature effect was observed. For example, the lifetime of triplet $C_{10}H_8$ changed from a value of 2.4 sec in EPA at 77°K to 1.5 sec in plastic polymethyl methacrylate at 298°K.[4] In the same temperature range, the lifetime of triplet $C_{10}D_8$ changed from 22 sec to 12.5 sec in plastic matrices.[4] On the contrary, a great and incongruous effect of temperature on the lifetime of triplet naphthalene in liquid solutions has been reported.[5-7] In a temperature range of -40°C to 25°C, the lifetime of triplet $C_{10}H_8$ was found to vary from 2 sec to 7.7 msec in glycerol[6] and from 1.7 sec to 0.55 msec in propylene glycol.[7] The viscosity in propylene glycol, for example, ranges from $\sim 3.5 \times 10^4$ centipoise at -40°C to 10 centipoise at 25°C.

Past results concerning the lifetime of triplet $C_{10}H_8$ in liquid solutions are shown in Table I. The main cause for the discrepancies among the various values was thought to be due to the varying purity of the samples used. The observed dependence on temperature or viscosity of the lifetime of triplet states can be ascribed to pseudo first-order decay controlled by diffusion processes involving impurities. See, for example, Refs. (6) and (8).

From Table I, it can be seen that the longest reported lifetime of triplet $C_{10}H_8$ in non-viscous fluid solutions measured with the flash technique is of the order of milliseconds. This is short compared with the 2.6 sec lifetime of $C_{10}H_8$ in EPA at 77°K obtained by means of phosphorescence.[9] Consequently, many discussions and speculations about the quenching process of phosphorescence in liquid solutions have resulted,[10] since Professor G. Porter presented this problem in the discussion of the Faraday Society ten years ago. The purpose of this investigation is to discover whether phosphorescence of compounds, such as naphthalene, with long-lived triplet states, exists in liquid solutions, even though in the past it has never been observed; and then to use the phosphorescence emissions to study the kinetics of triplet decay in fluid solution, especially under conditions of low exciting light intensity where the chance of producing impurities by the excitation source itself is minimized. The experimental results verify the idea that the dominant part of "liquid quenching" of the lowest

TABLE I. Lifetime of $C_{10}H_8$ in liquid solutions.

Solvent	Viscosity η (centipoise)	Technique	Lifetime τ (sec)	Reference
hexane	0.33	a	0.83×10^{-3}	11,12
hexane	0.33	a	0.36×10^{-3}	12
i-butanol	3.97	a	0.56×10^{-3}	6
ethylene glycol	19.9	a	4.54×10^{-3}	6
ethylene glycol	19.9	a	1.00×10^{-3}	12
propylene glycol	44.8	a	6.67×10^{-3}	6
propylene glycol	44.8	a	0.56×10^{-3}	7
glycerol	4.2	a	7.70×10^{-3}	6
benzene	0.65	a	0.50×10^{-3}	18
benzene	0.65	a	1.20×10^{-3}	this work
benzene	0.65	b	$\sim 40.00 \times 10^{-3}$	this work
3-methylpentane	0.65[c]	b	0.5	this work

[a] Flash technique.

[b] Phosphorescence.

[c] At temperature -48°C.

triplet state of naphthalene can be attributed to quenching by impurities, such as oxygen or other compounds of low-lying triplet states. These reulsts also indicate that the environment has very little effect on the intrinsic radiationless transitions.

The experimental set-up and sample preparations are described in detail in section 2, and the results are shown in section 3. A general theory of radiationless transitions is briefly outlined in section 4A. Both Robinson's theoretical model and a simpler model derived from Fano's autoionization are illustrated. The theoretical aspects for the phenomena observed in the experiment are included in section 4B.

2. EXPERIMENTAL

A. Sample Preparation

To investigate the long-lived phosphorescence of organic compounds in liquid solutions, we chose naphthalene because high-purity material can be obtained;[13] the triplet state of naphthalene lies relatively low and is therefore not so susceptible to quenching by energy transfer as would be benzene, for instance; and finally the triplet-triplet absorption spectrum is known[5] for naphthalene and could therefore be used to check the triplet state population during the early phases of the investigation.

In the study of phosphorescence in liquid solutions, avoidance of impurity contamination during every step of the procedure is very

important. For this reason, details about the preparation of the sample are described in this subsection.

Three Phillips' research grade solvents were selected: 3-methylpentane (3-MP), methylcyclopentane (MCP), and benzene. Pure 3-MP absorbs light only to the short wavelength side of 2000 Å, and therefore can be completely protected from any possible radiation damage from the light source. The appropriate filtering can be achieved by means of a solution made up of $1\frac{1}{2}$ volumes of 500 g/ℓ $CoCl_2$ solution[14] to one volume of a saturated solution[14] of $NiCl_2$ in 1 M HCl. This solution has a transmission band at 2300-3600 Å. 3-MP forms a clear glass at low temperatures facilitating experimental observations over a wide range of temperatures. Benzene was selected because it can be readily brought to a high degree of purity.[15] The viscosity of the three solvents is shown in Fig. 1. The viscosity of 3-MP was measured with an Ostwald viscosimeter in the temperature range of -100°C to 20°C. The data obtained from 0°C to 20°C are approximately the same as those in the International Critical Tables. The viscosity of C_6H_6 and MCP was obtained from the International Critical Tables. Note that the viscosity of benzene at room temperature is roughly equal to that of 3-MP at -48°C.

Naphthalene is purified using a procedure similar to that reported earlier.[13] The important parts of the purification process consist of preliminary zone-refining, followed by fusion with potassium at 100°C, and finally by a further extensive zone-

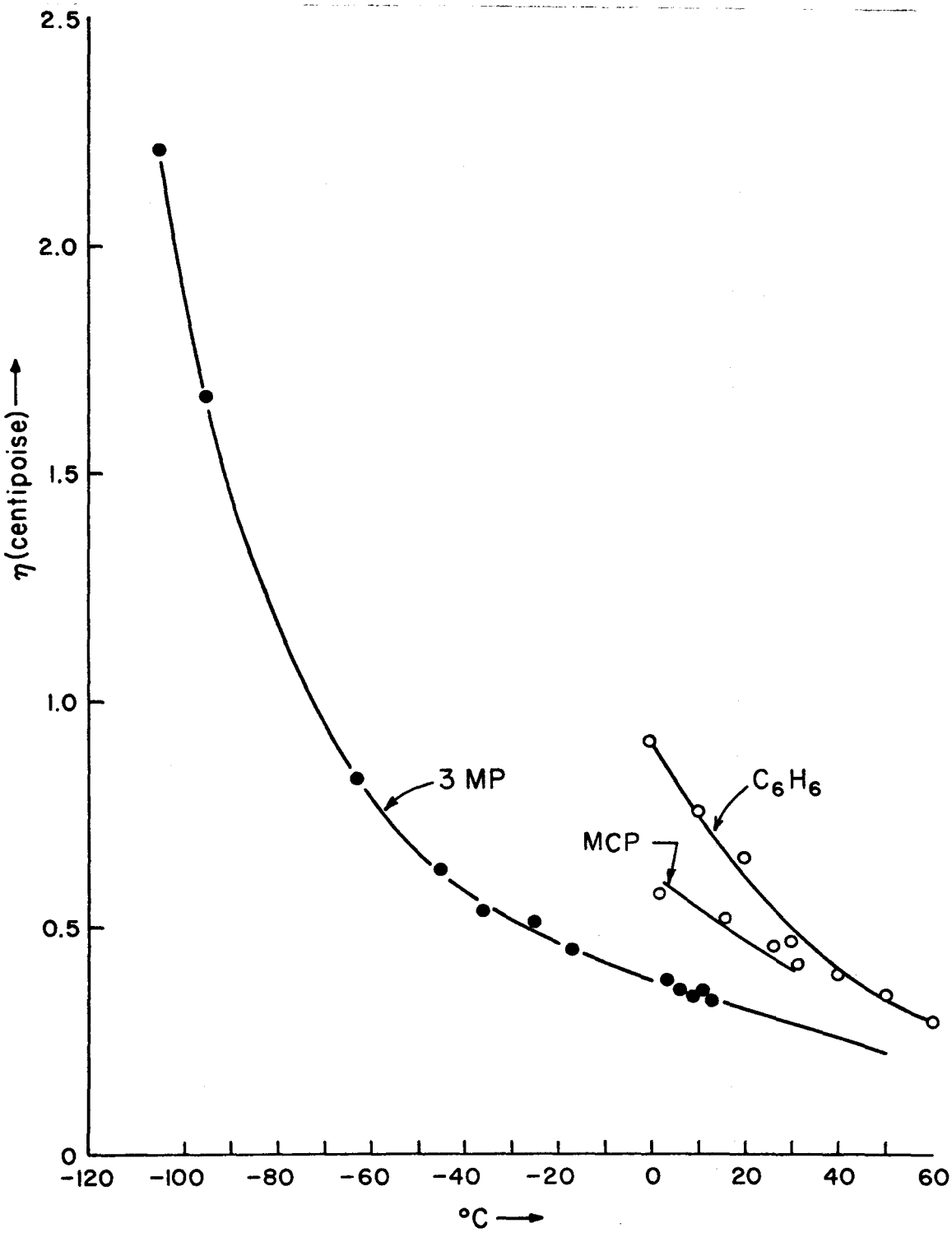

FIG. 1. Viscosity of different solvents (at 0°C, C_6H_6 is a supercooled liquid.

refining stage. A check of the purity of the naphthalene after such a procedure is made by examining the visible-ultraviolet spectrum of a 40-mm thick crystal at 4.2°K; the concentration of spectroscopically active impurities is usually found to be less than 1 part in 10^7.

To prevent subsequent contamination by oxygen or other foreign materials, the naphthalene is handled only in a "clean" vacuum system from the time it is fused with potassium. The vacuum system for the preparation of the naphthalene solution consists of a break-seal tube containing the highly purified naphthalene, and several 200-ml measuring bulbs each with a 10-mm O.D. quartz sample tube attached as shown in Fig. 2. The entire vacuum system is baked out at 250°C for about a day during which time the tube containing the naphthalene sample is kept immersed in ice to avoid thermal decomposition. The pressure in the vacuum system at the end of this procedure is lower than 5×10^{-7} Torr.

A 200-ml sample of naphthalene vapor at its room temperature vapor pressure (0.04 Torr[16]) is separated from the rest of the system by means of a greaseless "ball valve" (see Fig. 2). It is then frozen in the sample tube while the bulk sample is simultaneously being recooled to liquid nitrogen temperature. The "ball valve" is then opened and the system is again pumped down to $< 5 \times 10^{-7}$ mm Hg. The sample tube, containing the approximately 0.4 μmole of naphthalene, is sealed off from the vacuum system during the pumping procedure.

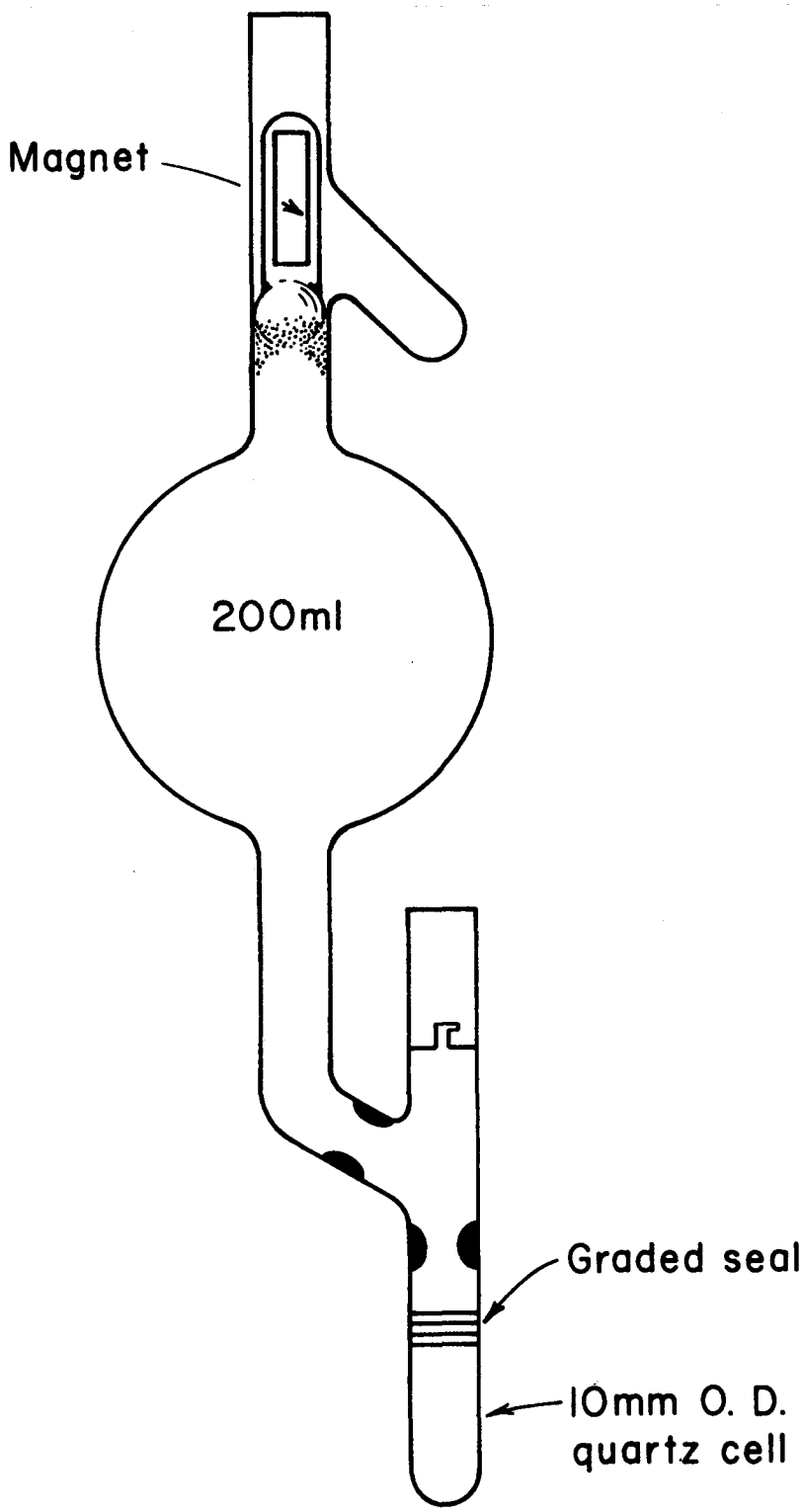

FIG. 2. "Ball valve" and sample tube. The "ball valve" is a pyrex ball with a ground-glass surface sealed to a pyrex tube containing a magnet. The "ball valve" fits in a ground-glass socket.

3-MP is degassed extensively by alternate freezing and melting until the pressure is less than 10^{-6} mm Hg. It is then refluxed at 80°C for an hour in a vacuum vessel on whose surface a thin layer of high-purity potassium has been distilled. After refluxing, 3-MP is degassed once more and is transferred to the sample tube that contains the purified naphthalene. The resulting concentration of naphthalene in the 3-MP is about 5×10^{-4} M/ℓ. MCP is purified with the same procedure.

The purification process for benzene is the same as that used in earlier work.[15] It includes degassing, drying over a thin layer of high-purity potassium ,and refluxing at 100°C for an hour in a vacuum vessel mirrored with high-purity cesium (Fisher Scientific Company).

B. Phosphorescence Experiments

A schematic diagram of the experimental apparatus used for measurements of the decay of the phosphorescence of the naphthalene is shown in Fig. 3. An Osram XBO 6500 Watt xenon arc lamp combined with the Kasha solution filter[14] described in the previous subsection is used to excite the naphthalene. A belt-driven rotating cylinder, with a choice of speeds, and having unappreciable frequency drift acts as a phosphoroscope. The light emitted from the sample passes through a series of lenses, then through Corning glass filters #3389 and #5031 into a 1/4-m Bausch and Lomb high-intensity grating monochromator with a bandpass of 180 Å. The

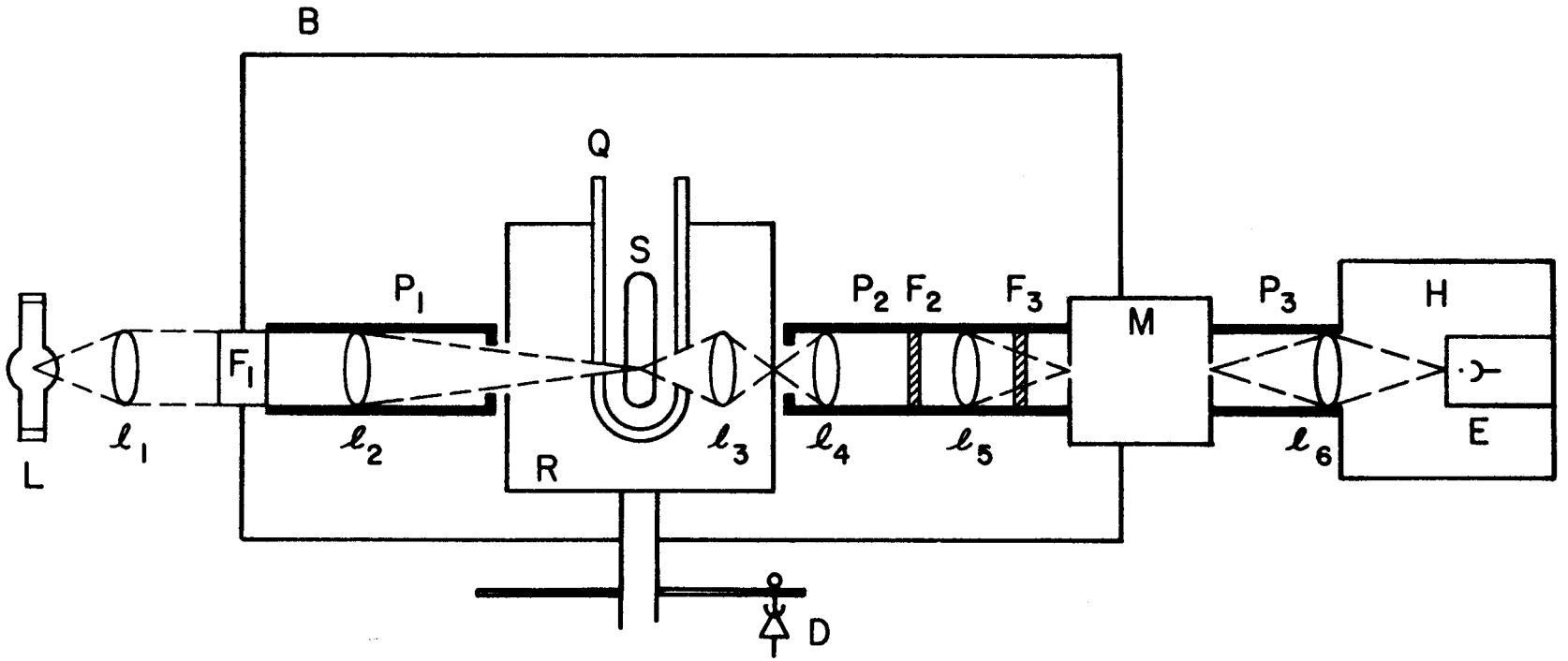

FIG. 3. Apparatus for phosphorescence. L = light source, ℓ = lenses, F_1 = filter solution, F_2, F_3 = Corning glass filters, P = light-tight pipes with baffles, R = rotating cylinder, D = photodiode, Q = quartz Dewar, S = sample tube, M = monochromator, H = photomultiplier housing, E = photomultiplier, B = black box to isolate the system from stray light.

output of the monochromator is detected by a high-gain, low-noise EMI photomultiplier #6256(S) that has been cooled to dry-ice temperature. The output from the photomultiplier is amplified either by a Tektronix oscilloscope #585 with a type 1A1 plug-in unit, or by a Keithley Multi-Range Electrometer, Model 610B. The amplified signal is then fed into a Nuclear Data memory unit in order to bring up the weak signal, which is otherwise buried by the noise.

The memory unit is constructed of three parts: Integrator and Time Base (ND 180 ITB), Analog to Digital Converter (ND 180 F), and 512 Channel Memory Unit (ND 180 M). The triggering for the ITB unit is taken from the output of a photodiode, which is synchronized with the rotating cylinder. The decay curve of the phosphorescence, with a fairly good signal-to-noise ratio can be obtained by time-averaging over 10 K to 100 K counts. After time-averaging, the decay is plotted out by means of a Hewlett-Packard X-Y recorder.

A wide range of temperatures in the experiment can be achieved by cooling the sample with nitrogen gas that has flowed through a copper coil immersed in a liquid nitrogen bath.[17] The temperature of the sample, which is placed in the center of the quartz Dewar, is measured by a calibrated copper-constantan thermocouple. The temperature can be maintained to within ± 1 °C for the duration of the experiment by adjustment of the flow rate of the nitrogen gas.

C. Triplet-Triplet Absorption Experiment

The conventional flash photolysis technique[1,2] is used to detect the decay of triplet-triplet absorption of $C_{10}H_8$ in benzene at room temperature. The actual apparatus employed was kindly loaned to us by Dr. W. G. Herkstroeter and is described in detail in his thesis.[18] A schematic diagram of this apparatus is shown in Fig. 4. A PEK-109 Hg-Xe lamp provides a monitoring light for the triplet-triplet absorption. Two E.G. & G. FX-45 xenon flash lamps are used for excitation. About 100 joules of energy from a flash lamp pulser is discharged in each flash. The decay of the absorbed light is measured with an RCA 1P28 photomultiplier and a Tektronix oscilloscope; it is photographed on Polaroid-Land Projection Film 46-L.

Two kinds of newly prepared filters[14] are placed around the flash lamps to avoid undesirable irradiation: one is 1 g/ℓ potassium acid phthalate in water with a wavelength cut-off below 3000 Å; the other is a solution of 0.4 ml of p-cymene in 1 ℓ CCl_4, which cuts off light of wavelengths shorter than 2600 Å.

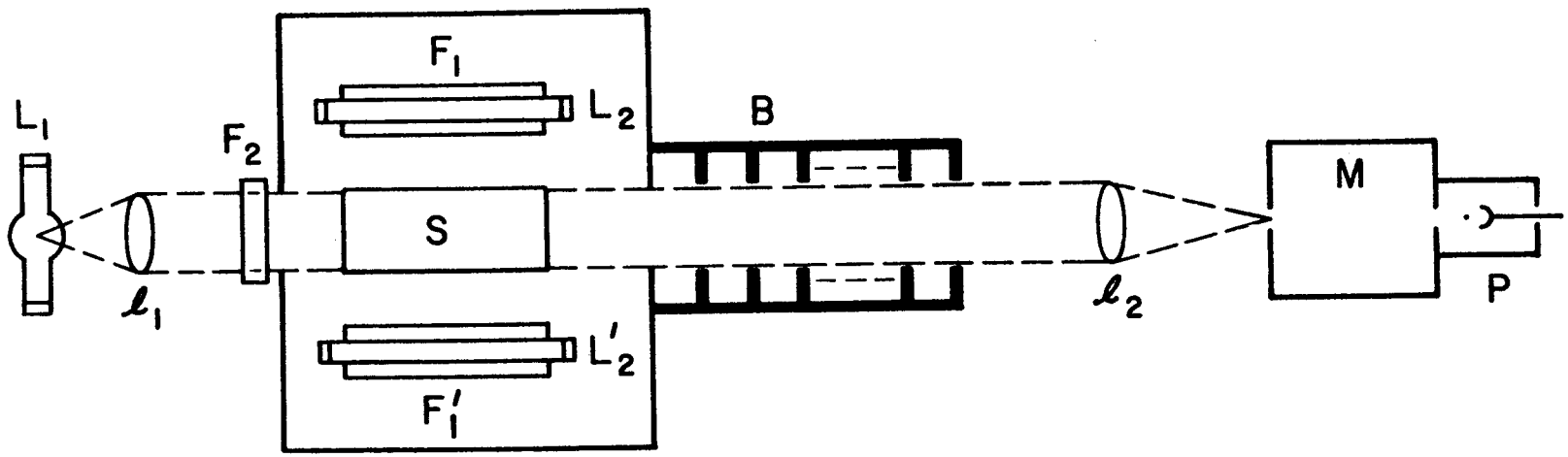

FIG. 4. Experimental apparatus for triplet-triplet absorption. L_1 = monitoring light for the triplet-triplet absorption; L_2, L_2' = flash lamps, F_1, F_1' = filter solution; F_2 = Corning glass filter; S = sample tube (18-cm long); B = baffles, ℓ_1, ℓ_2 = condensing lenses; M = 0.5 M Jarrell-Ash spectrometer; P = IP28 photomultiplier.

3. RESULTS AND DISCUSSION

A. Kinetic Analysis

A schematic representation of the excitation and decay of the lowest triplet state of naphthalene is shown in Fig. 5. Population of the triplet state of the naphthalene is accomplished by the excitation into the first two singlet states, utilizing the higher-lying $^1B_{2u} \leftarrow {}^1A_{1g}$ transition and the weaker $^1B_{3u} \leftarrow {}^1A_{1g}$ transition. Rapid internal conversion and intersystem crossing then cause a portion of the molecules to be excited into triplet states. Internal conversion and intersystem crossing into the triplet state are not rate determining and need not be considered.

Both unimolecular and bimolecular processes are important in the depopulation of the triplet state in fluid solutions. The former includes the radiative decay, which gives rise to phosphorescence: $T_1 \xrightarrow{k_p} S_0 + h\nu_p$; non-radiative decay: $T_1 \overset{k_n}{\rightsquigarrow} S_0$; and the pseudo first-order quenching by oxygen or other impurities: $T_1 + Q \overset{k_Q}{\rightsquigarrow} S_0 + Q^*$, where Q represents the ground state of the quencher, and Q^* the quencher in some state of excitation. The bimolecular processes consist of radiative and non-radiative triplet-triplet annihilations, $T_1 + T_1 \xrightarrow{k_2}$ products.

The rate equation for the concentration $[T_1]$ of the triplet state can be written as follows:

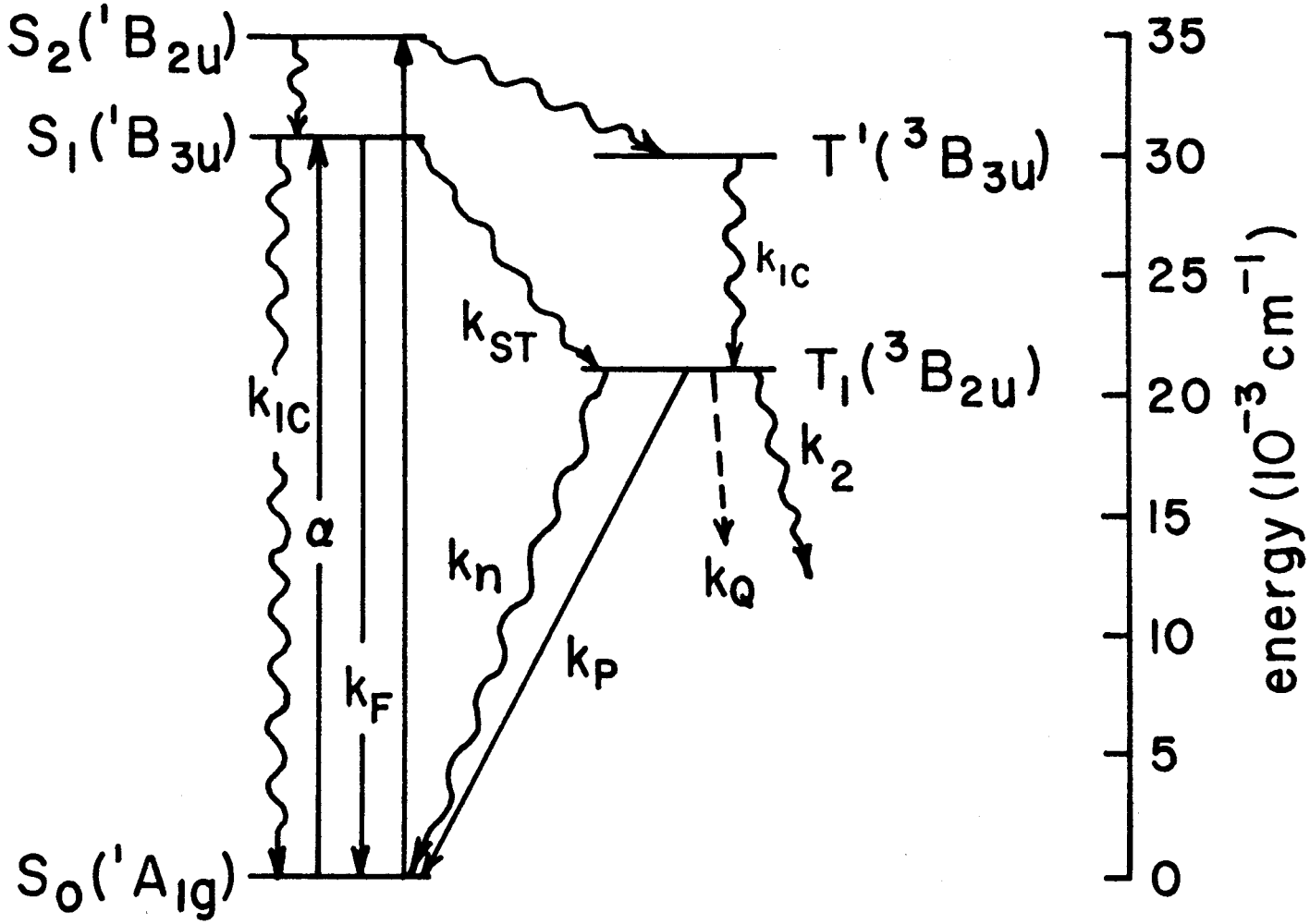

FIG. 5. Excitation and decay of the lowest triplet state of naphthalene.

$$-\frac{d[T_1]}{dt} = k_1[T_1] + k_2]T_1]^2 \qquad (1)$$

where

$$k_1 = k_n + k_p + k_Q[Q],$$

and $[Q]$ = the impurity concentration.

By integrating Eq. (1) and setting $I_p = ak_p[T_1]$, one obtains for the decay of phosphorescence intensity,

$$I_p = \frac{k_1 I_p^o}{(k_1 + \frac{k_2}{ak_p} I_p^o)e^{k_1 t} - \frac{k_2}{ak_p} I_p^o} \qquad (2)$$

where I_p^o designates the initial intensity of the phosphorescence, and a is a geometric and detection sensitivity factor.

Similarly, for the triplet-triplet absorption,

$$A_t = \frac{k_1 A_o}{(k_1 + \frac{k_2}{\epsilon \ell} A_o)e^{k_1 t} - \frac{k_2}{\epsilon \ell} A_o}. \qquad (3)$$

where $A_t \equiv \log \frac{I_o}{I_t} = \epsilon \ell [T_1]$ according to the Beer-Lambert Law. Here ℓ is the pathlength of the sample cell and ϵ is the molar extinction coefficient, which is about 10^4 for the 4150 Å triplet-triplet absorption of $C_{10}H_8$ in benzene,[5] and k_2 is of the order of 5×10^9 ℓmole^{-1} sec^{-1} (see Table II).

TABLE II. Second-order decay constant (k_2) of triplet $C_{10}H_8$ at room temperature by means of triplet-triplet absorption.

Solvent	Viscosity (centipoise)	k_2 (ℓ mole^{-1} sec^{-1})	References
n-hexane	0.30	2.1×10^9	11
benzene	0.65	8.8×10^9	18
benzene	0.65	5.8×10^9	this work

For $t \gg k_1^{-1} \equiv \tau$ (the "lifetime" of the triplet state), the decay in both cases is exponential. Consequently, the lifetime of the triplet state can be obtained from a plot of log I_p or log A_t vs t. However, for $t \lesssim \tau$, the decay is a combination of both first- and second-order processes. Consequently, the first-order rate constant obtained from a semilogarithmic plot can be considered as an upper limit. A more accurate value can be derived by means of a least-squares fit taking into account k_1 and k_2 simultaneously. Even so, gross inaccuracies can occur in the determination of k_1 for $t \lesssim k_1^{-1}$. Because of inadequate detection sensitivity, this time range has been the one employed in all past experiments on triplet decay in fluid solutions.

B. Triplet-Triplet Absorption

Highly purified solutions (see Sec. 2.A.) of $C_{10}H_8$ in benzene at room temperature were used. A typical decay curve traced with an oscilloscope is shown in Fig. 6. In the absence of the continuous monitoring light, no emission, except the stray light from the pulse of flash lamps, is observed as shown in the upper trace of Fig. 6. Table III gives the results obtained by neglecting the long tail which is barely above the noise level in the decay curves for a series of experiments on two different solutions under various conditions. The lifetime decreases slightly after a number of flashes. This is believed to be due to photogenerated impurities. Bimolecular processes dominate for a long period of time during the decay. These

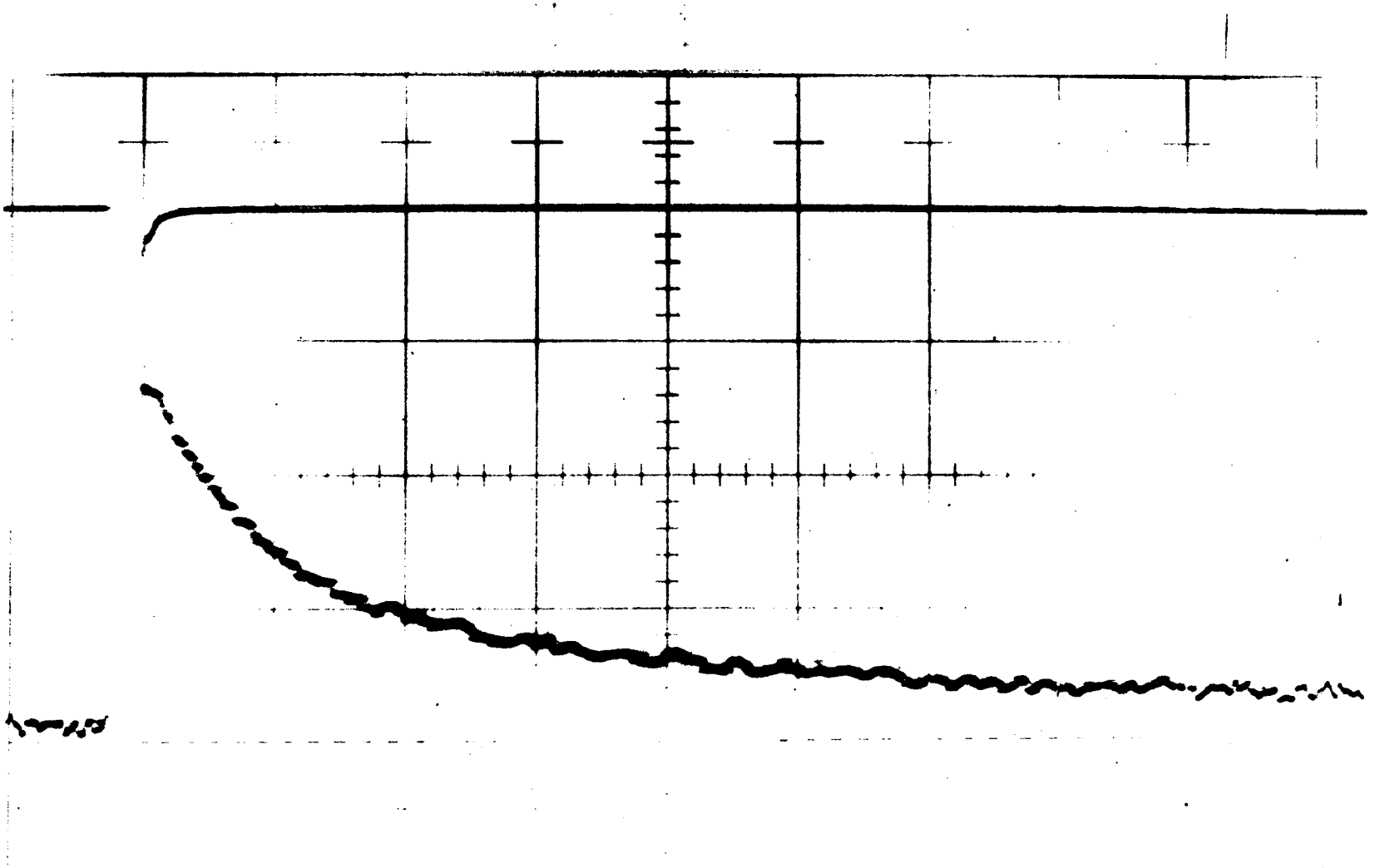

FIG. 6. Decay of triplet-triplet absorption of $C_{10}H_8$ in benzene at room temperature. A large division of the time scale is 100 μsec.

TABLE III. Lifetime of $C_{10}H_8$ in benzene at room temperature, measured by means of triplet-triplet absorption under various conditions.

Solution No.	Concentration M/ℓ	Excitation Wavelength λ_{ex}(Å)	Flash Number	Lifetime (k_1^{-1}) msec
I	$\sim 5 \times 10^{-4}$	$\geq$ 3000	1	0.54 ± 0.07
		> 2600	3[b]	0.54 ± 0.07
		> 2200	5	0.33 ± 0.07
		$\geq$ 3000	7	0.24 ± 0.02
		> 2200	9	0.14 ± 0.02[a]
II	$\sim 3 \times 10^{-5}$	> 2600	1	1.20 ± 0.40
		> 2600	3	1.10 ± 0.40

[a]Measured after standing 24 hours.

[b]The decay curve traced by an oscilloscope is shown in Fig. 6.

two phenomena also occur in the phosphorescence experiment which will be described in the next Section.

C. Phosphorescence

Phosphorescence spectra of $C_{10}H_8$ in 3-MP were obtained with either a 0.5-m Jarrell-Ash spectrometer or a Bausch and Lomb High Intensity Grating Monochromator equipped with a wavelength drive. Typical spectra are shown in Fig. 7. During the course of this work, no method for time-averaging an entire spectrum was available in our laboratory except through point-by-point measurements. Phosphorescence spectra at the higher temperatures are therefore obscured by noise.

Because of the great sensitivity of the time-averaging technique to measurement of phosphorescence decay curves, a number of precautions were taken to insure that it was the phosphorescence of naphthalene that was indeed being detected. Experiments with an empty sample tube and with a sample tube filled with pure solvent showed only a base-line signal when the monochromator was set at 4700 Å (the position of the first intense peak in the $C_{10}H_8$ phosphorescence spectrum--see Fig. 7). For a highly purified 3-MP solution of $C_{10}H_8$ at -45°C, identical lifetimes were obtained when the monochromator was set at 4700 Å and 5075 Å (see spectrum in Fig. 7). However, only a baseline was obtained when the monochromator was set at 4500 Å and 5400 Å (above and below the region of intense $C_{10}H_8$ phosphorescence emission.)

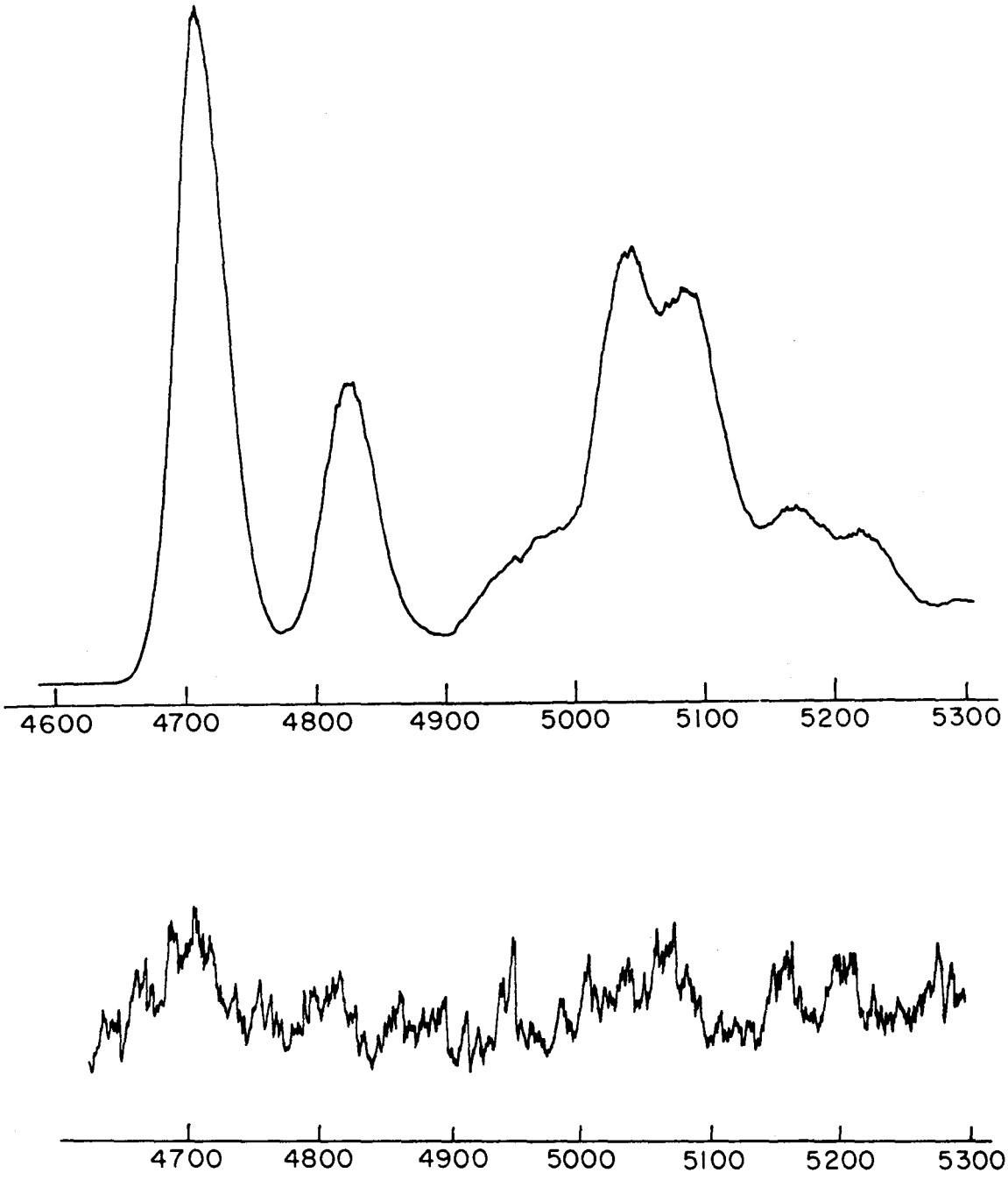

FIG. 7. Phosphorescence spectra of $C_{10}H_8$ in 3-MP with a concentration of 5×10^{-4} M/ℓ; (a) solid solution, and (b) liquid solution. The sensitivity used in (b) is about 200 times larger than that used in (a).

The phosphorescence decay of one sample of $C_{10}H_8$ in 3-MP, which was refluxed with potassium at 80°C for an hour, is given in Fig. 8 for a range of -48°C to +8°C. In this figure the lowest trace is the base line signal. The corresponding plots of log I_p vs t at temperatures of -48°C and -18°C are presented in Fig. 9. From the semilogarithmic plots, one can see that during the time of this observation (about half of the lifetime) the bimolecular processes are very efficient, and more dominant at high temperatures (low viscosities) than at low temperatures (high viscosities). One can also observe a slight dependence of the lifetime on temperature. This is believed to be caused by the diffusion-controlled process of quenching by the residual impurity. Thus the temperature dependence of k_1 can be depicted by the following equation[6]

$$k_1 = k_Q[Q] \exp(-\Delta E^{\ddagger}/RT) + k_1^0 , \qquad (5)$$

where $k_1^0 = K_n + k_p$ is independent of temperature, and the activation energy $\Delta E^{\ddagger}$ is expected to be equivalent to the energy of activation ΔE_η for the flow of non-viscous solvent in the same range of temperature:

$$\Delta E_\eta = [RTT'/(T' - T)] \ell n \eta/\eta' , \qquad (6)$$

in which η and η' designate viscosities of the solvent at temperatures T and T'. The experimental values of the activation energies $\Delta E^{\ddagger}$ and ΔE_η for 3-MP were found to be 1.5 kcal/mole and 1.3 kcal/mole, respectively, in the temperature range of -60°C to -18°C.

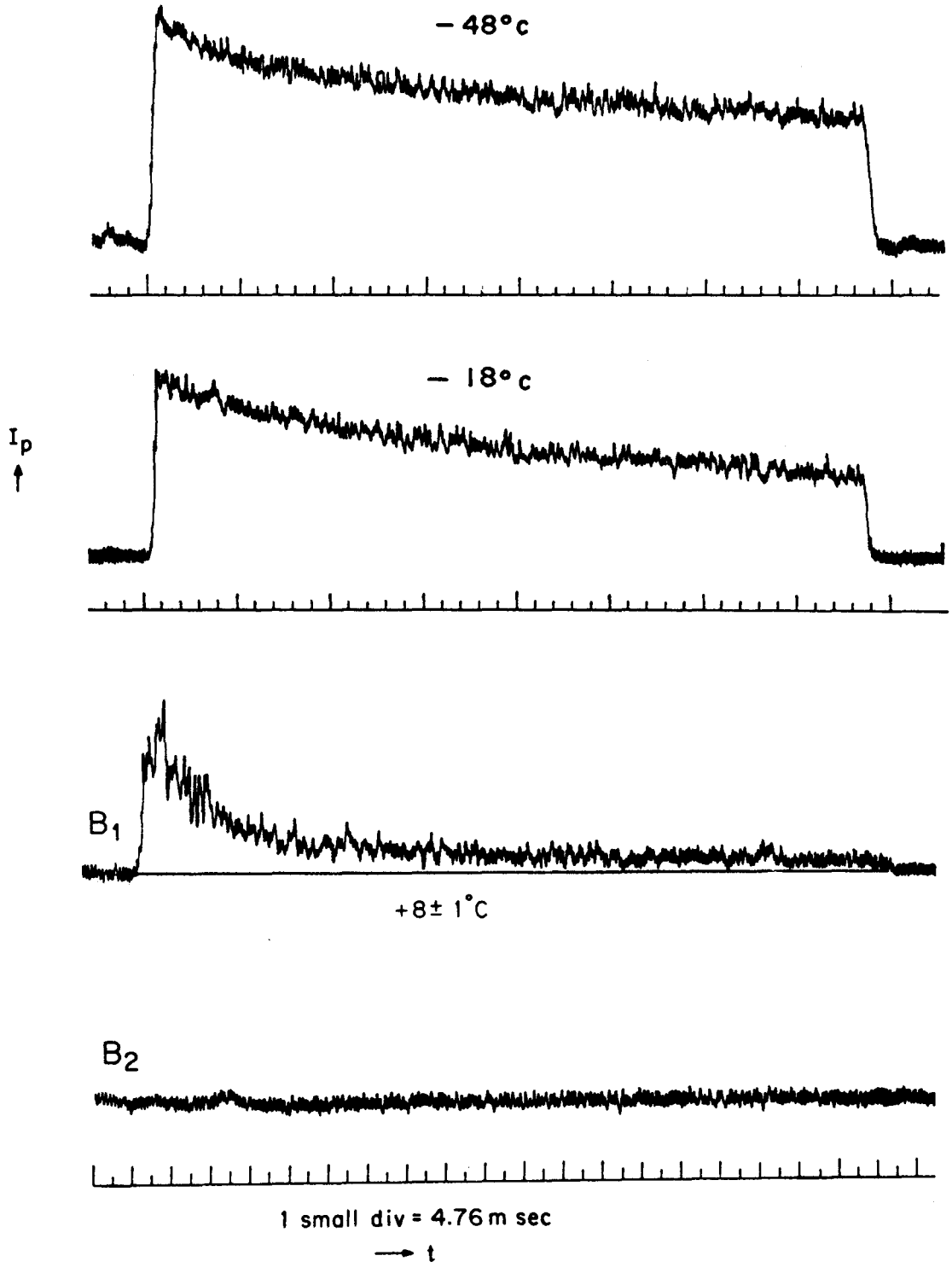

FIG. 8. Phosphorescence decay of a highly purified solution of $C_{10}H_8$ in 3-MP at various temperatures. One small division of the time scale is 4.76 msec.

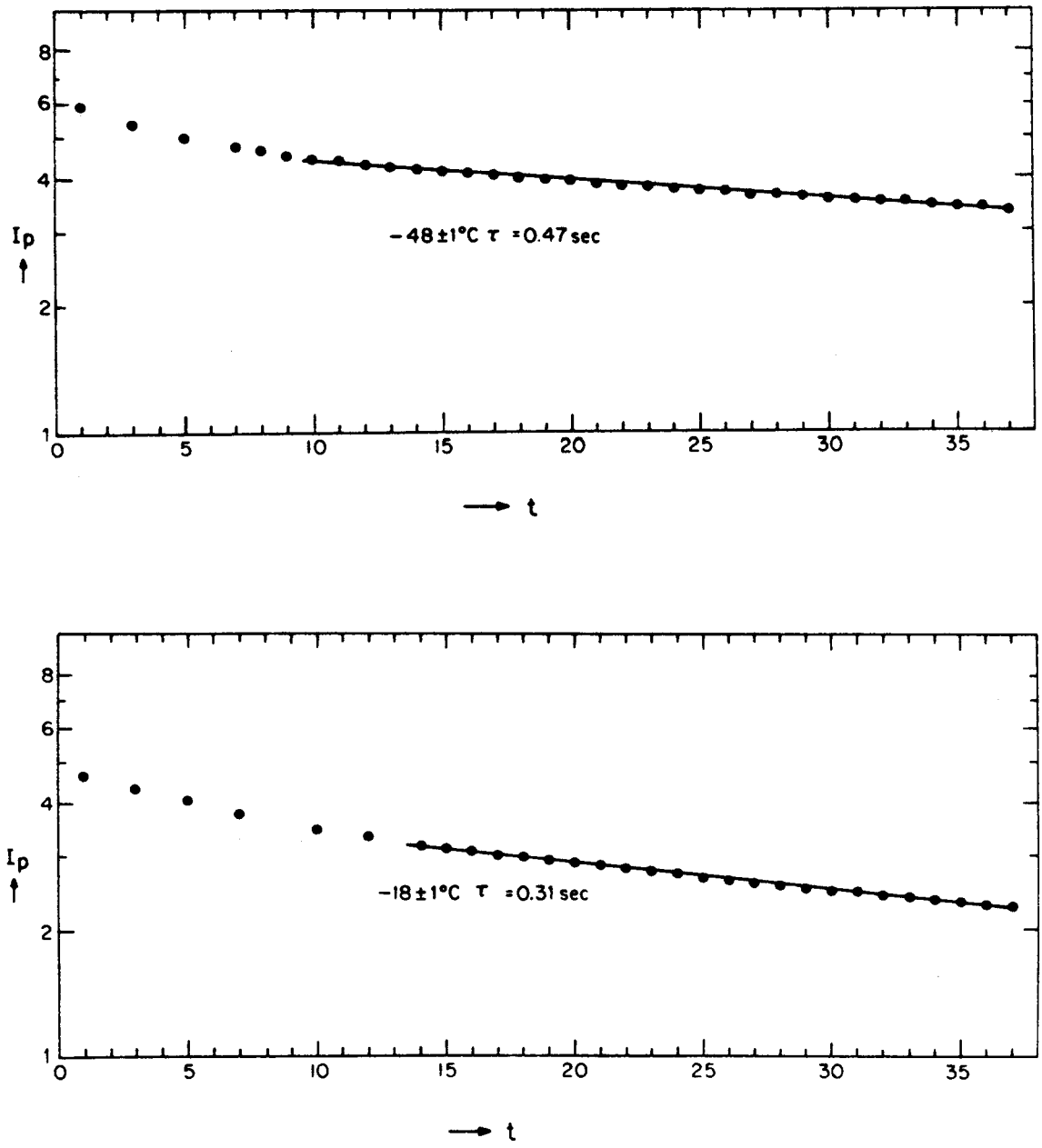

FIG. 9. Semilogarithmic plot of phosphorescence decay of $C_{10}H_8$ in 3-MP at -48°C and -18°C. One small division of the time scale is 4.76 msec.

Figure 10 depicts the phosphorescence decay of another sample in which the solvent was dried over potassium at 50°C, instead of being refluxed at 80°C for an hour. The lifetime was found to be 0.16 sec, about a factor of three shorter than that for the more rigorously purified sample.

The quenching effect of oxygen is shown in Fig. 11. In this case, a lifetime of 18 msec was measured for a sample that had been purified using the same procedure as the sample whose phosphorescence decay was shown in Fig. 10 and then exposed to the air at a pressure of approximately 10^{-2} mm Hg.

Figure 12 shows that the lifetime of triplet $C_{10}H_8$ in highly purified benzene at room temperature is much shorter than that in 3-MP at -48°C. In addition, the fact that the lifetime becomes shorter and shorter in the process of averaging seems to indicate the occurrence of a photoreaction. This phenomenon does not occur when 3-MP is used as the solvent. Therefore we speculate that the photo-impurities may arise in benzene through unavoidable irradiation.

D. Perdeuteronaphthalene Phosphorescence

Little or no deuterium effect on the lifetime of the triplet state of perdeuteronaphthalene in liquid solutions having residual impurities is expected.[19] Only in the purest solutions where the lifetime is intrinsic would a large deuterium effect be observed. If the phosphorescence lifetime of $C_{10}H_8$ in 3-MP at -45°C is 0.5 sec,

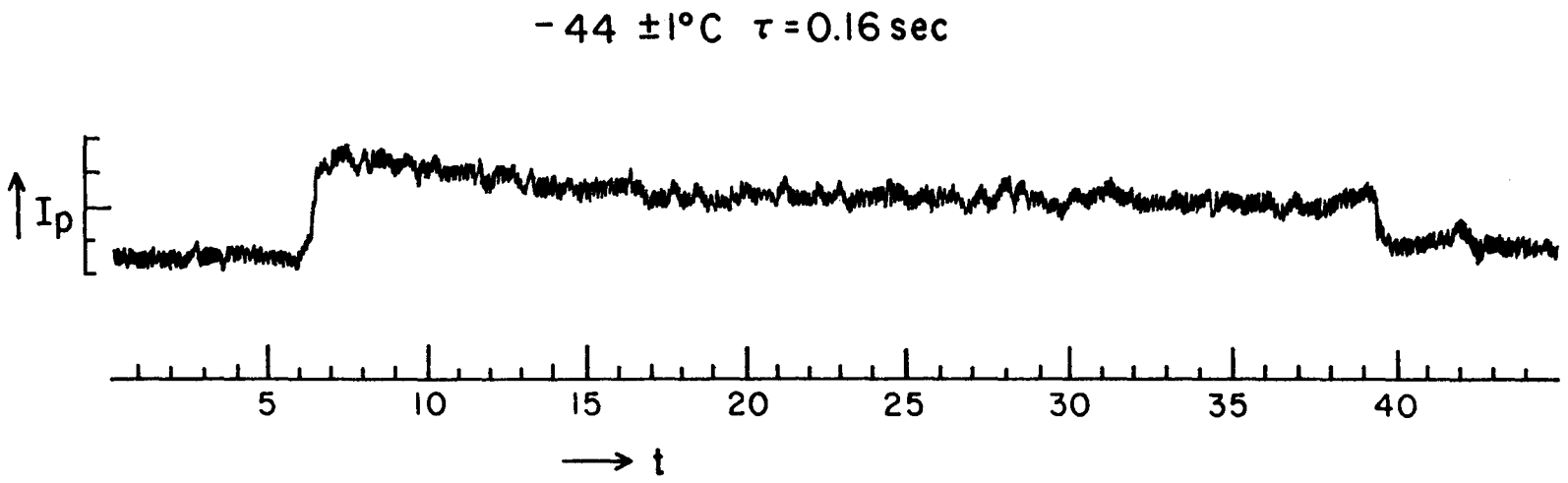

FIG. 10. Phosphorescence decay of another sample of $C_{10}H_8$ in 3-MP at -44° ± 1°C. One small division of the time scale is 2.08 msec.

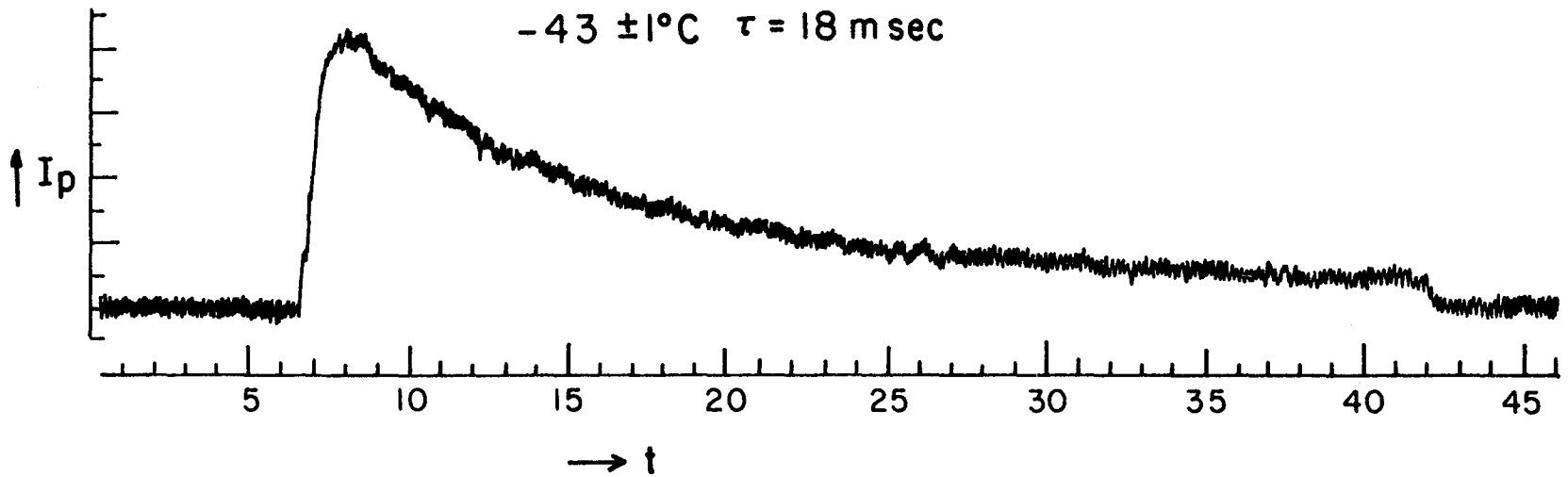

FIG. 11. Phosphorescence decay of $C_{10}H_8$ in 3-MP with a little air ($< 10^{-6}$ M/ℓ) at -43° ± 1°C. One small division of the time scale is 1.06 msec.

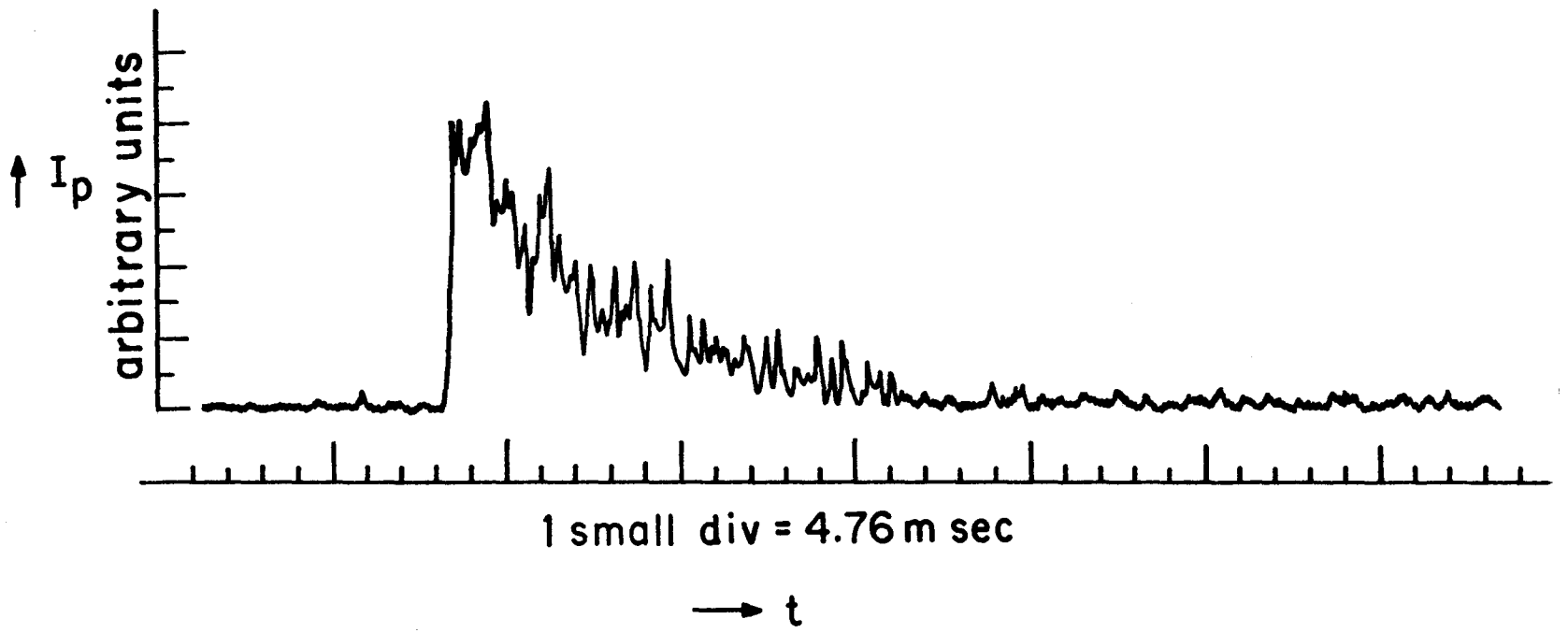

FIG. 12. Phosphorescence decay of $C_{10}H_8$ in benzene at room temperature.

compared with approximately 2 sec in a solid matrix, impurity quenching is still expected to be the dominant part of the first-order decay process. If one assumes similarly prepared samples of $C_{10}D_8$ in 3-MP have a very comparable impurity content as those of $C_{10}H_8$ in 3-MP, then, dividing the first-order rate into an isotopically independent radiative part ($k_p \approx 0.05\ sec^{-1}$), an isotopically dependent intrinsic non-radiative part ($k_n \approx 0.33\ sec^{-1}$ for $C_{10}H_8$; $k_n \approx 0$ for $C_{10}D_8$), and an isotopically independent impurity quenching part ($k_Q[Q] \approx 1.62\ sec^{-1}$), gives an expected overall lifetime of about 0.6 sec for $C_{10}D_8$ in 3-MP under the same conditions. This is indeed what has been observed as shown in Fig. 13. During the time scale of these observations, the decay curves are quite exponential as shown in Fig. 14. Similar experiments are also carried out in methyl cyclopentane. The results are shown in Table IV.

E. Conclusions

From the experimental results, it is concluded that quenching by impurities (those initially present or those produced by the intense excitation) and bimolecular depopulation are responsible for the previous failure to observe long-lived phosphorescence in liquid solutions. In highly purified solutions the bimolecular process is so effective compared to the first-order decay process that, when one attempts to approach the limit where the first-order process dominates, the concentration of the triplet state becomes too low to be measured by means of single-flash triplet-triplet absorption.

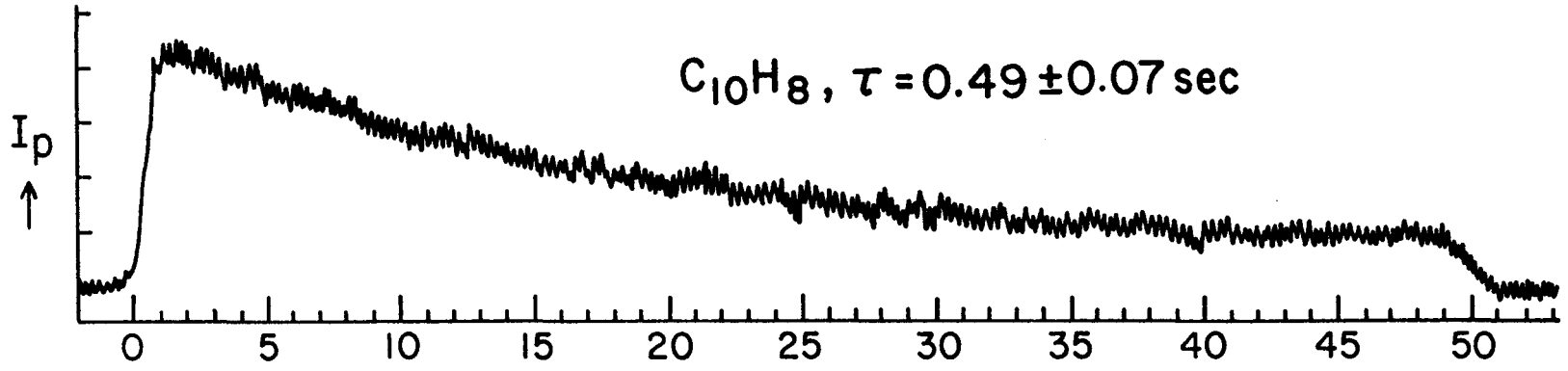

One small division of the time scale is 15.75 msec.

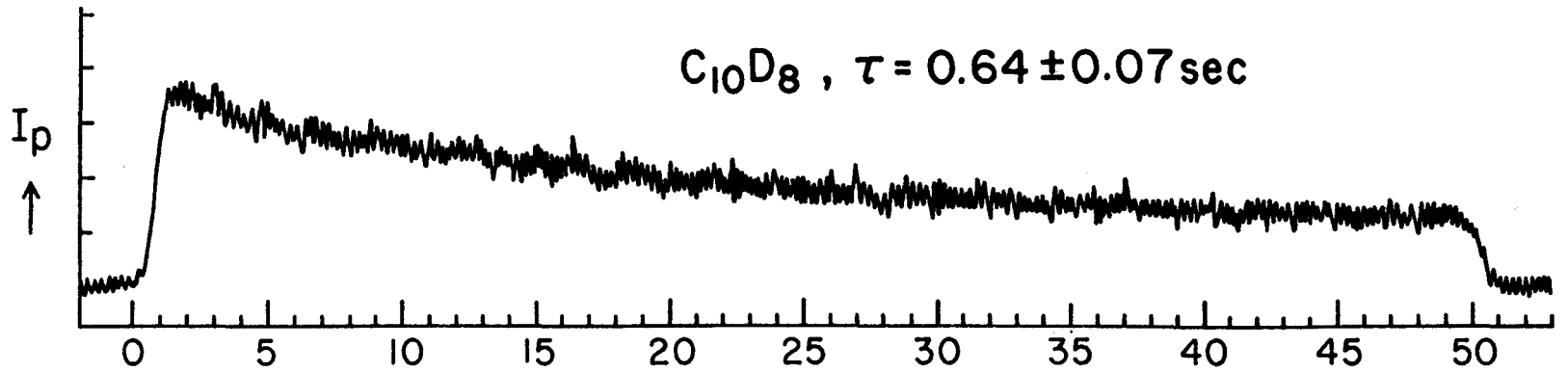

FIG. 13.

FIG. 14. Semilogarithmic plot of Fig. 13.

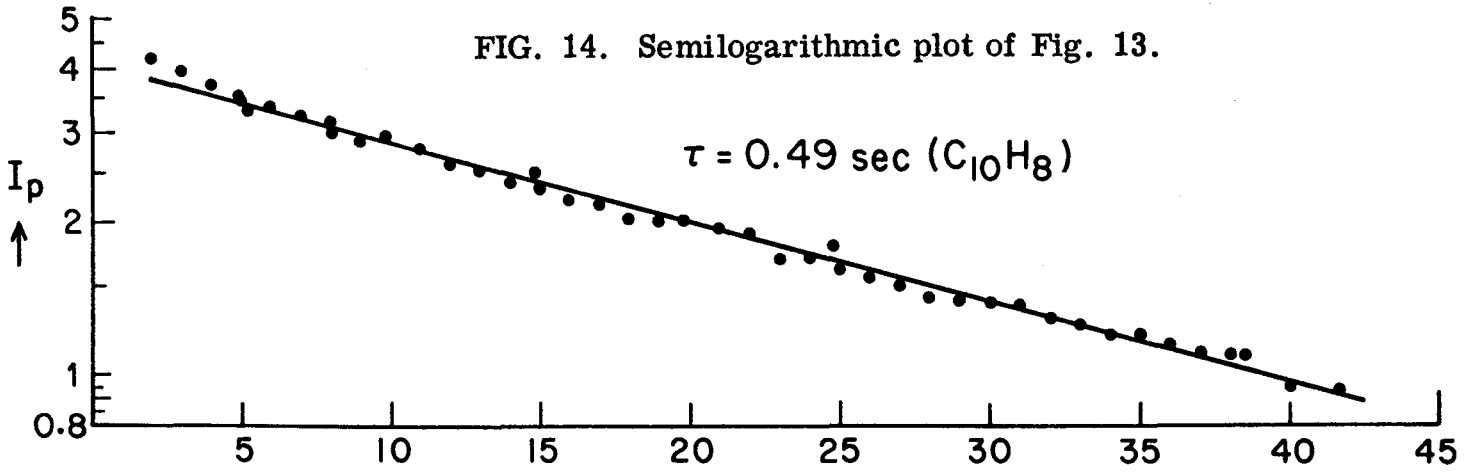

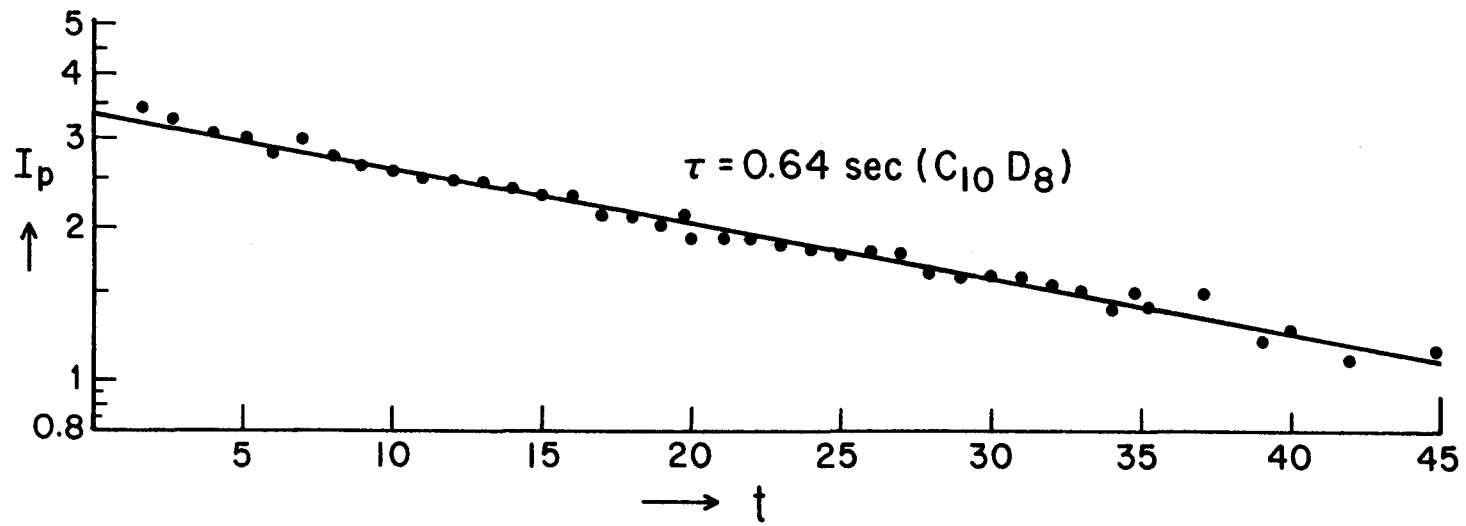

TABLE IV. Lifetime of Triplet Naphthalene in Different Solvents at Various Temperatures.

Expt. No.	Naphthalene	Solvent	Temperature °C	Lifetime sec
1	$C_{10}H_8$	3-MP	-48	0.47
		3-MP	-32	0.36
		3-MP	-18	0.31
2	$C_{10}H_8$	3-MP	-45	0.49
	$C_{10}D_8$	3-MP	-45	0.64
3	$C_{10}H_8$	3-MP	-46	0.47
	$C_{10}H_8$	MCP	-67	0.32
		MCP	-81	0.37
4	$C_{10}H_8$	MCP	-58	0.23
	$C_{10}D_8$	MCP	-50	0.25
		MCP	-64	0.31

The phosphorescence lifetime of triplet $C_{10}H_8$ in liquid solutions is 0.5 sec, which is of the same order of magnitude as that in plastic polymethyl methacrylate at room temperature.[4] Furthermore, only a little deuterium effect on the lifetime of triplet naphthalene was observed. We therefore think that the radiationless decay in liquid solutions is essentially the same as that in solid solutions.[19] The small discrepancy can be attributed to residual impurities, perhaps oxygen.

REFERENCES

1. G. Porter, Proc. Roy. Soc. (London) A200, 284 (1950).
2. G. Porter and M. W. Windsor, Discussions Faraday Soc. 17, 178 (1954).
3. S. G. Hadley, H. E. Rast, Jr. and R. A. Keller, J. Chem. Phys. 39, 705 (1963).
4. R. E. Kellogg and R. P. Schwenker, J. Chem. Phys. 41, 2860 (1964).
5. G. Porter and M. W. Windsor, Proc. Roy. Soc. (London) A245, 238 (1958).
6. R. Livingston and W. R. Ware, J. Chem. Phys. 39, 2593 (1963).
7. J. W. Hilpern, G. Porter and L. J. Stief, Proc. Roy. Soc. (London) 277A, 437 (1964).
8. G. Jackson and R. Livingston, J. Chem. Phys. 35, 2182 (1961).
9. D. S. McClure, J. Chem. Phys. 17, 905 (1949).
10. (a) Discussions Faraday Soc. 27, 94 (1959); (b) Proceedings of the Thirteenth Conference on Chemistry at the University of Brussels, Belgium, October, 1965, p. 79.
11. G. Porter and M. Wright, Discussions Faraday Soc. 27, 18 (1959).
12. G. Porter and F. Wilkinson, Proc. Roy. Soc. (London) A642, 1 (1961).

13. D. M. Hanson and G. W. Robinson, J. Chem. Phys. 43, 4174 (1965).

14. M. Kasha, J. Opt. Soc. Am. 38, 929 (1948); Appl. Optics 3, 361 (1964).

15. S. D. Colson and E. R. Bernstein, J. Chem. Phys. 43, 2661 (1965).

16. M. R. Andrews, J. Phys. Chem. 30, 1497 (1926).

17. C. H. Perr J. H. Fertel and T. F. McNelly, J. Chem. Phys. 47, 1619 (1967).

18. W. G. Herkstroeter, Ph.D. thesis, California Institute of Technology, 1965.

19. (a) G. W. Robinson and R. P. Frosch, J. Chem. Phys. 37, 1962 (1962); (b) G. W. Robinson, J. Chem. Phys. 47, 1967 (1967).

4. THEORETICAL

A. General Theory of Radiationless Transitions

a. Introduction

Theories of radiationless electronic relaxation have been discussed by Robinson and Frosch,[1] M. Gouterman,[2] S. H. Lin,[3] M. Bixon and J. Jortner.[4] These theories have the following in common: the zero-order state of an electronically excited but vibrationally unexcited molecule is mixed with a state in which the molecule is electronically unexcited and vibrationally excited; these zero-order states are nonstationary in the presence of a perturbation; the assumption is made that coupling between the molecule and its environment is required to dissipate the vibrational energy and to secure energy conservation by demanding that the energy spectrum of the coupled system is almost continuous.

Robinson and Frosch[1] discussed radiationless transitions for cases in which electronic relaxations are much slower than vibrational relaxations as happens frequently in organic compounds (i.e., electronic lifetime $\tau_{el} \gg \tau_{vib}$ vibrational lifetime). They considered zero-order states of the coupled system to be almost, but not quite, stationary. The time-development of these states is determined by the time-independent perturbations which are already present in the free molecule, such as intramolecular vibronic coupling and intramolecular spin-orbit coupling. The intramolecular

perturbations are so small that the Born-Oppenheimer approximation is assumed to be valid. The environment simply provides a manifold of states nearly degenerate with the initial state and a sink for vibrational relaxation processes. Therefore little environmental effect is expected to exist in most electronic relaxations. On the other hand, Gouterman[2] treats the environment as harmonic oscillators of a phonon field. He assumed that the interaction between the solute molecules and the environment can be represented by a force field, which is set up by lattice vibrations. The oscillating force field thus induces the radiationless transitions and leads to a considerable environmental effect, including a temperature effect, on the transition rate.

In contrast to Robinson's theory, Lin[3] and Jortner[4] took the deviation from the Born-Oppenheimer approximation as a source of perturbations which includes both intramolecular and intermolecular perturbations. Lin derived[3] a radiationless transition probability which is principally a function of electronic matrix elements $R_i(a\,b)$, vibrational frequency (ω_i) and the displacement of the normal mode of the two electronic states concerned. $R_i(a\,b) = \langle \Theta_a | \frac{\partial}{\partial Q_i} | \Theta_b \rangle$ where Θ_a and Θ_b represent respectively the electronic wavefunctions of the initial state a and the final state b; Q_i is the normal coordinate, and subscript i runs over all normal modes of molecular and lattice vibrations. From this theory, the electronic energy may convert directly into the lattice vibrational energy. However, because of the smallness of ω_i and $R_i(a\,b)$ for

lattice modes, this process is not likely to be important unless $R_i(ab)$ is zero for all intramolecular normal modes. For systems with a large number of internal vibrations, such as naphthalene, $R_i(ab)$'s for intramolecular normal modes have very little chance to vanish. It was therefore concluded that most of the electronic energy would first go into the internal normal nodes and then transfer to the lattice modes through vibrational relaxations. This conclusion is essentially the same as Robinson's assumption. Small environmental and temperature effects are expected from this theory, as well.

A theory of radiationless transitions, based on Robinson's theory, will be briefly outlined.

b. Theoretical Models

i) Transition between two discrete states:

Consider two non-resonant eigenstates ψ', ψ'' of an incomplete Hamiltonian H_0. These two states are separated with an energy gap Γ and have eigenvalues $(E - \frac{\Gamma}{2})$ and $(E + \frac{\Gamma}{2})$, respectively. They can be mixed together through a perturbation H' with the corresponding matrix element β. The energy matrix $H = H_0 + H'$ for these states is

$$\underset{\sim}{H} = \begin{bmatrix} E - \frac{\Gamma}{2} & \beta \\ \beta & E + \frac{\Gamma}{2} \end{bmatrix} \qquad (1)$$

We now wish to determine the first-order eigenstates ψ_1, ψ_2 of the matrix $\underset{\sim}{H}$ associated with the eigen-energies $E_1 = E - \frac{\epsilon}{2}$, $E_2 = E + \frac{\epsilon}{2}$, where $\epsilon \equiv (4\beta^2 + \Gamma^2)^{\frac{1}{2}}$:

$$\text{Let } \psi_1 = a\psi' + b\psi'' \tag{2}$$

From the normalization condition $a^2 + b^2 = 1$ and the following equations pertaining to the matrix $\underset{\sim}{H}$

$$(E - \frac{\Gamma}{2})\, a + \beta b = E_1 a \tag{3a}$$

$$\beta a + (E + \frac{\Gamma}{2})\, b = E_1 b \tag{3b}$$

one obtains

$$a = \left(\frac{\epsilon + \Gamma}{2\epsilon}\right)^{\frac{1}{2}} \qquad b = \left(\frac{\epsilon - \Gamma}{2\epsilon}\right)^{\frac{1}{2}} \tag{4}$$

Similarly, one obtains $\psi_2 = b\psi' - a\psi''$.

The time-development of the zero-order states ψ', ψ'', which are non-stationary under H, becomes

$$\begin{aligned} \psi'(\vec{x}, t) &= \left\{ a\psi_1 e^{-\frac{iE_1}{\hbar}t} + b\psi_2 e^{-\frac{iE_2}{\hbar}t} \right\} \\ \psi''(\vec{x}, t) &= \left\{ b\psi_1 e^{-\frac{iE_1}{\hbar}t} - a\psi_2 e^{-\frac{iE_2}{\hbar}t} \right\} \end{aligned} \tag{5}$$

Since we are interested in the transition probability $\omega(t)$ for $\psi'' \leftarrow \psi'$ at time t, we write out $\psi''(\vec{x}, t)$ explicitly in terms of ψ' and ψ''.

$$\psi''(\vec{x},t) = \left\{ ab\left(e^{\frac{i\epsilon t}{2\hbar}} - e^{-\frac{i\epsilon t}{2\hbar}}\right)\psi' + \left(b^2 e^{\frac{i\epsilon t}{2\hbar}} + a^2 e^{-\frac{i\epsilon t}{2\hbar}}\right)\psi'' \right\} e^{-\frac{iEt}{\hbar}}$$

Incorporating the initial conditions $|\psi'|^2 = 1$ and $|\psi''|^2 = 0$, we obtain the transition probability

$$\omega(t) = \langle \psi''(\vec{x},t) | \psi''(\vec{x},t) \rangle = \frac{4\beta^2}{(4\beta^2 + \Gamma^2)} \sin^2\left[\frac{t}{2\hbar}(4\beta^2 + \Gamma^2)^{\frac{1}{2}}\right] \qquad (6)$$

For very short times compared with the time scale $t \approx \hbar\beta^{-1}$, the probability for a transition from ψ' to states very near resonance is given by

$$\omega(t) \approx \frac{\beta^2 t^2}{\hbar^2} \qquad (t \ll \hbar\beta^{-1},\ \Gamma \approx \beta) \qquad (7)$$

while for states far-removed from resonance, one has

$$\omega(t) \approx \frac{4\beta^2}{\Gamma^2} \sin^2\left(\frac{\Gamma t}{2\hbar}\right) \qquad (\Gamma \gg \beta) \qquad (8)$$

ii) Transition from a discrete initial state to a directly coupled final state, being strongly coupled to N-1 discrete states in N steps:

Suppose in an idealized case, there is a single final state ψ''_n in near resonance with the initial state ψ'_0. Let ψ'_0 and ψ''_n be mixed through the matrix element β_n. Assume now that there exist (N-1) other final states ψ^i_0, i = I, II, ... N-1, which are coupled directly to each other and to ψ''_n, but indirectly to ψ'_0. For simplicity, we assume all the matrix elements α directly mixing these final states to be equal. We also neglect the indirect coupling between ψ'_0 and ψ^i_0. This model is illustrated in Fig. 1.

FIG. 1. (a) Schematic energy level idagram illustrating the coupling parameters α and β_n. The figure shows how the directly coupled final state ψ_n'' interacts weakly with the initial state ψ_0' but strongly with the set of indirectly coupled final states ψ_0^I, ψ_0^{II}, $\ldots\psi_0^{N-1}$. For simplicity, only a single molecular mode and a single lattice mode are shown. In general a variety of such modes is involved. When there are many lattice modes, a number of final states having the same molecular vibrational energy as ψ_0^I may exist. There may also be many ψ_0^{II}, etc. The parameter α used in the text of the paper represents an average over all these final states.
(b) This figure schematically represents the coupling between the initial state and the final state band. It is the integration over all final states in this band which yields $\omega_n(t)$. The scale in this figure has been greatly magnified compared with that in Fig. 1(a) since $\alpha \sim 1$ cm^{-1} while generally $\Delta E > 1000$ cm^{-1}.

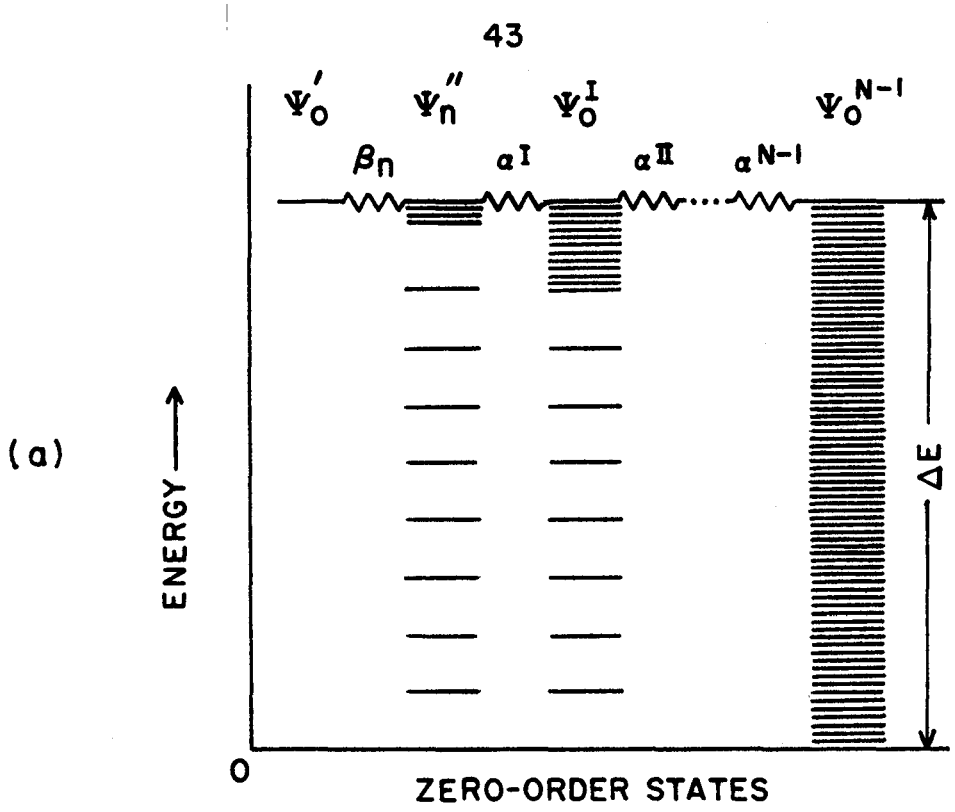
(a)
Ψ_0'
Ψ_n''
Ψ_0^I
Ψ_0^{N-1}
β_n
α^I
α^{II}
α^{N-1}
ENERGY
ΔE
0
ZERO-ORDER STATES

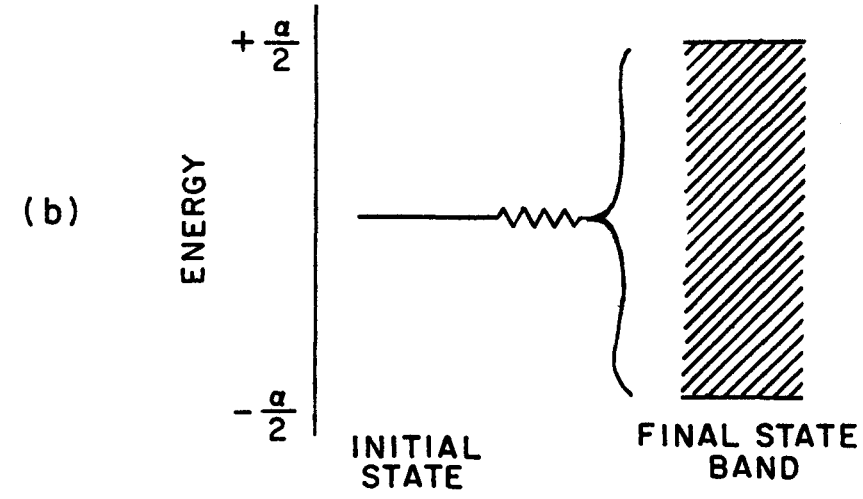
(b)
$+\frac{a}{2}$
ENERGY
$-\frac{a}{2}$
INITIAL STATE
FINAL STATE BAND

Fig. 1

Then we choose a representation which is diagonal in the absence of β_n and α, and assume the initial zero-order state ψ_0' and all the N final zero-order states ψ_n'', ψ_0^i to be degenerate with one another. The (N+1)-order Hamiltonian matrix $\underset{\sim}{H}$ for such a problem is

$$\underset{\sim}{H} = \begin{bmatrix} E & \beta_n & 0 & 0 & \cdot & \cdot \\ \beta_n & E & \alpha & 0 & \cdot & \cdot \\ 0 & \alpha & E & \alpha & \cdot & \cdot \\ 0 & 0 & \alpha & E & \alpha & \cdot \\ \cdot & \cdot & \cdot & \cdot & \cdot & \cdot \\ \cdot & \cdot & \cdot & \cdot & \cdot & E \end{bmatrix}_{N+1} \tag{9}$$

If $\beta_n = 0$, the matrix $\underset{\sim}{H}$ is diagonalized by the symmetrical orthogonal matrix $\underset{\sim}{T}$ whose elements are,[6]

$$\begin{aligned} &T_{1,1} = 1, \\ &T_{1,s+1} = T_{s+1,1} = 0 \\ \text{and} \quad &T_{s+1,t+1} = \sqrt{\frac{2}{N+1}} \sin\left(\frac{st\pi}{N+1}\right) \end{aligned} \tag{10}$$

for s, t = 1, 2, ...N. The perturbation α removes the degeneracy of the N zero-order final states ψ_n'', ψ_0^i. The new eigenvalues become

$$\begin{aligned} &E_1 = E, \\ &E_{s+1} = E + 2\alpha \cos\left(\frac{s\pi}{N+1}\right) \quad s = 1, 2, \ldots N \end{aligned} \tag{11}$$

When $\beta_n \neq 0$, the transformation

$$\underset{\sim}{\mathcal{K}} = T^{-1} \underset{\sim}{H} T \tag{12}$$

diagonalizes $\underset{\sim}{H}$ except for the occurrence of the element β_n with diminished coefficients

$$T_{1,s+1} = \sqrt{\frac{2}{N+1}} \sin\left(\frac{s\pi}{N+1}\right) \quad s = 1, 2, \ldots N \tag{13}$$

along the first row and column of $\underset{\sim}{\mathcal{K}}$. Since $\hbar\alpha^{-1}$ is of the order of the relaxation time, per quantum of molecular vibration, and since the electronic radiationless transition is slow compared with vibrational relaxation, we assume the inequality $\beta_n \ll \alpha$. Therefore a first-order perturbation calculation can be used to find the time-dependence of the nonstationary state ψ_0'. Using β_n with its diminished coefficients for the matrix elements and the eigenvalues of Eq. (11) for calculating the energy gap Γ, one obtains, according to Eq. (8), the transition probability to any one of the final states r

$$\omega_r(t) = \frac{2\beta_n^2 \sin^2\left(\frac{r\pi}{N+1}\right)}{(N+1)\alpha^2 \cos^2\left(\frac{r\pi}{N+1}\right)} \sin^2\left[\frac{\alpha t}{\hbar} \cos\left(\frac{r\pi}{N+1}\right)\right] \tag{14}$$

$$r = 1, 2, \ldots . N.$$

Summation over r yields[1] the total transition probability per unit time $\frac{\omega_n(t)}{t}$ for the process associated with β_n.

$$\frac{\omega_n(t)}{t} = \frac{2|\beta_n|^2}{\alpha\hbar} \sec^{-1} \tag{15}$$

To simplify mathematics, r has been taken to be ∞. This did not introduce any significant error because the dominant terms of the summation arise from that part of the final state band relatively near the origin.

iii) Transition from a single state to a discrete final state which strongly couples with a continuum:

Instead of coupling with (N-1) final states as described in the previous model, ψ''_n now couples strongly with a continuum of states $\psi_{E'}$. We also assume that β_n is much smaller than the coupling elements of $\psi_{E'}$ with ψ''_n or with $\psi_{E''}$. Therefore to a first-order approximation, we can separate the subset of states ψ''_n, $\psi_{E'}$'s from ψ'_0. The energy matrix for the subset can be indicated by

$$\langle \psi''_n \,|\, H \,|\, \psi''_n \rangle = E_\varphi \tag{16a}$$

$$\langle \psi_{E'} \,|\, H \,|\, \psi''_n \rangle = V_{E'} \tag{16b}$$

$$\langle \psi_{E'} \,|\, H \,|\, \psi_{E''} \rangle = E' \delta (E' - E'') \tag{16c}$$

Not only the zero-order states ψ'_0, ψ''_n are non-degenerate and orthogonal, the Dirac δ factor in Eq. (16c) implies as well that the submatrix belonging to the more limited subset of states $\psi_{E'}$ has previously been diagonalized in the zero-order approximation. It is understood that the discrete energy E_φ lies within the continuous range of values of E'.

We now wish to determine the first-order eigenstate Ψ_E of the matrix (16), associated with an eigenvalue E which is within the

range of E′. Ψ_E has the form

$$\Psi_E = a\psi''_n + \int dE'\, b_{E'}\psi_{E'} \tag{17}$$

The coefficients $\underline{a}$ and $b_{E'}$, which are functions of E, can be evaluated as solutions of the following equations pertaining to the energy matrix of Eq. (16).

$$E_q a + \int dE'\, V_{E'} b_{E'} = E a \tag{18a}$$

$$V_{E'} a + E' b_{E'} = E b_{E'} \tag{18b}$$

The solution of this system can be carried out exactly,[7] so that the diagonalization of the energy matrix can be achieved.

Since E is within E′, there is a singularity when $b_{E'}$ is expressed in terms of $\underline{a}$, utilizing Eq. (18b). This obstacle can be circumvented by following Dirac's[8] procedure of introducing the formal solution of Eq. (18b)

$$b_{E'} = \left[\frac{1}{E - E'} + z(E)\,\delta(E - E')\right] V_{E'} a \tag{19}$$

with the understanding that, upon substitution into Eq. (18a), one shall take the principal part of the integral over $(E - E')^{-1}$. The value of z(E) is determined by substituting Eq. (19) into Eq. (18a). The coefficient $\underline{a}$ factors out so that Eq. (18a) reduces to

$$E_\varphi + F(E) + z(E)\left|V_E\right|^2 = E \tag{20}$$

where $F(E) = P\int dE' \dfrac{\left|V_{E'}\right|^2}{E - E'}$ (21)

and P indicates "principal part of". We have then

$$z(E) = \frac{E - E_{\varphi} - F(E)}{|V_E|^2} \tag{22}$$

Notice that $|V_E|^2$, an index of the strength of the interaction, has the dimensions of energy since $\psi_{E'}$ is normalized "per unit energy" according to Eq. (16c).

The coefficient $\underline{a}$ is determined by normalization. The orthonormalization condition of the continuous spectrum gives

$$\langle \Psi_E | \Psi_E \rangle = a^*(\bar{E})\, a(E) + \int dE' b^*_{E'}(\bar{E})\, b_{E'}(E) = \delta(\bar{E} - E) \tag{23}$$

Substitution of Eq. (19) yields

$$a^*(E)\, a(E) \left\{ 1 + \int dE' V^*_{E'} \left[\frac{1}{\bar{E} - E'} + z(E)\, \delta(\bar{E} - E') \right] \times \right.$$

$$\left. \left[\frac{1}{E - E'} + z(E)\, \delta(E - E') \right] V_{E'} \right\} = \delta(\bar{E} - E) \tag{24}$$

The factor $\dfrac{1}{(\bar{E} - E')(E - E')}$ is properly resolved[7] into

$$\frac{1}{(\bar{E} - E')(E - E')} = \frac{1}{(\bar{E} - E)} \left(\frac{1}{E - E'} - \frac{1}{\bar{E} - E'} \right)$$

$$+ \pi^2 \delta(E - E)\, \delta\left[E' - \tfrac{1}{2}(E + E)\right] \tag{25}$$

Substituting Eq. (25) into Eq. (24) and considering that $\delta(\bar{E} - E')\, \delta(E - E') = \delta(\bar{E} - E)\, \delta[E' - \frac{1}{2}(E + \bar{E})]$ and that $\delta(E - E')\, f(E') = \delta(E - E')\, f(E)$, one finds

$$|a(E)|^2 |V_E|^2 [\pi^2 + z^2(E)] \delta(\bar{E} - E)$$

$$+ a^*(\bar{E}) \left\{ 1 + \frac{1}{E - \bar{E}} [F(E) - F(\bar{E}) + z(E)|V_E|^2 - z(\bar{E})|V_{\bar{E}}|^2] \right\} a(E)$$

$$= \delta(\bar{E} - E). \tag{26}$$

The expression in braces vanishes because of Eq. (22), so that

$$|a(E)|^2 = \frac{1}{|V_E|^2 [\pi^2 + z^2(E)]}$$

$$= \frac{|V_E|^2}{[E - E_\varphi - F(E)]^2 + \pi^2 |V_E|^4} \tag{27}$$

This result shows that the discrete state ψ_n'' is diluted throughout a band of actual stationary states with half-width $\pi |V_E|^2$.

Referring to Eq. (19) and assuming an arbitrary phase of a, one can finally write

$$a = \frac{\sin \Delta}{\pi V_E} \tag{28a}$$

$$b_{E'} = \frac{V_{E'}}{\pi V_E} \frac{\sin \Delta}{E - E'} - \cos \Delta \, \delta(E - E') \tag{28b}$$

$$\text{where } \Delta = -\arctan \frac{\pi |V_E|^2}{E - E_\varphi - F(E)} \tag{29}$$

From the first-order time-dependent perturbation theory one can write the transition probability per unit time[10] for the radiationless transition $n \leftsquigarrow 0$.

$$\frac{\omega_n(t)}{t} = \frac{2\pi\rho}{\hbar} \left| H'_{no} \right|^2 \qquad (30)$$

where ρ is the density of final states $\underline{n}$, H'_{no} is the matrix element of the time-independent perturbation Hamiltonian for the transition $n \rightsquigarrow 0$.

Combining Eqs. (17), (28) and (30), and neglecting the weak indirect coupling between ψ'_0 and $\psi_{E'}$, one obtains the transition rate

$$\frac{\omega_n(t)}{t} = \frac{2\pi}{\hbar} \cdot \frac{\left|V_E\right|^2}{\left[E - E_\varphi - F(E)\right]^2 + \pi^2 \left|V_E\right|^4} \left|\beta_n\right|^2 \qquad (31)$$

Because of the energy conservation in non-radiative transitions, only states in near resonance give important contributions to $\frac{\omega_n(t)}{t}$. Eq. (31) is therefore simplified:

$$\frac{\omega_n(t)}{t} \approx \frac{2}{\hbar\pi \left|V_E\right|^2} \left|\beta_n\right|^2 \qquad (32)$$

Notice that α in Eq. (15) has the same meaning as the interaction half-width $\pi \left|V_E\right|^2$ in Eq. (32). These two equations are therefore exactly the same.

c. Physical Implications

In real physical problems, it is assumed that there is a set of molecular vibrational levels ψ''_n of the final electronic state, which in the free molecule are in near resonance with the initial state ψ'_0. Each one of the final states ψ_n is directly coupled to the initial state

with a matrix element β_n. Summation over all of the directly coupled final states yields the total transition probability $\frac{W(t)}{t}$, or the rate constant k, for the radiationless transition

$$k = \frac{W(t)}{t} = \sum_n \frac{2}{\hbar\alpha} |\beta_n|^2 \qquad (33)$$

The introduction of an environment provides a way to dissipate the vibrational energy of the directly coupled final states and enormously increases the number of final states which are indirectly coupled to the initial state. Even in the absence of the environment, the density* of the final states in large molecules such as naphthalene is so great that intramolecular radiationless transitions can take place.

Using the Born-Oppenheimer approximation, the total wavefunction ψ can be resolved into an electronic and a vibrational part

---

*According to Bixon and Jortner[4], to make the intersystem crossing feasible for an energy gap of 10^4 cm^{-1}, more than 10^4 states per cm^{-1} are required. However, an estimate of the vibrational densities of states in a 10-atom molecule, characterized by equal vibrational frequencies of 1000 cm^{-1}, yields 4×10^5 states per cm^{-1}. Robinson[5] estimated 3×10^5 vibrational states per cm^{-1} for an energy gap of 8570 cm^{-1} between the $^1B_{2u}$ and $^3B_{1u}$ states of benzene. The density of the vibrational states of ground naphthalene state with an energy gap of 21,000 cm^{-1} (i.e., below the first triplet state) is expected to be much larger than this value.

$$\psi(\vec{x}, Q) = \Theta(\vec{x})\,\phi(Q) \tag{34}$$

where $\vec{x}, Q$ are electronic and vibrational coordinates respectively. β_n is related therefore to the electronic matrix element $\beta_e = \langle \Theta_n'' | H' | \Theta_0' \rangle$ through vibrational overlap integrals

$$\beta_n = \beta_e \langle \phi_n'' | \phi_0' \rangle \tag{35}$$

Eq. (33) is thus reduced to

$$k = \frac{2}{\hbar\alpha}\,\beta_e^2 \sum_n{}' \left| \langle \phi_n'' | \phi_0' \rangle \right|^2 \equiv \frac{2}{\hbar\alpha}\,\beta_e^2 \cdot F \tag{36}$$

The environment has no effect on β_e and has an effect on β_n only through the presence of lattice contributions to the Franck-Condon factor F. The dependence of the transition rate k on α is not as apparent as Eq. (36) indicates, because as α increases in magnitude, more states are brought into play in the Franck-Condon factor.

We assume that the initial state is in the zeroth vibrational level. The final vibrational level ϕ_n'' consists, in general, of a superposition of many quanta of a large number of vibrational modes, the vibrational overlap integral thus being a product

$$\langle \phi_n'' | \phi_0' \rangle = \prod_r \langle \phi_{v_r}(Q_r'') | \phi_0(Q_r') \rangle \tag{37}$$

providing the oscillations are harmonic and the appropriate linear combinations are used for ϕ_{v_r} when the vibrations are degenerate. In Eq. (37), v_r is the quantum number for the rth normal mode and Q_r is the rth normal coordinate. The product is over all molecular and lattice normal modes which contribute to the final level ϕ_n''.

For tractable quantitative calculations, the assumptions concerning the Born-Oppenheimer approximation in Eq. (34) and harmonic oscillations in Eq. (37) are desirable. The validity of the harmonic oscillator approximation is fairly good in large polyatomic molecules, where many atoms are involved in the normal vibrations. Anharmonicities cannot be neglected for large quantum numbers v_r, for example, $v_r \geq 10$ in benzene.[1] Fortunately, since there are so many vibrational normal modes in large molecules, one is seldom forced to use quantum numbers greater than ten for a single normal mode to fill the electronic energy difference. In addition, the most important contribution to the Franck-Condon factor F is derived from vibrations of quantum numbers much smaller than ten.

The validity of Eq. (34) depends on the neglect[9] of terms in the total vibronic Hamiltonian which have to do with the dependence of the zero-order electronic eigenfunctions upon nuclear coordinates. Such terms can mix zero-order vibronic states. The vibronic coupling as well as spin-orbit coupling, H_{SO}, can be treated as a perturbation. We expand the Hamiltonian, $H_0 + H_{SO}$ in terms of Taylor's series of normal coordinates Q_i of a suitable electronic state to first-order in nuclear displacement. Therefore we obtain the perturbation Hamiltonian[11]

$$H' = H_{SO}^{o} + \sum_i \left(\frac{\partial H_0}{\partial Q_i}\right)_0 Q_i + \sum_i \left(\frac{\partial H_{SO}}{\partial Q_i}\right)_0 Q_i$$

$$= H_1 + H_2 + H_3 \qquad (38)$$

where the superscript zero in the leading term refers to the equilibrium nuclear position at which the partial derivatives are also evaluated. H_0 contains the kinetic and potential energy for the electrons. Both H_0 and H_{SO} contain nuclear coordinates as parameters.

In Eq. (38), H_1 is a magnetic perturbation which is required for multiplicity-forbidden transitions. The vibronic couplings H_2, when they arise from nontotally symmetric vibrations in a polyatomic molecule, will be responsible for multiplicity-allowed radiationless transitions between electronic states not having the same symmetry. The spin-vibronic couplings H_3 may modify multiplicity-forbidden transitions. The direct product of the irreducible representation of the two electronic states to be mixed by H_2 or H_3 must be identical with or include the irreducible representation of the perturbing vibration Q_i. This is because both H_2 and H_3 are energy expressions, invariant to symmetry operations, therefore $\left(\frac{\partial H_0}{\partial Q_i}\right)_0$ in H_2 and $\left(\frac{\partial H_{SO}}{\partial Q_i}\right)_0$ in H_3 should have the symmetry properties in electronic coordinates identical with that of Q_i in nuclear coordinates. An example will be given in the following section.

All of the above-mentioned perturbations are simply time-independent terms which are already present in free molecules. They play by far the greatest role in the radiationless transition processes. Time-dependent perturbations such as oscillatory electric fields caused by lattice vibrations or coupling between lattice vibrations and magnetic perturbations (spin-orbit coupling,

for example) must be small compared to the time-independent intramolecular perturbations.

The breakdown of the Born-Oppenheimer approximation may also be responsible for the introduction of correction terms to the vibrational overlap integrals since, in general, the vibronic zero-order states are mixed through vibronic coupling with other states. Such an effect may be important for the high vibrational quantum numbers necessary when ΔE is large. For low-lying electronic states, however, the density of electronic zero-order states is sufficiently small. Coupling of states which have quite different zero-order energies is expected to be small because, in the language of perturbation theory, the energy denominators are large. In addition, interactions, for which large differences exist in the initial and final vibrational quantum numbers, are expected to be weak because of the Franck-Condon effect. It is expected therefore that in the absence of electronic degeneracies, or near degeneracies, these effects will not greatly influence the calculation of vibrational factors for radiationless transitions.

B. Applications

a. Intrinsic Non-Radiative Relaxation of the Lowest Triplet State $^3B_{2u}$ of Naphthalene

Consider the radiationless transition $^3B_{2u} \rightsquigarrow {}^1A_{1g}$ of naphthalene as an example. The symmetry species of naphthalene belong to the irreducible representations of D_{2h}. The spin-orbit couplings and

the vibronic couplings for naphthalene derived from symmetry consideration are shown in tables I and II, respectively. For the radiationless transition $^3B_{2u} \rightsquigarrow {}^1A_{1g}$, there are three paths: first, the transition is induced by the spin-vibronic coupling through the normal coordinates Q_i (b_{2u}); second, the electronic state $^1A_{1g}$ can be mixed with the intermediate state $^3B_{1g}$ by the spin-orbit coupling σ_z, and $^3B_{1g}$ with $^3B_{2u}$ by the vibronic coupling through the normal coordinates Q_i of symmetry b_{3u}; third, the state $^3B_{2u}$ mixes with the intermediate state $^1B_{3u}$ by the spin-orbit coupling σ_z, and the state $^1B_{3u}$ with the state $^1A_{1g}$ by vibronic coupling through the normal coordinate Q_i (b_{3u}).

These processes can be depicted as follows:

i) spin vibronic coupling $^3B_{2u} \overset{b_{2u}}{\rightsquigarrow} {}^1A_{1g}$

ii) vibronic coupling in the triplet manifold with spin-orbit coupling $^3B_{2u} \overset{b_{3u}}{\rightsquigarrow} {}^3B_{1g} \overset{\sigma_z}{\rightsquigarrow} {}^1A_{1g}$

iii) spin-orbit coupling with vibronic coupling in the singlet manifold $^3B_{2u} \overset{\sigma_z}{\rightsquigarrow} {}^1B_{3u} \overset{b_{3u}}{\rightsquigarrow} {}^1A_{1g}$

The electronic matrix element β_e corresponding to the perturbations in Eq. (38) is

TABLE I. Spin-Orbit Coupling for Naphthalene (D_{2h})

	σ_x	σ_y	σ_z
$^3A_{1g}$	$^1B_{3g}$	$^1B_{2g}$	$^1B_{1g}$
$^3B_{1g}$	$^1B_{3g}$	$^1B_{3g}$	$^1A_{1g}$
$^3B_{2u}$	$^1B_{1u}$	$^1A_{1u}$	$^1B_{3u}$
$^3B_{3u}$	$^1A_{1u}$	$^1B_{1u}$	$^1B_{2u}$

TABLE II. Vibronic coupling for naphthalene (D_{2h})

	A_{1g}	B_{1g}	B_{2u}	B_{2u}
A_{1g}	a_{1g}	b_{1g}	b_{1u}	b_{3u}
B_{1g}	b_{1c}	a_{1g}	b_{3u}	b_2
B_{2u}	b_{2u}	b_{3u}	a_{1g}	b_{1g}
B_{3u}	b_{3u}	b_{2u}	b_{1g}	a_{1g}

$$\beta_e = \langle {}^3B_{2u} | H_3 (b_{2u}) | {}^1A_{1g} \rangle \qquad (39)$$

$$+ \frac{\langle {}^3B_{2u} | H_2 (b_{3u}) | {}^3B_{1g} \rangle \langle {}^3B_{1g} | H_1 (\sigma_z) | {}^1A_{1g} \rangle}{E({}^3B_{2u}) - E({}^3B_{1g})}$$

$$+ \frac{\langle {}^3B_{2u} | H_1 (\sigma_z) | {}^1B_{3u} \rangle \langle {}^1B_{3u} | H_2 (b_{3u}) | {}^1A_{1g} \rangle}{E({}^3B_{2u}) - E({}^1B_{3u})}$$

b. Deuterium Effect on Intrinsic Radiationless Transitions

The Franck-Condon factor F in Eq. (36) can lead to a large deuterium effect on the intramolecular non-radiative $T_1 \rightarrow S_0$ transition as follows:

For a sufficiently large electronic energy difference ΔE to be converted into vibrational energy, the dominant contribution to the Franck-Condon factor comes from high-frequency modes associated with normal coordinates and frequency differences in the initial and final electronic states. For the same energy gap, low-frequency vibrations correspond to high quantum numbers and thus yield small Franck-Condon factors. Therefore, unless the density of high-frequency modes is much smaller than that of low-frequency modes, the predominant path of electronic relaxation is via high-frequency modes. For instance, in benzene and naphthalene, the high-frequency C—H and C—D modes are more effective than the low-frequency C—C modes.

The Deuterium effect is a result of decreased radiationless transition probability in perdeuterated compounds as compared to

that in perprotonated species. This is due to the relatively smaller value of the vibrational overlap integral between the zero-point wavefunction of the triplet state and that of the isoenergetic C—D vibration modes of the ground state. More specifically, we consider the transition $^3B_{2u} \rightsquigarrow {}^1A_{1g}$ of naphthalene, which corresponds to an energy difference $\Delta E = 21,000\ cm^{-1}$. In regard to the most dominant vibrational mode, we need approximately seven quanta of the C—H stretching mode, while ten quanta of the C—D stretching mode are necessary to match the energy difference. The Franck-Condon factor in the former is larger than that in the latter. Therefore the intrinsic radiationless transition rate in naphthalene is larger in perprotonated species. This is evidenced by the shorter intrinsic lifetime of $C_{10}H_8$[12] compared with that of $C_{10}D_8$.[13]

c. Oxygen Quenching of Phosphorescence

The interaction of molecular oxygen with electronically excited molecules is important in both the physical quenching of emission and the photochemical or photosensitized oxidation. This is especially true for triplet states in liquid solutions, where even a trace of oxygen is sufficient to quench phosphorescence completely. This occurs because of the long lifetime of triplet states. In regard to this a number of mechanisms have been proposed to account for the ability of oxygen to quench excited triplet and singlet molecules:

i) Energy transfer:

This mechanism was first proposed by Kautsky[14] and can

be formulated as follows:

$$^3D + {}^3O_2\,(X^3\Sigma_g^-) \rightarrow {}^1D + {}^1O_2(b^1\Sigma_g^+ \text{ or } a^1\Delta_g) \qquad (40)$$

where $^{3,1}D$ represents an excited triplet or a ground singlet state of donor molecules. This process is quite similar to the transfer of triplet-state excitation between two organic molecules. Energy transfer to oxygen is unusual only in that oxygen starts out in a ground triplet state and is excited to a metastable singlet state. Recent observations have confirmed Kautsky's original proposal. For example, singlet-state molecular oxygen produced in the reaction of sodium hypochlorite and hydrogen peroxide,[15] or in rf discharge,[16] reacts with various unsaturated organic compounds to give products which are identical to those produced in photosensitized oxidation of these compounds.[17,18] Furthermore, the relative rates of photooxidation of various compounds are found to be independent of the nature of the sensitizer.[19] These findings confirm the suggestion[14,19] that a common excited-state intermediate may actually be involved in physical quenching of phosphorescence and sensitized photochemical reactions.

ii) Enhanced Intersystem Crossing:

Evans demonstrated that oxygen reversibly enhances singlet-triplet transitions in organic molecules.[20] A number of enhancement mechanisms[20-25] have been proposed. Evans[20] and others[21,22] suggested that the enhanced intersystem crossing was attributed to a spin-orbit perturbation of the triplet level of the

organic molecule by the inhomogeneous field of the paramagnetic oxygen molecule. This effectively introduces a slight degree of singlet character into the triplet level. Tsubomura and Mulliken have theoretically evaluated the magnitude of the inhomogeneous-magnetic-field effect and have shown it to be of negligible importance.[23] Furthermore, Porter and Wright in their studies of the quenching of triplet states by paramagnetic ions found no correlation between the quenching efficiency and the magnetic moment of the paramagnetic ions.[26] Hoijtink[25] suggested that direct mixing of the initial and final states of the colliding organic and oxygen molecules through intermolecular exchange interaction could lead to the enhancement. On the other hand, Tsubomura and Mullikan[23] and Murrell[24] discussed an indirect mixing which involves the charge-transfer states of the organic donor-O_2 complex as intermediates.

In fact, the two mechanisms--Energy Transfer and Enhanced Intersystem Crossing--have the following in common: both require intermolecular exchange interaction* of a triplet-state molecule with triplet-state oxygen, and neglect the spin-orbit coupling; both can undergo radiationless transitions directly or via charge transfer states to the appropriate final states. The triplet organic molecule returns to its ground state in both mechanisms. However, the oxygen either is excited electronically to the low-lying singlet states ($a\,^1\Delta_g$) or ($b\,^1\Sigma_g^+$) by means of energy transfer mechanism, or stays in the

*The exchange interaction of two triplets leads to the formation of singlet, triplet, or quintet.

ground state by means of enhanced intersystem crossing. This can be depicted as follows:

(i) Energy Transfer.

Direct: $^1\psi_1 (^3B_{2u}, X^3\Sigma_g^-) \rightsquigarrow {}^1\psi_2 (^1A_{1g}, b^1\Sigma_g^+)$

or $^1\psi_3^{\pm} (^1A_{1g}, a^1\Delta_g)$

Indirect: $^1\psi_1 (^3B_{2u}, X^3\Sigma_g^-) \rightsquigarrow {}^1\psi_{CT}^{\pm} \rightsquigarrow {}^1\psi_2 (^1A_{1g}, b^1\Sigma_g^+)$

or $^1\psi_3^{\pm} (^1A_{1g}, a^1\Delta_g)$

(ii) Enhanced Intersystem Crossing.

Direct: $^3\psi_1 (^3B_{2u}, X^3\Sigma_g^-) \rightsquigarrow {}^3\psi_4 (^1A_{1g}, X^3\Sigma_g^-)$

Indirect: $^3\psi_1 (^3B_{2u}, X^3\Sigma_g^-) \rightsquigarrow {}^3\psi_{CT}^{\pm} \rightsquigarrow {}^3\psi_4 (^1A_{1g}, X^3\Sigma_g^-)$

where $^i\psi_j (A, B)$ is the wavefunction of the system with the organic molecule (naphthalene) in state A and oxygen in state B; i is the multiplicity. $^{3,1}\psi_{CT}^{\pm}$ are wavefunctions of the charge transfer intermediate states.

The rate of oxygen quenching of triplet states by means of direct mixing of initial and final states or indirect mixing via charge transfer states can be calculated from Eq. (36) with the following electronic matrix elements:

$$\beta_e = \langle \Theta_n'' | H' | \Theta_0' \rangle \quad \text{for direct mixing} \tag{41a}$$

$$\beta_e = \frac{\langle \Theta_n'' | H' | \Theta_i \rangle \langle \Theta_i | H' | \Theta_0' \rangle}{E_0 - E_i} \quad \text{for indirect mixing} \tag{41b}$$

where Θ_n'', Θ_0', and Θ_i are electronic wavefunction of final, initial, and intermediate states respectively; E_0 and E_i are eigenvalues of Θ_0' and Θ_i. In Eq. (41) the perturbation Hamiltonian H′ is the intermolecular exchange interaction between O_2 and the triplet organic molecule.

Kawaoka, Khan, and Kearns[27] estimated that the electronic matrix elements β_e's for direct mixing of the initial and the final states in both energy transfer and enhanced intersystem crossing are approximately 2 cm^{-1}. They also found that indirect mixing via charge transfer intermediate states in both mechanisms yield nearly identical electronic matrix elements. The electronic matrix elements connecting the initial state with the charge transfer state, and the charge transfer states with the final states were found[27] to be 600 cm^{-1} and 200 cm^{-1}, respectively. We assume the charge transfer states of the naphthalene and O_2 complex lie slightly below the $^1B_{2u}$ state of naphthalene which could induce strong mixing of the charge transfer state and the final states, i.e., $E_0 - E_i \approx 10,000\,cm^{-1}$. According to Eq. (41b) the effective electronic matrix elements for indirect mixing are estimated to be 10 cm^{-1}. It is, therefore, concluded that charge transfer intermediate states appeared to be of essential importance in the quenching processes.

Using Siebrand's semi-empirical method,[28] the variation of the Franck-Condon factor F with the electronic energy difference ΔE in cm^{-1} can be expressed:

$$F = 0.15 \times 10^{-(\Delta E - 4000)/5000} \qquad (42)$$

For naphthalene of triplet energy $E_T \approx 21,000\ cm^{-1}$, Franck-Condon factors for enhanced intersystem crossing, energy transfer to $\left(a^1\Delta_g\right)$, and energy transfer to $\left(b^1\Sigma_g^+\right)$ are respectively 6×10^{-5}, 3×10^{-3}, and 2.5×10^{-2}. The Franck-Condon factors for quenching through energy transfer are always orders of magnitude larger than that through enhanced intersystem crossing. Because of the large difference of Franck-Condon factors and the similarity of the electronic matrix elements for different quenching mechanisms, it is concluded that O_2 quenching of triplet-state molecules by transfer of electronic energy to O_2 could be more importnat (by a factor of 100 ~ 1000) than quenching by enhanced intersystem crossing.

For a qualitative calculation, assuming $\beta_e \approx 5\ cm^{-1}$, $\alpha \approx 1\ cm^{-1}$,[1] one obtains, according to Eq. (36) the rate of oxygen quenching of triplet naphthalene due to energy transfer

$$k_Q \approx 10^{13} \cdot F \approx 3 \times 10^{10} \sim 10^{12}\ sec^{-1}$$

while that due to enhanced intersystem crossing is only $10^9\ sec^{-1}$. Taking into account the fact that O_2 quenches the triplet state in a diffusion controlled process, the quenching rate must be rapid

compared to 10^{10} sec^{-1} (the reciprocal of the lifetime of a collision complex in solutions). It is therefore concluded that quenching by energy transfer mechanism satisfactorily accounts for the O_2 quenching of triplet states, whereas the enhanced intersystem crossing mechanism is insufficient. Although the absolute transition rates might not be very reliable, it is fairly certain that quenching by energy transfer is more important than quenching by enhanced intersystem crossing.

5. FINAL REMARKS

The experimental results of this work are important in the theory of radiationless transitions. According to the ideas presented by Robinson and Frosch,[1] there would be no mechanism by which the non-radiative lifetime of an electronic state could be changed by environmental perturbations of magnitude $kT \ll \Delta E$, where ΔE is the quantum of electronic energy to be given up to the environment. Environmental perturbation affecting the non-radiative loss of electronic energy in a molecule can take place: (i) for temperatures where $kT \sim \Delta E$; (ii) for very high pressure[29] (> 7 Kbar), where a change in the relative position of the potential surfaces of the initial and final states can lead to an increase of the vibrational overlap integrals;[30] (iii) when the solvent furnishes a specific perturbation greater than that mixing states in the free molecule (e.g., external heavy atom effect); or (iv) when there are solvent-solute interactions strong enough to change the essential character

of the molecule in solution (e.g., hydrogen bonding). For the solvent-solute systems used here, none of these special situations are expected to exist, so no environmental effect on the radiationless transition would be anticipated. It is gratifying that there is now experimental evidence to support this view.

REFERENCES

1. G. W. Robinson, P. R. Frosch, J. Chem. Phys. 37, 1962 (1962); J. Chem. Phys. 38, 1187 (1963).
2. M. Gouterman, J. Chem. Phys. 36, 2846 (1962).
3. S. H. Lin, J. Chem. Phys. 44, 3759 (1966).
4. M. Bixon and J. Jortner, J. Chem. Phys. 48, 715 (1968).
5. G. W. Robinson, J. Chem. Phys. 47, 1967 (1967).
6. C. A. Coulson, Proc. Roy. Soc. (London) A169, 413 (1939).
7. U. Fano, Phys. Rev. 124, 1866 (1961).
8. P. A. M. Dirac, Z. Physik. 44, 585 (1927).
9. M. Born and J. R. Oppenheimer, Ann. Physik. 84, 457 (1927); D. R. Bates, A. Fundaminsky and H. S. W. Massey, Phil. Trans. Roy. Soc. (London) A243, 93 (1950).
10. W. Heitler, The Quantum Theory of Radiation (Clarendon Press, Oxford, 1954), Third Edition, p. 140.
11. A.C. Albrecht, J. Chem. Phys. 38, 354 (1963).
12. D. S. McClure, J. Chem. Phys. 17, 905 (1949).
13. R. E. Kellogg and R. P. Schwenker, J. Chem. Phys. 41, 2860 (1964).
14. H. Kautsky, Trans. Faraday Soc. 35, 216 (1939).
15. A. U. Khan and M. Kasha, J. Chem. Phys. 39, 2105 (1963).
16. S. J. Arnold, E. A. Ogryzlo and H. Witzke, J. Chem. Phys. 40, 1769 (1964).
17. C. S. Foote and S. Wexler, J. Am. Chem. Soc. 86, 3879 (1964).

18. E. J. Corey and W. C. Taylor, J. Am. Chem. Soc. 86, 3881 (1964).

19. T. Wilson, J. Am. Chem. Soc. 88, 2898 (1966).

20. D. F. Evans, J. Chem. Soc. 1957, 1351 (1957)

21. D. S. McClure, J. Chem. Phys. 17, 905 (1949).

22. P. Yuster and S. I. Weissman, J. Chem. Phys. 17, 1182 (1949).

23. H. Tsubomura and R. S. Mulliken, J. Am. Chem. Soc. 82, 5966 (1960).

24. J. N. Murrell, Mol. Phys. 3, 319 (1960).

25. G. J. Hoijtink, Mol. Phys. 3, 67 (1960).

26. G. Porter and M. R. Wright, J. Chem. Phys. 55, 705 (1958).

27. K. Kawaoka, A. U. Khan and D. R. Kearns, J. Chem. Phys. 46, 1842 (1967).

28. W. Siebrand, J. Chem. Phys. 44, 4055 (1966).

29. B. A. Baldwin and H. W. Offen, J. Chem. Phys. 48, 5358 (1968).

30. M. A. El-Sayed, J. Chem. Phys. 37, 1568 (1962).

II. WHY IS CONDENSED OXYGEN BLUE?

1. INTRODUCTION

Solid, liquid and compressed gaseous oxygen is blue. The color is mostly derived from double transitions,

$$(a\ ^1\Delta_g)(a\ ^1\Delta_g) \leftarrow (X\ ^3\Sigma_g^-)(X\ ^3\Sigma_g^-) \qquad \lambda(0,0) = 6299\ \text{Å}$$

$$(a\ ^1\Delta_g)(b\ ^1\Sigma_g^+) \leftarrow (X\ ^3\Sigma_g^-)(X\ ^3\Sigma_g^-) \qquad \lambda(0,0) = 4770\ \text{Å}$$

$$(b\ ^1\Sigma_g^+)(b\ ^1\Sigma_g^+) \leftarrow (X\ ^3\Sigma_g^-)(X\ ^3\Sigma_g^-) \qquad \lambda(0,0) = 3803\ \text{Å}$$

and their vibrational additions. Salow and Steiner,[1] and V. I. Dianov-Klokov[2] have investigated the pressure dependence of these bands. They found that the position of the absorption and the band shape do not change appreciably with the pressure or the physical state of the oxygen; but the logarithm of the peak intensity is proportional to the square of the oxygen pressure and is independent of the pressure of foreign gas. Other support for the double transition idea was obtained by Bader and Ogryzlo[3] who studied electrically discharged oxygen at room temperature. They showed that the intensity of the 6299 Å emission transition is proportional to the square of the $O_2(a\ ^1\Delta_g)$ concentration.

To determine whether the O_2-O_2 pair is simply a colliding pair or a more strongly bound complex, Arnold, Browne and Ogryzlo[4] measured the temperature dependence of the absolute intensity of the emission from -50 °C to 200 °C. Their results show that the

emitting complex has a negative bond dissociation energy, indicating that it is not bound.

In the colliding pair, it is assumed that through the intermolecular force the states $(a\ ^1\Delta_g)(a\ ^1\Delta_g)$, $(a\ ^1\Delta_g)(b\ ^1\Sigma_g^+)$, and $(b\ ^1\Sigma_g^+)(b\ ^1\Sigma_g^+)$ are mixed with the state $(B\ ^3\Sigma_u^-)(X\ ^3\Sigma_g^-)$. Also the states $(a\ ^1\Delta_g)(\ ^1\Delta_u)$, $(b\ ^1\Sigma_g^+)(\ ^1\Delta_u)$, $(a\ ^1\Delta_g)(\ ^1\Sigma_u^+)$, and $(b\ ^1\Sigma_g^+)(\ ^1\Sigma_u^+)$ are mixed with the state $(X\ ^3\Sigma_g^-)(X\ ^3\Sigma_g^-)$. In the first instance, the intensity of the double transition is borrowed from the dipole-allowed transition (Schumann-Runge transition) $\underline{B}\ ^3\Sigma_u^- \leftarrow \underline{X}\ ^3\Sigma_g^-$, whose center of gravity lies at 68,000 cm^{-1} and whose oscillator strength f = 0.2. In the other cases, the allowed transitions $^1\Delta_u \leftarrow a\ ^1\Delta_g$, $^1\Sigma_u^+ \leftarrow b\ ^1\Sigma_g^+$ are responsible. These last transitions have not been observed, but theoretically they should have intensities of the same order of magnitude as that of the Schumann-Runge transition. The "single-molecule" transitions

$$(a\ ^1\Delta_g)(X\ ^3\Sigma_g^-) \leftarrow (X\ ^3\Sigma_g^-)(X\ ^3\Sigma_g^-)$$
$$(b\ ^1\Sigma_g^+)(X\ ^3\Sigma_g^-) \leftarrow (X\ ^3\Sigma_g^-)(X\ ^3\Sigma_g^-)$$

are assumed to be enhanced by a similar mechanism.[5]

2. THEORY

A general theory of perturbed transitions has been previously published.[5] In this paper we present a theoretical calculation of the intensity of the particular double transition $(a\,^1\Delta_g)(a\,^1\Delta_g) \leftarrow (X\,^3\Sigma_g^-)(X\,^3\Sigma_g^-)$ based on a pair of oxygen molecules at a separation of 3.81 Å (see Sec. 4 and Ref. 6). One molecule designated as molecule 1 is assumed fixed in space with internuclear axis along the $z_1 = Z$ direction. The other called molecule 2 is oriented in some arbitrary manner as shown in Fig. 1. The angles θ and φ are just the conventional polar coordinates of the internuclear z_2-axis of molecule 2 with respect to the coordinate system (x_2', y_2', z_2'). The latter coordinate system is one that has been displaced along the X-axis by the intermolecular distance R_{12} and whose origin coincides with the center of molecule 2. The molecule-fixed coordinate system (x_2, y_2, z_2) is chosen in such a way that the following relation holds:

$$\begin{bmatrix} x_2 \\ y_2 \\ z_2 \end{bmatrix} = \begin{bmatrix} \cos\theta\cos\varphi & \cos\theta\sin\varphi & -\sin\theta \\ -\sin\varphi & \cos\varphi & 0 \\ \sin\theta\cos\varphi & \sin\theta\sin\varphi & \cos\theta \end{bmatrix} \begin{bmatrix} x_2' \\ y_2' \\ z_2' \end{bmatrix} \qquad (1)$$

The intermolecular force depends sensitively on the intermolecular separation, which is fixed at 3.81 Å, and the relative orientation of the two molecules. In addition, it is different depending upon whether the perturbing state is localized in molecule 1 or molecule 2. These two cases are respectively designated as case 1 and case 2. The calculations are carried out for both cases. To obtain the angular dependence of the interactions, three non-trivial[7]

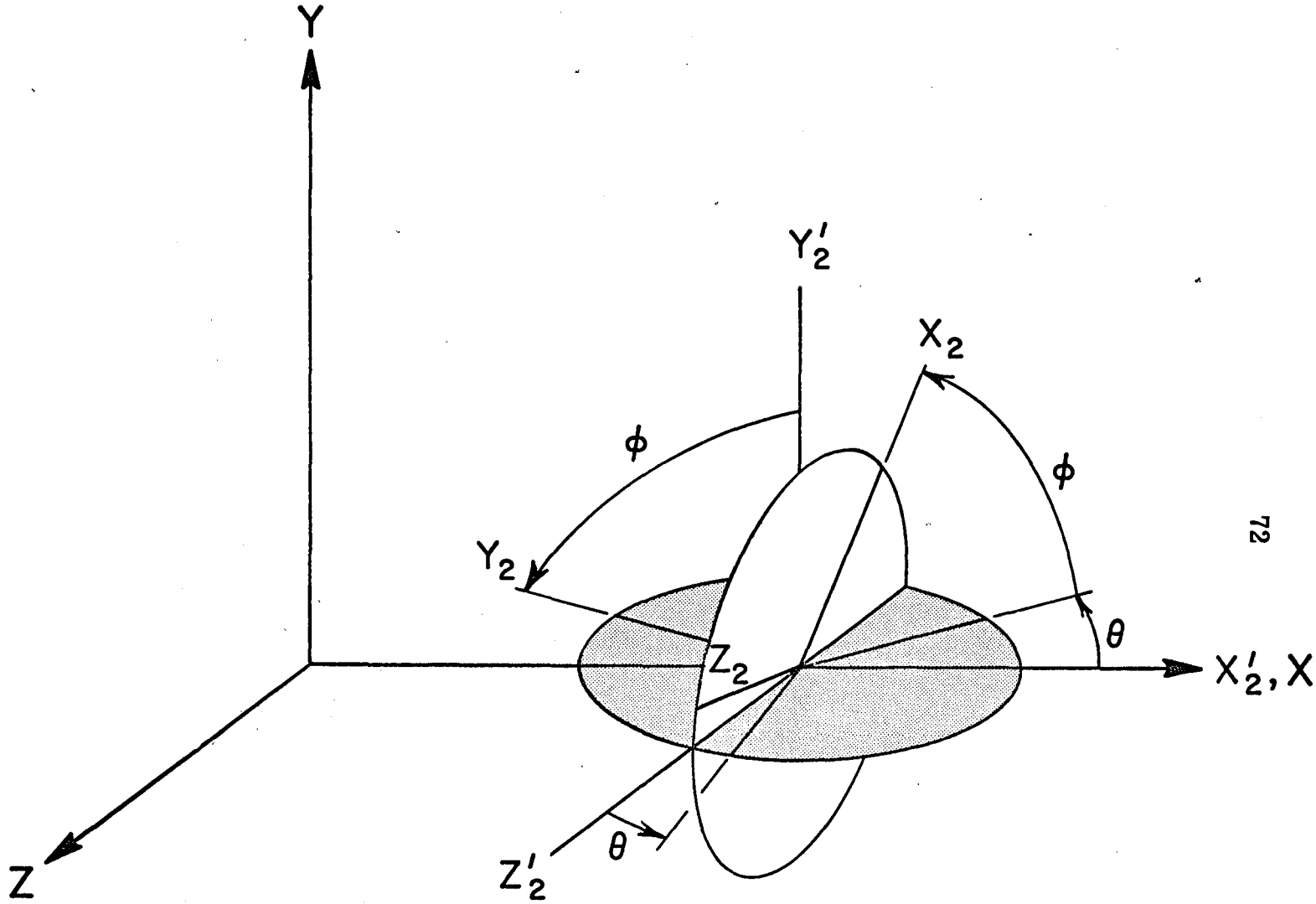

Fig. 1 (θ, ϕ)

orientations are chosen. The orientation-dependent interaction is then derived by fitting the results to an analytical expression in the variables θ and φ.

Now briefly reviewing the theory[5] of double transitions as it pertains to oxygen, we consider a pair of interacting O_2 molecules. The total Hamiltonian is given by,

$$\mathcal{H} = H_1 + H_2 + H', \tag{2}$$

where H_1 and H_2 are the full Hamiltonians for the isolated molecules 1 and 2. Since, within the framework of our theoretical treatment, only two electron terms can contribute to the mixing of doubly-excited and singly-excited states of the pair system, we neglect intermolecular electron-nucleus and nucleus-nucleus interactions. H′ then consists only of the intermolecular electronic repulsion terms.

Within the framework of the Born-Oppenheimer approximation, the vibronic wavefunctions can be expressed as a product of purely electronic and purely vibrational parts. Using first-order perturbation theory, the distorted molecular wavefunction $\Psi_{k\ell}^{m\mu}$ is expanded in terms of product wavefunctions $\Phi^{p\nu}\chi_{st}^{p\nu} \equiv \phi_1^p \phi_2^\nu \eta_1^{ps} \eta_2^{\nu t}$ of the free molecules 1 and 2. Here ϕ_1^p represents the $p^{\underline{th}}$ electronic state of molecule 1, ϕ_2^ν is the $\nu^{\underline{th}}$ electronic state of molecule 2, and the η's represent the $s^{\underline{th}}$ and $t^{\underline{th}}$ vibrational states, respectively, that correspond to these electronic states. We thus write for the corrected pair vibronic eigenfunctions,

$$\Psi_{k\ell}^{m\mu} = \Phi^{m\mu}\chi_{k\ell}^{m\mu} - \sum_{p\nu st} \frac{C^{p\nu;m\mu}\langle \chi_{st}^{p\nu} | \chi_{k\ell}^{m\mu}\rangle}{E_{st}^{p\nu} - E_{k\ell}^{m\mu}} \Phi^{p\nu}\chi_{st}^{p\nu} \ . \tag{3}$$

In Eq. (3) $C^{p\nu;m\mu} \equiv \langle \Phi^{p\nu} | H' | \Phi^{m\mu} \rangle$. $E_{k\ell}^{m\mu}$, for example, is the eigenvalue of $\Phi^{m\mu} \chi_{k\ell}^{m\mu}$ in zeroth order.

The electric dipole length for the pair system is given by

$$\underset{\sim}{R} = \underset{\sim}{R}_1 + \underset{\sim}{R}_2 = \sum_{i=1}^{N_1} \underset{\sim}{r}_{i_1} + \sum_{j=N_1+1}^{N_1+N_2} \underset{\sim}{r}_{j_2} , \tag{4}$$

where $\underset{\sim}{r}_{i_1}$ and $\underset{\sim}{r}_{j_2}$ are molecule-fixed coordinates of electron i and j in molecule 1 and 2, respectively; and N_1 and N_2 represent the number of electrons in molecules 1 and 2. Consider now the double transition $\underline{aa} \leftarrow \underline{XX}$, where we are interested explicitly in the $(a\ ^1\Delta_g)(a\ ^1\Delta_g)$ excited state, represented by the notation $\underline{aa}$, with wavefunction $\Psi_{k\ell}^{aa}$; and the ground vibronic state $(X\ ^3\Sigma_g^-)(X\ ^3\Sigma_g^-)$, represented by $\underline{XX}$, with wavefunction $\Psi_{00}^{XX} \equiv \Psi^{XX}$. Since the zero-order transition is highly forbidden, we proceed to the first-order approximation. The dipole transition moment, which is a product of the electronic dipole moment and the vibrational overlap integrals of the free molecule, is simply given by the expression,

$$\langle \Psi_{k\ell}^{aa} | \underset{\sim}{R} | \Psi^{XX} \rangle = \underset{\sim}{R}_{aa;XX} \langle \eta_k^a | \eta_0^X \rangle \langle \eta_\ell^a | \eta_0^X \rangle ,$$

where, following Eqs. (3) and (4),

$$\underset{\sim}{R}_{aa;XX} = -\left(\sum_{p\nu}{}' \frac{C^{p\nu;aa}}{\overline{E}_{p\nu} - \overline{E}_{aa}} \underset{\sim}{R}_{p\nu;XX} + \sum_{q\beta}{}' \frac{C^{q\beta;XX}}{\overline{E}_{q\beta} - \overline{E}_{XX}} \underset{\sim}{R}_{aa;q\beta} \right). \tag{5}$$

$\underset{\sim}{R}_{p\nu;XX}$ has been summed over all vibronic bands, and $\overline{E}_{p\nu}$ refers to the approximate center of gravity of this vibrational structure.

The two types of terms occurring in Eq. (5) can be depicted by the diagrams, [5]

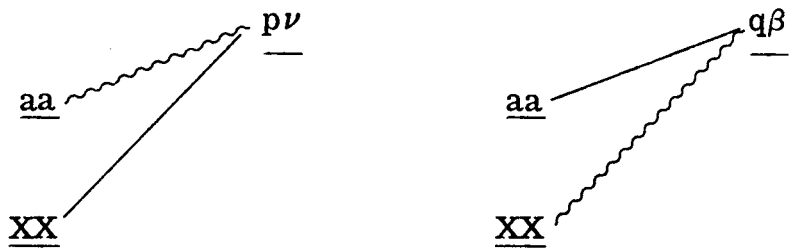

where the solid line represents a transition and the wiggly line an interaction.

The assumption that the intensity enhancement is derived from the mixing $(a\ ^1\Delta_g)(a\ ^1\Delta_g) \sim\sim (B\ ^3\Sigma_u^-)(X\ ^3\Sigma_g^-)$ and $(a\ ^1\Delta_g)(^1\Delta_u) \sim\sim (X\ ^3\Sigma_g^-)(X\ ^3\Sigma_g^-)$ ignores all diagrams of type A except the one for which $p\nu = (B\ ^3\Sigma_u^-)(X\ ^3\Sigma_g^-)$ and all those of type B except the one for which $q\beta = (a\ ^1\Delta_g)(^1\Delta_u)$. This clearly seems a rather gross approximation, since the excited configuration of $O_2(KK\sigma_g^2\sigma_u^2\sigma_g^2\pi_u^4\pi_g^1\sigma_u^1)$ leads to a $^3\Pi_u$ state that can undergo an allowed dipole transition with the ground state, and a $^1\Pi_u$ state that can similarly combine with the $\underline{a}\ ^1\Delta_g$ state. However, these two excited states lie fairly high. For example, the transition $^3\Pi_u^- \leftarrow \underline{X}\ ^3\Sigma_g^-$ is near 1290 Å. See Fig. 2. [8] In addition, as can also be seen in the figure, the integrated absorption coefficient of this transition is much smaller than that of the Schumann-Runge continuum. Because of its low intensity and its high energy the $^3\Pi_u^- \leftarrow \underline{X}\ ^3\Sigma_g^-$ transition is therefore neglected in the consideration of intensity enhancement. For similar reasons the $^1\Pi_u$ state is ignored. It is also assumed that Rydberg states and the ionization continuum

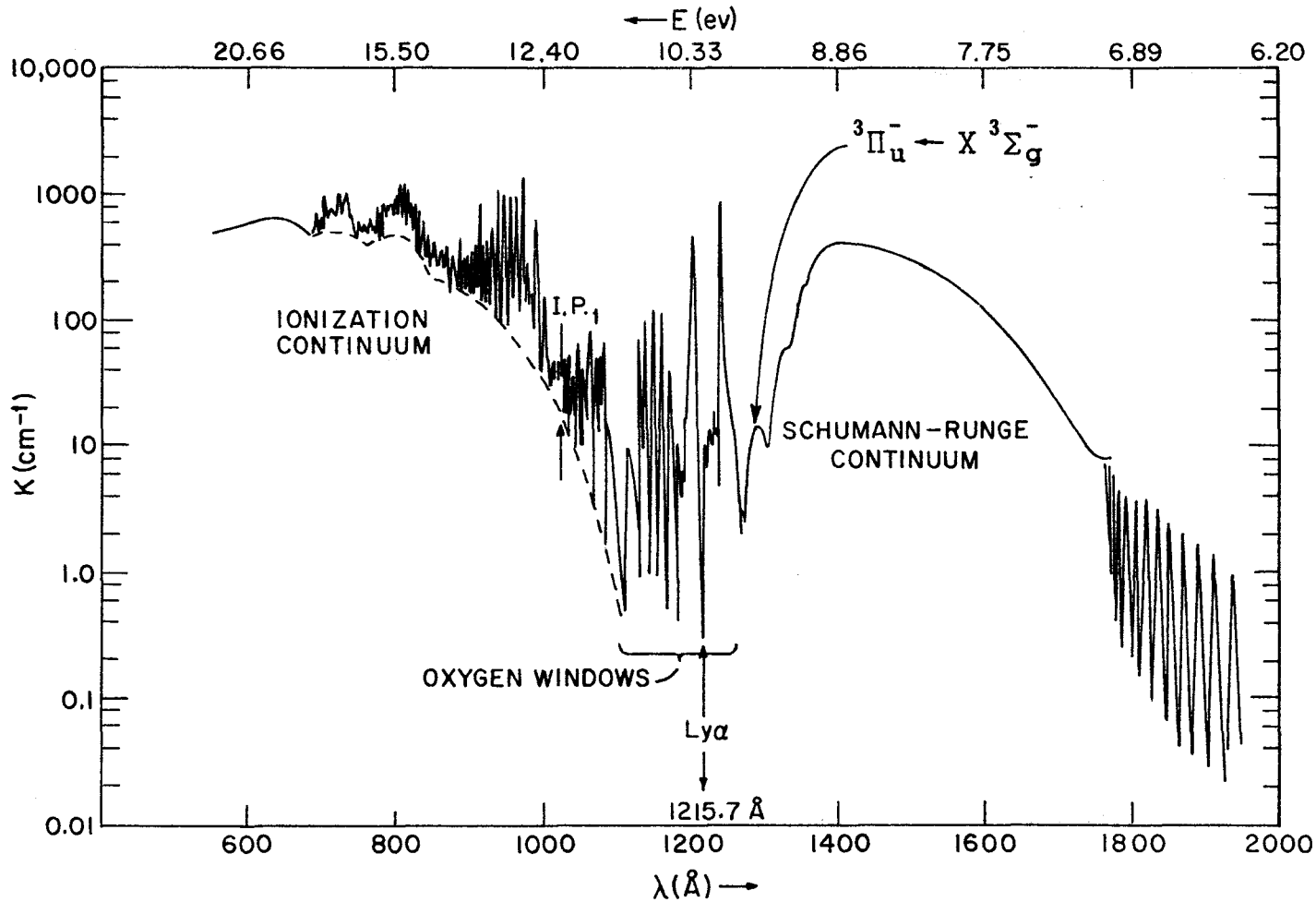
←E (ev)
20.66
15.50
12.40
10.33
8.86
7.75
6.89
6.20
10,000
1000
100
10
1.0
0.1
0.01
K (cm⁻¹)
$^3\Pi_u^- \leftarrow X\ ^3\Sigma_g^-$
IONIZATION CONTINUUM
I.P.1
SCHUMANN-RUNGE CONTINUUM
OXYGEN WINDOWS
Lyα
1215.7 Å
600
800
1000
1200
1400
1600
1800
2000
λ(Å) →

Fig. 2

can be left out of our calculation not only because of their high energy but also because of probable lack of much spatial overlap of their eigenfunctions with those of the lower states. We believe that these simplifying assumptions cannot introduce an error in the final calculated intensity of the double transition of more than a factor of two, but one would have to do some trial calculations to make certain of this point.

Neglecting therefore all but the two contributions to the perturbed intensity, the transition moment for the double transition $\underline{aa} \leftarrow \underline{XX}$ is,

$$\underset{\sim}{R}_{aa;XX} = -\left(\frac{C^{BX;aa}}{\overline{E}_{BX} - \overline{E}_{aa}} \underset{\sim}{R}_{BX} + \frac{C^{au;XX}}{\overline{E}_{au} - \overline{E}_{XX}} \underset{\sim}{R}_{au} \right) \quad . \qquad (6)$$

where $C^{BX;aa}$ and $C^{au;XX}$ include matrix elements for both case 1 and case 2.

The transition $^1\Delta_u \leftarrow \underline{a}\ ^1\Delta_g$ has not been observed experimentally. Since the $^1\Delta_u$ state arises from the configuration $(KK\sigma_g^2\sigma_u^2\sigma_g^2\pi_u^3\pi_g^3\sigma_u^0)$, the "orbital jump" $\pi_g \leftarrow \pi_u$ is the same as that for the Schumann-Runge transition. We therefore assume the transition moment for the $^1\Delta_u \leftarrow \underline{a}\ ^1\Delta_g$ transition to be the same as that for the $\underline{B}\ ^3\Sigma_u^- \leftarrow \underline{X}\ ^3\Sigma_g^-$ transition. Energy denominators associated with the $^1\Delta_u$ state can be estimated from the theoretical value[9] of the $^1\Delta_u$ energy ($87,000\ cm^{-1}$). Substituting the state wavefunctions as shown in the next section into the matrix elements, it is found that $C^{au;XX} = (\sqrt{2}/3)C^{BX;aa}$. Therefore Eq. (6) can be expressed as follows:

$$\underset{\sim}{R}_{aa;XX} = -\left[\frac{1}{\overline{E}_{BX} - \overline{E}_{aa}} + \frac{\sqrt{2}}{3(\overline{E}_{au} - \overline{E}_{XX})}\right] \underset{\sim}{R}_{BX} \cdot C^{BX;aa}, \qquad (7)$$

where $C^{BX;aa}$ is measured in cm^{-1}, $\overline{E}_{aa}$ is taken to be 16, 800 cm^{-1} for the center of gravity of the vibronic structure of the double transition $\underline{aa} \leftarrow \underline{XX}$.

3. CALCULATION

A. Electronic Matrix Elements

For simplicity, we use a four-electron π-orbital approximation for the pair system.

It is assumed that the state wavefunctions of the pair system can be represented as antisymmetrized products of one-electron molecular orbitals (MO). The orthonormal MO's of one molecule are not necessarily orthogonal to those of the other molecule. In order to simplify the calculation, we orthonormalize the MO's of molecule 2 with respect to those of molecule 1 by a procedure which will be described shortly. Two different sets of orthonormalized MO's were used in the two different cases:

Case 1, when the perturbing state is localized in molecule 1,

$$\nu_1 = \pi^-_{g_1}$$

$$\omega_1 = \pi^-_{u_1} \qquad (8a)$$

$$\mu_2 = \frac{1}{\sqrt{N}} \left[\pi^-_{g_2} - \pi^-_{g_1}(\pi^-_{g_1}|\pi^-_{g_2}) - \pi^+_{g_1}(\pi^+_{g_1}|\pi^-_{g_2}) - \pi^-_{u_1}(\pi^-_{u_1}|\pi^-_{g_2}) - \pi^+_{u_1}(\pi^+_{u_1}|\pi^-_{g_2})\right] \cdot$$

Case 2, when the perturbing state is localized in molecule 2,

$$\nu_1 = \pi^-_{g_1}$$

$$\nu_2 = \frac{1}{\sqrt{N}}\left[\pi^-_{g_2} - \pi^+_{g_1}(\pi^+_{g_1}|\pi^-_{g_2}) - \pi^-_{g_1}(\pi^-_{g_1}|\pi^-_{g_2})\right] \tag{8b}$$

$$\omega_2 = \frac{1}{\sqrt{N}}\left[\pi^-_{u_2} - \pi^-_{g_1}(\pi^-_{g_1}|\pi^-_{u_2}) - \pi^+_{g_1}(\pi^+_{g_1}|\pi^-_{u_2})\right] .$$

The subscripts 1 and 2 signify the MO's in the molecule-fixed coordinate system of molecules 1 and 2, respectively. N is a normalization factor that is approximately equal to 1. By this procedure, the MO's of molecule 2 are orthogonal to those of molecule 1 to within the square of an intermolecular overlap integral. For practical purposes, they may be considered to be rigorously orthogonal.

Because H′ does not contain an appreciable spin-orbit term, the multiplicity is invariant in this case. Therefore, we shall only need to consider the singlet components of $(B\ ^3\Sigma^-_u)(X\ ^3\Sigma^-_g)$ and $(X\ ^3\Sigma^-_g)(X\ ^3\Sigma^-_g)$, which arise through intermolecular electron exchange. The spin functions[10] of the singlet component of triplet+triplet and singlet+singlet are, respectively,

$$\frac{1}{\sqrt{12}}\{2(\alpha\alpha\beta\beta + \beta\beta\alpha\alpha) - (\alpha\beta\alpha\beta + \alpha\beta\beta\alpha + \beta\alpha\beta\alpha + \beta\alpha\alpha\beta)\}$$

$$\frac{1}{2}(\alpha\beta\alpha\beta - \beta\alpha\alpha\beta - \alpha\beta\beta\alpha + \beta\alpha\beta\alpha).$$

For case 2, the zero-order antisymmetrized orthonormal eigenfunctions of states $(X\ ^3\Sigma^-_g)_1(B\ ^3\Sigma^-_u)_2$, $(X\ ^3\Sigma^-_g)(X\ ^3\Sigma^-_g)$, $(a\ ^1\Delta^+_g)(a\ ^1\Delta^+_g)$, $(a\ ^1\Delta^-_g)(a\ ^1\Delta^-_g)$, $(a\ ^1\Delta^+_g)_1(^1\Delta^+_u)_2$, and $(a\ ^1\Delta^-_g)_1(^1\Delta^-_u)_2$ are, respectively,[11]

$$\Phi^{XB} = \frac{1}{\sqrt{24}} \{2 \left| \nu_1^*(1)\nu_1(2)\bar{\omega}_2^*(3)\bar{\nu}_2(4) \right| -2 \left| \nu_1^*(1)\nu_1(2)\bar{\omega}_2(3)\bar{\nu}_2^*(4) \right|$$

$$+2 \left| \bar{\nu}_1^*(1)\bar{\nu}_1(2)\omega_2^*(3)\nu_2(4) \right| -2 \left| \bar{\nu}_1^*(1)\bar{\nu}_1(2)\omega_2(3)\nu_2^*(4) \right|$$

$$- \left| \nu_1^*(1)\bar{\nu}_1(2)\omega_2^*(3)\bar{\nu}_2(4) \right| + \left| \nu_1^*(1)\bar{\nu}_1(2)\omega_2(3)\bar{\nu}_2^*(4) \right|$$

$$- \left| \nu_1^*(1)\bar{\nu}_1(2)\bar{\omega}_2^*(3)\nu_2(4) \right| + \left| \nu_1^*(1)\bar{\nu}_1(2)\bar{\omega}_2(3)\nu_2^*(4) \right|$$

$$- \left| \bar{\nu}_1^*(1)\nu_1(2)\bar{\omega}_2^*(3)\nu_2(4) \right| + \left| \bar{\nu}_1^*(1)\nu_1(2)\bar{\omega}_2(3)\nu_2^*(4) \right|$$

$$- \left| \bar{\nu}_1^*(1)\nu_1(2)\omega_2^*(3)\nu_2(4) \right| + \left| \bar{\nu}_1^*(1)\nu_1(2)\omega_2(3)\bar{\nu}_2^*(4) \right| \}$$

$$\Phi^{XX} = \frac{1}{\sqrt{12}} \{2 \left| \nu_1^*(1)\nu_1(2)\bar{\nu}_2^*(3)\bar{\nu}_2(4) \right| +2 \left| \bar{\nu}_1^*(1)\bar{\nu}(2)\nu_2^*(3)\nu_2(4) \right|$$

$$- \left| \nu_1^*(1)\bar{\nu}_1(2)\nu_2^*(3)\bar{\nu}_2(4) \right| - \left| \nu_1^*(1)\bar{\nu}_1(2)\bar{\nu}_2^*(3)\nu_2(4) \right| \qquad (9)$$

$$- \left| \bar{\nu}_1^*(1)\nu_1(2)\bar{\nu}_2^*(3)\nu_2(4) \right| - \left| \bar{\nu}_1^*(1)\nu_1(2)\nu_2^*(3)\bar{\nu}_2(4) \right| \}$$

$$\Phi^{aa}_{\pm\pm} = \frac{1}{4} \{ \left| \nu_1^*(1)\bar{\nu}_1^*(2)\nu_2^*(3)\bar{\nu}_2^*(4) \right| \pm \left| \nu_1^*(1)\bar{\nu}_1^*(2)\nu_2(3)\bar{\nu}_2(4) \right|$$

$$\pm \left| \nu_1(1)\bar{\nu}_1(2)\nu_2^*(3)\bar{\nu}_2^*(4) \right| + \left| \nu_1(1)\bar{\nu}_1(2)\nu_2(3)\bar{\nu}_2(4) \right|$$

$$- \left| \bar{\nu}_1^*(1)\nu_1^*(2)\nu_2^*(3)\bar{\nu}_2^*(4) \right| \mp \left| \bar{\nu}_1^*(1)\nu_1^*(2)\nu_1(3)\bar{\nu}_2(4) \right|$$

$$\mp \left| \bar{\nu}_1(1)\nu_1(2)\nu_2^*(3)\bar{\nu}_2^*(4) \right| - \left| \bar{\nu}_1(1)\nu_1(2)\nu_2(3)\bar{\nu}_2(4) \right|$$

$$- \left| \nu_1^*(1)\bar{\nu}_1^*(2)\bar{\nu}_2^*(3)\nu_2^*(4) \right| \mp \left| \nu_1^*(1)\bar{\nu}_1^*(2)\bar{\nu}_2(3)\nu_2(4) \right|$$

$$\mp \left| \nu_1(1)\bar{\nu}_1(2)\bar{\nu}_2^*(3)\nu_2^*(4) \right| - \left| \nu_1(1)\bar{\nu}_1(2)\bar{\nu}_2(3)\nu_2(4) \right|$$

$$+ \left| \bar{\nu}_1^*(1)\nu_1^*(2)\bar{\nu}_2^*(3)\nu_2^*(4) \right| \pm \left| \bar{\nu}_1^*(1)\nu_1^*(2)\bar{\nu}_2(3)\nu_2(4) \right|$$

$$\pm \left| \bar{\nu}_1(1)\nu_1(2)\bar{\nu}_2^*(3)\nu_2^*(4) \right| + \left| \bar{\nu}_1(1)\nu_1(2)\bar{\nu}_2(3)\nu_2(4) \right| \}$$

$$\Phi^{au}_{\pm\pm} = \frac{1}{4}\{ |\nu_1^*(1)\bar{\nu}_1^*(2)\nu_2^*(3)\bar{\omega}_2^*(4)| \pm |\nu_1^*(1)\bar{\nu}_1^*(2)\nu_2(3)\bar{\omega}_2(4)|$$

$$\pm |\nu_1(1)\bar{\nu}_1(2)\nu_2^*(3)\bar{\omega}_2^*(4)| + |\nu_1(1)\bar{\nu}_1(2)\nu_2(3)\bar{\omega}_2(4)|$$

$$- |\bar{\nu}_1^*(1)\nu_1^*(2)\nu_2^*(3)\bar{\omega}_2^*(4)| \mp |\bar{\nu}_1^*(1)\nu_1^*(2)\nu_2(3)\bar{\omega}_2(4)|$$

$$\mp |\bar{\nu}_1(1)\nu_1(2)\nu_2^*(3)\bar{\omega}_2^*(4)| - |\bar{\nu}_1(1)\nu_1(2)\nu_2(3)\bar{\omega}_2(4)|$$

$$- |\nu_1^*(1)\bar{\nu}_1^*(2)\bar{\nu}_2^*(3)\omega_2^*(4)| \mp |\nu_1^*(1)\bar{\nu}_1^*(2)\bar{\nu}_2(3)\omega_2(4)| \qquad (9)$$

$$\mp |\nu_1(1)\bar{\nu}_1(2)\bar{\nu}_2^*(3)\omega_2^*(4)| - |\nu_1(1)\bar{\nu}_1(2)\bar{\nu}_2(3)\omega_2(4)|$$

$$+ |\bar{\nu}_1^*(1)\nu_1^*(2)\bar{\nu}_2^*(3)\omega_2^*(4)| \pm |\bar{\nu}_1^*(1)\nu_1^*(2)\bar{\nu}_2(3)\omega_2(4)|$$

$$\pm |\bar{\nu}_1(1)\nu_1(2)\bar{\nu}_2^*(3)\omega_2^*(4)| + |\bar{\nu}_1(1)\nu_1(2)\bar{\nu}_2(3)\omega_2(4)| \} \quad .$$

The upper signs on the right-hand side are to be used with the upper two signs on the left-hand side of these equations. The zero-order antisymmetrized orthonormal eigenfunction $\Phi^{aa}_{\pm\mp}$ and $\Phi^{au}_{\pm\mp}$ for the states $(a\ ^1\Delta_g^{\pm})_1(a\ ^1\Delta_g^{\mp})_2$ and $(a\ ^1\Delta_g^{\pm})(\ ^1\Delta_u^{\mp})$ can be obtained similarly. For case 1, the zero-order antisymmetrized eigenfunctions Φ^{BX}, $\Phi^{ua}_{\pm\pm}$ and $\Phi^{ua}_{\pm\mp}$ for the states $(B\ ^3\Sigma_u^-)_1(X\ ^3\Sigma_g^-)_2$, $(\ ^1\Delta_u^{\pm})_1(a\ ^1\Delta_g^{\pm})_2$ and $(\ ^1\Delta_u^{\pm})_1(a\ ^1\Delta_g^{\mp})_2$ can be obtained simply by replacing the appropriate MO's in Φ^{XB}, $\Phi^{au}_{\pm\pm}$ and $\Phi^{au}_{\pm\mp}$, respectively. Substituting the zero-order antisymmetrized eigenfunctions into the electronic matrix elements,[12] one obtains:

For case 1,

$$\sqrt{2/3}\, C^{BX}_{\pm\pm} = \sqrt{3}\, C^{ua}_{\pm\pm} = (\mp\langle \omega_1(1)\mu_2^*(2)\left|\frac{1}{r_{12}}\right|\mu_2(1)\nu_1^*(2)\rangle + \langle \omega_1^*(1)\mu_2^*(2)\left|\frac{1}{r_{12}}\right|\mu_2(1)\nu_1(2)\rangle) + c.c.$$

$$-\sqrt{2/3}\, C^{BX}_{\pm\mp} = -\sqrt{3}\, C^{ua}_{\pm\mp} = (\mp\langle \omega_1(1)\mu_2^*(2)\left|\frac{1}{r_{12}}\right|\mu_2(1)\nu_1^*(2)\rangle + \langle \omega_1^*(1)\mu_2^*(2)\left|\frac{1}{r_{12}}\right|\mu_2(1)\nu_1(2)\rangle) - c.c., \tag{10a}$$

For case 2,

$$\sqrt{2/3}\, C^{XB}_{\pm\pm} = \sqrt{3}\, C^{au}_{\pm\pm} = (\mp\langle \nu_1(1)\omega_2^*(2)\left|\frac{1}{r_{12}}\right|\nu_2(1)\nu_1^*(2)\rangle + \langle \nu_1^*(1)\omega_2^*(2)\left|\frac{1}{r_{12}}\right|\nu_2(1)\nu_1(2)\rangle) + c.c.$$

$$-\sqrt{2/3}\, C^{XB}_{\pm\mp} = -\sqrt{3}\, C^{au}_{\pm\mp} = (\mp\langle \nu_1(1)\omega_2^*(2)\left|\frac{1}{r_{12}}\right|\nu_2(1)\nu_1^*(2)\rangle + \langle \nu_1^*(1)\omega_2^*(2)\left|\frac{1}{r_{12}}\right|\nu_2(1)\nu_1(2)\rangle) - c.c. \tag{10b}$$

In Eq.(10) c.c. means the complex conjugate of the terms inside the preceding parentheses; matrix elements are abbreviated as C^{BX} and C^{ua} in case 1, and as C^{XB} and C^{au} in case 2. Note that $C^{XB;aa}$ in Eq.(7) includes both C^{BX} and C^{XB}. This holds for $C^{au;XX}$ as well.

Substituting Eq.(8) into Eq.(10), one obtains:

$$
\begin{aligned}
C^{BX}_{\pm\pm} &= \sqrt{3/2}\ \{[(2\,1\,2\,1)_1 - (2\,1\,1\,1)_1 + (1\,1\,1\,1)_1] + \text{c.c.}\} \\
-C^{BX}_{\pm\mp} &= \sqrt{3/2}\ \{[(2\,1\,2\,1)_1 - (2\,1\,1\,1)_1 + (1\,1\,1\,1)_1] - \text{c.c.}\} \\
C^{XB}_{\pm\pm} &= \sqrt{3/2}\ \{[(2\,1\,2\,1)_2 - (2\,1\,1\,1)_2 + (1\,1\,1\,1)_2] + \text{c.c.}\} \\
-C^{XB}_{\pm\mp} &= \sqrt{3/2}\ \{[(2\,1\,2\,1)_2 - (2\,1\,1\,1)_2 + (1\,1\,1\,1)_2] - \text{c.c.}\}
\end{aligned}
\qquad (11)
$$

where

$$
\begin{aligned}
(2\,1\,2\,1)_2 &= \mp(\pi^+_{u_2}\pi^+_{g_1}\,|\,\pi^-_{g_2}\pi^-_{g_1}) + (\pi^+_{u_2}\pi^-_{g_1}\,|\,\pi^-_{g_2}\pi^+_{g_1}) \\
(2\,1\,1\,1)_2 &= (\pi^+_{u_2}\,|\,\pi^+_{g_1})[\mp(\pi^-_{g_2}\pi^-_{g_1}\,|\,\pi^+_{g_1}\pi^+_{g_1})^* + (\pi^-_{g_2}\pi^+_{g_1}\,|\,\pi^+_{g_1}\pi^-_{g_1})^*] \\
&\quad + (\pi^+_{u_2}\,|\,\pi^-_{g_1})[\mp(\pi^-_{g_2}\pi^-_{g_1}\,|\,\pi^-_{g_1}\pi^+_{g_1})^* + (\pi^-_{g_1}\pi^+_{g_1}\,|\,\pi^-_{g_1}\pi^-_{g_1})^*] \\
&\quad + (\pi^+_{g_2}\,|\,\pi^-_{g_1})[\mp(\pi^+_{u_2}\pi^+_{g_1}\,|\,\pi^+_{g_1}\pi^-_{g_1}) + (\pi^+_{u_2}\pi^-_{g_1}\,|\,\pi^+_{g_1}\pi^+_{g_1})] \\
&\quad + (\pi^+_{g_2}\,|\,\pi^+_{g_1})[\mp(\pi^+_{u_2}\pi^+_{g_1}\,|\,\pi^-_{g_1}\pi^-_{g_1}) + (\pi^+_{u_2}\pi^-_{g_1}\,|\,\pi^-_{g_1}\pi^+_{g_1})]
\end{aligned}
$$

$$
\begin{aligned}
(1\,1\,1\,1)_2 &= (\pi^+_{u_2}\,|\,\pi^+_{g_1})(\pi^+_{g_2}\,|\,\pi^+_{g_1})[\mp(\pi^-_{g_1}\pi^-_{g_1}\,|\,\pi^+_{g_1}\pi^+_{g_1}) + (\pi^+_{g_1}\pi^-_{g_1}\,|\,\pi^-_{g_1}\pi^+_{g_1})] \\
&\quad + (\pi^+_{u_2}\,|\,\pi^-_{g_1})(\pi^+_{g_2}\,|\,\pi^-_{g_1})[\mp(\pi^-_{g_1}\pi^+_{g_1}\,|\,\pi^+_{g_1}\pi^-_{g_1}) + (\pi^+_{g_1}\pi^+_{g_1}\,|\,\pi^-_{g_1}\pi^-_{g_1})] \\
&\quad + (\pi^+_{u_2}\,|\,\pi^+_{g_1})(\pi^+_{g_2}\,|\,\pi^-_{g_1})[\mp(\pi^-_{g_1}\pi^+_{g_1}\,|\,\pi^+_{g_1}\pi^+_{g_1}) + (\pi^+_{g_1}\pi^+_{g_1}\,|\,\pi^-_{g_1}\pi^+_{g_1})] \\
&\quad + (\pi^+_{u_2}\,|\,\pi^-_{g_1})(\pi^+_{g_2}\,|\,\pi^+_{g_1})[\mp(\pi^-_{g_1}\pi^-_{g_1}\,|\,\pi^+_{g_1}\pi^-_{g_1}) + (\pi^+_{g_1}\pi^-_{g_1}\,|\,\pi^-_{g_1}\pi^-_{g_1})]
\end{aligned}
$$

$$(2\,1\,2\,1)_1 = \mp(\pi^+_{g_2}\pi^+_{g_1}|\pi^-_{g_2}\pi^-_{u_1}) + (\pi^+_{g_2}\pi^-_{g_1}|\pi^-_{g_2}\pi^+_{u_1})$$

$$\begin{aligned}(2\,1\,1\,1)_1 = (\pi^+_{g_2}|\pi^+_{g_1})[&\mp(\pi^+_{g_2}\pi^+_{g_1}|\pi^-_{g_1}\pi^-_{u_1}) \mp (\pi^+_{g_2}\pi^+_{g_1}|\pi^-_{g_1}\pi^-_{u_1}) \\ &+ (\pi^+_{g_2}\pi^-_{g_1}|\pi^-_{g_1}\pi^+_{u_1}) + (\pi^+_{g_2}\pi^-_{u_1}|\pi^-_{g_1}\pi^+_{g_1})] \\ + (\pi^+_{g_2}|\pi^-_{g_1})[&\mp(\pi^+_{g_2}\pi^+_{g_1}|\pi^+_{g_1}\pi^-_{u_1}) \mp (\pi^+_{g_2}\pi^+_{u_1}|\pi^+_{g_1}\pi^-_{g_1}) \\ &+ (\pi^+_{g_2}\pi^-_{g_1}|\pi^+_{g_1}\pi^+_{u_1}) + (\pi^+_{g_2}\pi^-_{u_1}|\pi^+_{g_1}\pi^+_{g_1})] \\ + (\pi^+_{g_2}|\pi^+_{u_1})[&\mp(\pi^+_{g_2}\pi^+_{g_1}|\pi^-_{u_1}\pi^-_{u_1}) \mp (\pi^+_{g_2}\pi^+_{u_1}|\pi^-_{u_1}\pi^-_{g_1}) \\ &+ (\pi^+_{g_2}\pi^-_{g_1}|\pi^-_{u_1}\pi^+_{u_1}) + (\pi^+_{g_2}\pi^-_{u_1}|\pi^-_{u_1}\pi^+_{g_1})] \\ + (\pi^+_{g_2}|\pi^-_{u_1})[&\mp(\pi^+_{g_2}\pi^+_{g_1}|\pi^+_{u_1}\pi^-_{u_1}) \mp (\pi^+_{g_2}\pi^+_{u_1}|\pi^+_{u_1}\pi^-_{g_1}) \\ &+ (\pi^+_{g_2}\pi^-_{g_1}|\pi^+_{u_1}\pi^+_{u_1}) + (\pi^+_{g_2}\pi^-_{u_1}|\pi^+_{u_1}\pi^+_{g_1})]\end{aligned}$$

$$\begin{aligned}(1\,1\,1\,1)_1 = (\pi^+_{g_2}|\pi^+_{g_1})(\pi^+_{g_2}|\pi^+_{g_1}) \quad &[\mp(\pi^+_{g_1}\pi^+_{g_1}|\pi^-_{g_1}\pi^-_{u_1}) + (\pi^+_{g_1}\pi^-_{g_1}|\pi^-_{g_1}\pi^+_{u_1})] \\ + (\pi^+_{g_2}|\pi^-_{g_1})(\pi^+_{g_2}|\pi^-_{g_1})[&\mp(\pi^-_{g_1}\pi^+_{g_1}|\pi^+_{g_1}\pi^-_{u_1}) + (\pi^-_{g_1}\pi^-_{g_1}|\pi^+_{g_1}\pi^+_{u_1})] \\ + (\pi^+_{g_2}|\pi^+_{u_1})(\pi^+_{g_2}|\pi^+_{u_1})[&\mp(\pi^+_{u_1}\pi^+_{g_1}|\pi^-_{u_1}\pi^-_{u_1}) + (\pi^+_{u_1}\pi^-_{g_1}|\pi^-_{u_1}\pi^+_{u_1})] \\ + (\pi^+_{g_2}|\pi^-_{u_1})(\pi^+_{g_2}|\pi^-_{u_1})[&\mp(\pi^-_{u_1}\pi^+_{g_1}|\pi^+_{u_1}\pi^-_{u_1}) + (\pi^-_{u_1}\pi^-_{g_1}|\pi^+_{u_1}\pi^+_{u_1})] \\ + (\pi^+_{g_2}|\pi^+_{g_1})(\pi^+_{g_2}|\pi^+_{u_1})[&\mp(\pi^+_{g_1}\pi^+_{g_1}|\pi^-_{u_1}\pi^-_{u_1}) \mp (\pi^+_{u_1}\pi^+_{g_1}|\pi^-_{g_1}\pi^-_{u_1}) \\ &+ (\pi^+_{g_1}\pi^-_{g_1}|\pi^-_{u_1}\pi^+_{u_1}) + (\pi^+_{u_1}\pi^-_{g_1}|\pi^-_{g_1}\pi^+_{u_1})] \\ + (\pi^+_{g_2}|\pi^-_{g_1})(\pi^+_{g_2}|\pi^-_{u_1})[&\mp(\pi^-_{g_1}\pi^+_{g_1}|\pi^+_{u_1}\pi^-_{u_1}) \mp (\pi^-_{u_1}\pi^+_{g_1}|\pi^+_{g_1}\pi^-_{u_1}) \\ &+ (\pi^-_{g_1}\pi^-_{g_1}|\pi^+_{u_1}\pi^+_{u_1}) + (\pi^-_{u_1}\pi^-_{g_1}|\pi^+_{g_1}\pi^+_{u_1})] \quad .\end{aligned}$$

Note that

$$(\pi^{+}_{u_2}\pi^{+}_{g_1}|\pi^{-}_{g_2}\pi^{-}_{g_1}) = \int \pi^{+*}_{u_2}(1)\,\pi^{+}_{g_1}(1)\,\frac{1}{r_{12}}\,\pi^{-}_{g_2}(2)\pi^{-*}_{g_1}(2)\,d\underset{\sim}{r}_1 \cdot d\underset{\sim}{r}_2 ,$$

etc. All of these integrals are in terms of molecule-fixed coordinates. The MO's are Slater type wavefunctions obtained by means of the SCF method.[13] In all the calculations we use π_u and π_g orbitals from the ground state of O_2, $X\ ^3\Sigma_g^-$ ($\cdots\pi_u^4\pi_g^2$). The π_u and π_g orbitals for the $B\ ^3\Sigma_u^-$ ($\cdots\pi_u^3\pi_g^3$) excited state could be somewhat different than the ground state orbitals. However, self-consistent calculations have not been reported yet for the $B\ ^3\Sigma_u^-$ state. The exponents of the set of basis functions of the MO's are 1.46838 and 2.88398 with corresponding vector components 0.63394 and 0.51164. The results for the three selected orientations $[(\pi/2), 0]$, $[(\pi/4), 0]$ and $[(\pi/4), (\pi/4)]$ in both cases are shown in Tables I and II. From these tables, it can be seen that the largest contribution to the matrix elements are derived from $(1\,1\,1\,1)_1$ and $(1\,1\,1\,1)_2$, which contain products of two intermolecular overlap integrals and one intramolecular electron repulsion integral. The intramolecular electron repulsion integrals are approximately 10^5 times as large as the intermolecular ones. Therefore when the intermolecular overlap integral is of the order of 5×10^{-3} a.u., the product of the two intermolecular overlap integrals and one intramolecular electron repulsion integral is still dominating.

The approximation that takes the MO's of $\underline{B}\ ^3\Sigma_u^-$ identical to those of the ground state is probably fairly good for case 2, while it could result in matrix elements for case 1 that are quite a bit too large. One suspects this might be the case from a qualitative examination of the largest terms $(1\,1\,1\,1)_1$ and $(1\,1\,1\,1)_2$ in Eq. (11). Only one intermolecular

overlap integral involving the MO's of $\underline{B}\ ^3\Sigma_u^-$ occurs in each term of $(1\,1\,1\,1)_2$, while a product of two intermolecular overlap integrals and an intramolecular electron repulsion integral involving the MO's of $\underline{B}\ ^3\Sigma_u^-$ occurs in that of $(1\,1\,1\,1)_1$. In order to test more quantitatively the sensitivity of our results to such changes in the π_u and π_g orbitals, we have taken the orbitals from a self-consistent calculation on the ground state of O_2^+, $X\ ^2\Pi_g$, $(\cdots\pi_u^4\pi_g)$.[13] (It would be more appropriate to use the orbitals from the $^2\Pi_u$ $(\cdots\pi_u^3\pi_g^2)$ state of O_2^+; however, calculations for this state have not been reported yet.)

We found that using the $X\ ^2\Pi_g$ orbitals for the $B\ ^3\Sigma_u^-$ state led to matrix elements for case 2 and case 1 that are respectively 0.7 and 0.3 those shown in Tables I and II.

B. Angular Dependence of Interaction

To get the analytical expression of the angular-dependent matrix elements, we first derive from Eq. (1) the relation between an MO in the molecule-fixed coordinate $(x_2,\ y_2,\ z_2)$ and one in the coordinate system $(x_2',\ y_2',\ z_2')$:

TABLE I. Matrix elements for case 2 when the perturbing state is localized in molecule 2.

(θ, φ)	$\sqrt{6}\ (2121)_2$			$\sqrt{6}\ (2111)_2$		$\sqrt{6}\ (1111)_2$				
	2C EX[a]	3C EX	4C EX	2C HD[b]	3C EM[c]	1C CM[d]	2C CM	EX	HD	Sum
				$(X\ ^3\Sigma_g^-)_1(B\ ^3\Sigma_u^-)_2 \sim\sim (a\ ^1\Delta_g^+)(a\ ^1\Delta_g^+)$						C_{++}^{XB}
$(\frac{\pi}{2}, 0)$	-0.29	-0.12	0	0	0	0.57	-0.01	0	0	0.15
$(\frac{\pi}{4}, 0)$	13.17	-12.43	0	0.04	/[e]	-0.05	-0.03	-0.01	0.04	0.73
$(\frac{\pi}{4}, \frac{\pi}{4})$	-5.91	5.51	0	-0.25	/	-0.66	-0.32	-0.05	0.40	-1.26
				$(X\ ^3\Sigma_g^-)_1(B\ ^3\Sigma_u^-)_2 \sim\sim (a\ ^1\Delta_g^-)(a\ ^1\Delta_g^-)$						C_{--}^{XB}
$(\frac{\pi}{2}, 0)$	7.84	0.45	/	-14.04	-2.84	25.96	13.44	2.15	-17.71	15.25
$(\frac{\pi}{4}, 0)$	34.30	-32.01	0	0.13	/	-0.20	-0.09	-0.02	0.12	2.23
$(\frac{\pi}{4}, \frac{\pi}{4})$	-11.60	9.23	0	0.18	/	-3.07	-1.60	-0.26	2.11	-5.02
				$(X\ ^3\Sigma_g^-)_1(B\ ^3\Sigma_u^-)_2 \sim\sim (a\ ^1\Delta_g^+)_1(a\ ^1\Delta_g^-)_2$						C_{+-}^{XB}
$(\frac{\pi}{2}, 0)$	0	0	0	0	0	0	0	0	0	0
$(\frac{\pi}{4}, 0)$	0	0	0	0	0	0	0	0	0	0
$(\frac{\pi}{4}, \frac{\pi}{4})$	-5.21i	3.69i	/	0.09i	/	0.06i	0	0	0	-1.37i

TABLE I. (continued)

(θ, φ)	$\sqrt{6}\ (2\,1\,2\,1)_2$			$\sqrt{6}\ (2\,1\,1\,1)_2$		$\sqrt{6}\ (1\,1\,1\,1)_2$				
	2C EX[a]	3C EX	4C EX	2C HD[b]	3C EM[c]	1C CM[d]	2C CM	EX	HD	Sum
	$(X\ ^3\Sigma_g^-)_1(B\ ^3\Sigma_u^-)_2 \sim\sim (a\ ^1\Delta_g^-)_1(a\ ^1\Delta_g^+)_2$									C_{-+}^{XB}
$(\frac{\pi}{2}, 0)$	0	0	0	0	0	0	0	0	0	0
$(\frac{\pi}{4}, 0)$	0	0	0	0	0	0	0	0	0	0
$(\frac{\pi}{4}, \frac{\pi}{4})$	-24.68i	15.67i	0	-0.75i	/[e]	2.73i	1.41i	0.23i	-1.86i	-7.25i

[a] EX = exchange integrals.

[b] HD = hybrid integrals.

[c] EM = exchange and coulomb integrals.

[d] CM = coulomb integrals

[e] / means that the contribution is so small that it is neglected.

TABLE II. Matrix elements for case 1, when the perturbing state is localized in molecule 1.

(θ, φ)	$\sqrt{6}\ (2121)_1$			$\sqrt{6}\ (2111)_1$		$\sqrt{6}\ (1111)_1$				
	2C EX[a]	3C EX	4C EX	2C HD[b]	3C EM[c]	1C CM[d]	2C CM	EX	HD	Sum
				$(B\ ^3\Sigma_u^-)_1(X\ ^3\Sigma_g^-)_2 \sim\sim (a\ ^1\Delta_g^+)(a\ ^1\Delta_g^+)$						C_{++}^{BX}
$(\frac{\pi}{2}, 0)$	-6.99	1.10	/[e]	-0.34	-3.88	34.56	18.30	-1.47	-0.53	40.75
$(\frac{\pi}{4}, 0)$	2.21	0.67	/	-4.88	0.21	12.98	6.88	3.48	32.66	54.21
$(\frac{\pi}{4}, \frac{\pi}{4})$	-1.48	0.45	/	0.51	/	-6.64	-3.52	-1.74	-16.55	-28.98
				$(B\ ^3\Sigma_u^-)_1(X\ ^3\Sigma_g^-)_2 \sim\sim (a\ ^1\Delta_g^-)(a\ ^1\Delta_g^-)$						C_{--}^{BX}
$(\frac{\pi}{2}, 0)$	1.29	0	/	0	0.02	-34.56	-18.30	1.17	10.25	-40.13
$(\frac{\pi}{4}, 0)$	-0.02	3.49	/	-11.63	-0.21	-12.32	-6.93	9.10	80.38	61.87
$(\frac{\pi}{4}, \frac{\pi}{4})$	-8.92	2.86	/	15.28	/	6.31	3.54	1.45	-21.51	-2.88
				$(B\ ^3\Sigma_u^-)_1(X\ ^3\Sigma_g^-)_2 \tilde{\sim}\sim (a\ ^1\Delta_g^+)_1(a\ ^1\Delta_g^-)_2$						C_{+-}^{BX}
$(\frac{\pi}{2}, 0)$	0	0	0	0	0	0	0	0	0	0
$(\frac{\pi}{4}, 0)$	0	0	0	0	0	0	0	0	0	0
$(\frac{\pi}{4}, \frac{\pi}{4})$	-1.45i	-0.28i	/	1.03i	/	-2.66i	-1.41i	-0.89i	-8.23i	-13.89i

TABLE II. (continued)

(θ, φ)	$\sqrt{6}\ (2121)_1$			$\sqrt{6}\ (2111)_1$		$\sqrt{6}\ (1111)_1$				
	2C	3C	4C	2C	3C	1C	2C			
	EX[a]	EX	EX	HD[b]	EM[c]	CM[d]	CM	EX	HD	Sum
				$(B\ ^3\Sigma_u^-)_1(X\ ^3\Sigma_g^-)_2 \sim\sim (a\ ^1\Delta_g^-)_1(a\ ^1\Delta_g^+)_2$						C_{-+}^{BX}
$(\frac{\pi}{2}, 0)$	0	0	0	0	0	0	0	0	0	0
$(\frac{\pi}{4}, 0)$	0	0	0	0	0	0	0	0	0	0
$(\frac{\pi}{4}, \frac{\pi}{4})$	-0.26i	-3.21i	/[e]	12.51i	/	2.52i	1.42i	-4.57i	-45.34i	-36.92i

[a] EX exchange integrals.

[b] HD ≡ hybrid integrals.

[c] EM ≡ exchange and coulomb integrals.

[d] CM ≡ coulomb integrals.

[e] / means that the contribution is so small that it is neglected.

$$\begin{bmatrix} \delta_2^+ \\ \delta_2^- \\ z_2 \end{bmatrix} = \begin{bmatrix} \frac{1}{2}(\cos\theta\cos\varphi + \cos\varphi - i\sin\varphi - i\cos\theta\sin\varphi) & \frac{1}{2}(\cos\theta\cos\varphi - \cos\varphi - i\sin\varphi + i\cos\theta\sin\varphi) & -\frac{1}{\sqrt{2}}\sin\theta \\ \frac{1}{2}(\cos\theta\cos\varphi - \cos\varphi + i\sin\varphi - i\cos\theta\sin\varphi) & \frac{1}{2}(\cos\theta\cos\varphi + \cos\varphi + i\sin\varphi + i\cos\theta\sin\varphi) & -\frac{1}{\sqrt{2}}\sin\theta \\ \frac{1}{\sqrt{2}}(\sin\theta\cos\varphi - i\sin\theta\sin\varphi) & \frac{1}{\sqrt{2}}(\sin\theta\cos\varphi + i\sin\theta\sin\varphi) & \cos\theta \end{bmatrix} \begin{bmatrix} \delta_{2'}^+ \\ \delta_{2'}^- \\ z_2' \end{bmatrix} \quad (12)$$

where $\delta_j^{\pm} = \frac{1}{\sqrt{2}}(x_j \pm i y_j)$. We now employ the transformation of Eq. (12) in Eq. (11) and use the symmetry conditions,

$$C^{BX;aa}(\theta, \tfrac{\pi}{2}) = C^{BX;aa}(0, 0) = 0$$

$$C^{BX;aa}(\theta, -\varphi) = C^{BX;aa}(\theta, \varphi) = C^{BX;aa}(-\theta, \varphi) \qquad (13)$$

$$C^{BX;aa}(\pi + \theta, \varphi) = C^{BX;aa}(\theta, \varphi) = C^{BX;aa}(\theta, \pi + \varphi).$$

Because of these conditions, $C^{BX;aa}$ has been assumed to have the following form:

$$C^{BX;aa}(\theta, \varphi) = A\cos^2\theta\cos 2\varphi + B\cos 2\varphi + C\cos^2\theta + D\cos^4\theta + B + F\cos^2\theta\cos^2 2\varphi + D\cos^4\theta\cos 2\varphi , \qquad (14)$$

where $A + 2B + C + 2D + F = 0$ and $A = C + F$. This expression is equivalent to an expansion in spherical harmonics $Y_{\ell, m}(\theta, \varphi)$, where terms satisfying the symmetry conditions up to $\ell = 4$, $m = 4$ have been retained, and where, because of the limitation on the number of theoretical points, terms in $\cos^2 2\varphi$ and $\cos^4\theta\cos^2 2\varphi$ have been ignored. Since the θ-dependence of $C^{BX;aa}(\theta, \varphi)$ seems to be more prominent than the φ-dependence, the assumption is reasonable.

The coefficients are now determined from the matrix elements given in Tables I and II. These results are shown in Table III. The last column in Table III is the root mean square of the matrix elements over all orientations, which is defined by

TABLE III. Coefficients in Eq. (14) and $(\overline{|C|^2})^{\frac{1}{2}}$ in cm^{-1}.

	A	B	C	D	F	$(\overline{\lvert C\rvert^2})^{\frac{1}{2}}$
C^{XB}_{++}	1.24	0.08	-2.01	-1.31	3.25	0.7
C^{XB}_{--}	-18.43	7.63	-30.70	10.80	12.27	6.2
C^{XB}_{+-}	0	0	-2.74	0	2.74	0.7
C^{XB}_{-+}	0	0	-14.50	0	14.50	3.9
C^{BX}_{++}	47.30	20.38	-64.88	-67.67	112.17	32
C^{BX}_{--}	183.95	-20.07	116.32	-163.88	67.63	22
C^{BX}_{+-}	0	0	-27.78	0	27.78	7.6
C^{BX}_{-+}	0	0	-73.84	0	73.84	20.2

$$(\overline{|C|^2})^{\frac{1}{2}} \equiv \left(\frac{1}{4\pi}\int_{\theta=0}^{\pi} d\theta \int_{\varphi=0}^{2\pi} d\varphi \, |C^{BX;aa}(\theta,\varphi)|^2 \sin\theta\right)^{\frac{1}{2}}$$

$$= \left(\frac{1}{10}A^2 + \frac{1}{5}C^2 + \frac{3}{2}B^2 + \frac{1}{6}D^2 + \frac{3}{40}F^2 + BC + \frac{3}{5}BD \right. \qquad (15)$$

$$\left. + \frac{2}{3}BF + \frac{3}{7}CD + \frac{1}{5}CF + \frac{2}{7}DF\right)^{\frac{1}{2}} .$$

The polarization in case 1 is along the Z-axis, while that in case 2 is arbitrary. When unpolarized light is used, both cases are equally probable. In this case the matrix element to be used in Eq. (7) takes the form,

$$|M|^2 \equiv \frac{1}{2}\left(\overline{|C^{XB}|^2} + \overline{|C^{BX}|^2}\right),$$

where $\overline{|C^{XB}|^2}$ and $\overline{|C^{BX}|^2}$ are respectively the square of $(\overline{|C|^2})^{\frac{1}{2}}$ for case 2 and case 1, which is defined in Eq. (15). (Note that $C^{BX;aa}$ in Eq. (15), as mentioned earlier, refers to both case 1 and case 2.) The results are given in Table IV. The dipole length in Eq. (7) is then given as follows:

$$|\underset{\sim}{R}_{aa;XX}|^2 = \gamma^2 |\underset{\sim}{R}_{BX}|^2 \cdot |M|^2 ,$$

where

$$\gamma = \frac{1}{\overline{E}_{BX} - \overline{E}_{aa}} + \frac{\sqrt{2}}{3(\overline{E}_{au} - \overline{E}_{XX})} .$$

Alternatively, starting with states $2^{-\frac{1}{2}}(\Phi^{XB} \pm \Phi^{BX})$ and considering the different polarizations, we obtain from Eq. (7)

TABLE IV. Matrix elements and oscillator strength.

Transition	Matrix Element ($\|M\|$ in cm^{-1})	Oscillator Strength f_{00}	Oscillator Strength f
$(a\ ^1\Delta_g^+)(a\ ^1\Delta_g^+) \leftarrow (X\ ^3\Sigma_g^-)(X\ ^3\Sigma_g^-)$	22.7	1.3×10^{-8}	1.4×10^{-8}
$(a\ ^1\Delta_g^-)(a\ ^1\Delta_g^-) \leftarrow (X\ ^3\Sigma_g^-)(X\ ^3\Sigma_g^-)$	18.0	0.8×10^{-8}	0.9×10^{-8}
$(a\ ^1\Delta_g^+)_1(a\ ^1\Delta_g^-)_2 \leftarrow (X\ ^3\Sigma_g^-)(X\ ^3\Sigma_g^-)$	5.4	0.1×10^{-8}	0.1×10^{-8}
$(a\ ^1\Delta_g^-)_1(a\ ^1\Delta_g^+)_2 \leftarrow (X\ ^3\Sigma_g^-)(X\ ^3\Sigma_g^-)$	14.6	0.5×10^{-8}	0.6×10^{-8}
Sum of Four Components	32.9	2.6×10^{-8}	3.0×10^{-8}
Experimental value ÷ 3 for solid γ-O_2 [a]		1.7×10^{-8}	5.2×10^{-8}

[a] See Ref. 15 for experimental value. The factor of 3 in the table is introduced in order to compare the calculated pairwise intensity enhancement with the intensity in solid O_2 where each molecule is adjacent to more than one neighbor. See text.

$$|\underset{\sim}{R}_{aa;XX}|^2 = \frac{\gamma^2}{2} |\underset{\sim}{R}_{BX}|^2 \frac{1}{4\pi} \int_{\theta=0}^{\pi} d\theta \int_{\varphi=0}^{2\pi} d\varphi \sin\theta \{ |C^{BX}(\theta, \varphi) + C^{XB}(\theta, \varphi)\cos\theta|^2 + |C^{XB}(\theta, \varphi)|^2 (\sin^2\theta \sin^2\varphi + \sin^2\theta \cos^2\varphi)\} \quad (16a)$$

$$= \frac{\gamma^2}{2} |\underset{\sim}{R}_{BX}|^2 \frac{1}{4\pi} \iint \{ |C^{BX}(\theta,\varphi)|^2 + 2|C^{BX}(\theta, \varphi)| |C^{XB}(\theta, \varphi)|\cos\theta + |C^{XB}(\theta, \varphi)|^2\} \sin\theta d\theta d\varphi. \quad (16b)$$

Since the second term in the parentheses of Eq. (16b) vanishes because of symmetry, one obtains the same result for $|\underset{\sim}{R}_{aa;XX}|^2$ as above.

C. Franck-Condon Factors

The Franck-Condon factor for the (k, 0) band of the transition $\underline{a}\ ^1\Delta_g \leftarrow \underline{X}\ ^3\Sigma_g^-$ is defined by,

$$F_{k0} \equiv |\langle \eta_k^a | \eta_0^X \rangle|^2 .$$

It seems reasonable to assume that the first few vibrations are harmonic. Hence F_{k0} can be simplified: [14]

$$F_{k0}^{\frac{1}{2}} = \frac{1}{\alpha} \left(\frac{2\pi}{1+f}\right)^{\frac{1}{2}} \exp\left[\frac{-f\alpha^2\delta^2}{2(1+f)}\right] \left(\frac{\omega}{\pi\hbar}\right)^{\frac{1}{4}} \left[\left(\frac{\omega'}{\pi\hbar}\right)^{\frac{1}{2}} \left(\frac{1}{k!\,2^k}\right)\right]^{\frac{1}{2}} \left(\frac{1-f}{1+f}\right)^{k/2} H_k\left[\frac{\alpha\sqrt{f}\,\delta}{(1-f^2)^{\frac{1}{2}}}\right] , \quad (18)$$

where $\alpha = \left(\frac{\omega}{\hbar}\right)^{\frac{1}{2}}$, $f = \frac{\omega'}{\omega}$, $\delta = Q'_e - Q_e$, $H_k\left[\frac{\alpha\sqrt{f}\,\delta}{(1-f^2)^{\frac{1}{2}}}\right]$ is an Hermite polynomial with argument $\left[\frac{\alpha\sqrt{f}\,\delta}{(1-f^2)^{\frac{1}{2}}}\right]$, Q'_e, ω' and Q_e, ω are equilibrium

normal coordinate and angular frequency of the excited $\underline{a}\ ^1\Delta_g$ and the ground $\underline{X}\ ^3\Sigma_g^-$ state, respectively. The Franck-Condon factors for the (0, 0), (1, 0) and (2, 0) bands were found to be 0.95248, 0.04718 and 0.00033.

D. Oscillator Strength

The oscillator strength for the $(k\ell, 0)$ band of the double transition $\underline{aa} \leftarrow \underline{XX}$ is given by

$$f_{k\ell,0} \approx 5.65 \times 10^{-10} \frac{\nu_{aa}}{\nu_B} f^{BX} |M|^2 F_{k0} \cdot F_{\ell 0} , \qquad (19)$$

where ν_{aa} and ν_B are centers of gravity of the vibronic bands of $(a\ ^1\Delta_g)(a\ ^1\Delta_g)$ and $\underline{B}\ ^3\Sigma_u^-$ being considered. $k\ell$ represents the vibronic state of $\underline{aa}$ in which one molecule is in the $k^{\underline{th}}$ and the other in the $\ell^{\underline{th}}$ vibrational level. f^{BX} is the oscillator strength of the Schumann-Runge transition. For the (0, 0) band of $\underline{aa} \leftarrow \underline{XX}$, Eq. (19) yields,

$$f_{00} \approx 0.24 \times 10^{-10} |M|^2 . \qquad (20a)$$

Summation over the vibronic structure of $\underline{aa} \leftarrow \underline{XX}$ yields for the overall oscillator strength,

$$f \approx 0.27 \times 10^{-10} |M|^2 . \qquad (20b)$$

The experimental[15] and the theoretical values of f_{00} and f are listed in Table IV. Since the four components of the degenerate state are not resolvable experimentally, the observed oscillator strength of the double transition should be equal to the sum of the four theoretical oscillator strengths.

E. Possible Vibronic Effects

It is well known that intermolecular integrals are very sensitive to the intermolecular distance. Therefore, a change of intermolecular overlap of electronic wavefunctions due to nuclear vibrational motion might not be negligible. In other words, an increase of electronic matrix elements with increasing vibrational amplitude could occur, and is perhaps responsible for the stronger observed[15] intensity in condensed O_2 of the (1, 0) band, compared to that of the (0, 0) band. This is of course in opposition to the prediction of simple Franck-Condon theory. The presence of such a vibronic effect would therefore contribute to a lack of agreement between experimental and theoretical oscillator strengths. (See the next section for a discussion of the comparison between calculated and observed intensities.)

4. CONCLUSION

Calculation of the intensity enhancement of the double transition $\underline{aa} \leftarrow \underline{XX}$ can be divided into two parts in the framework of the Born-Oppenheimer approximation: (1) electronic matrix elements of the intermolecular exchange interaction between the perturbed and the perturbing states, and (2) the Franck-Condon factor, which is approximately unity for the (0, 0) band.

As we have mentioned in the previous section, the matrix elements draw the largest contributions from the terms $(1\,1\,1\,1)_1$ and $(1\,1\,1\,1)_2$. From Table V it can be seen that all the orientations considered for case 1 and the orientation $(\frac{\pi}{2}, 0)$ in case 2 have intermolecular overlap

TABLE V. Intermolecular overlap integrals in 10^2 a.u.

Case 1				
	(θ, φ)	$(\pi^+_{g_2}\|\pi^+_{u_1})$	$(\pi^+_{g_2}\|\pi^-_{u_1})$	$(\pi^+_{g_2}\|\pi^-_{g_1})$
	$(\frac{\pi}{2}, 0)$	-0.344582	0.344582	0.430530
	$(\frac{\pi}{4}, 0)$	-0.765316	-1.179490	-0.106242
	$(\frac{\pi}{4}, \frac{\pi}{4})$	(-0.447027 -0.513171i)	(-0.412639 -0.801237i)	(-0.032327 -0.204104i)
Case 2				
	(θ, φ)	$(\pi^+_{u_2}\|\pi^+_{g_1})$	$(\pi^+_{u_2}\|\pi^-_{g_1})$	$(\pi^+_{g_2}\|\pi^+_{g_1})$
	$(\frac{\pi}{2}, 0)$	0.504493	0.504493	0.430530
	$(\frac{\pi}{4}, 0)$	0.104781	0.037486	-0.018134
	$(\frac{\pi}{4}, \frac{\pi}{4})$	(0.125948 -0.105253i)	(0.132530 -0.131008i)	(-0.006808 -0.187506i)

integrals $\gtrsim 10^{-3}$ a.u., and therefore give most of the contribution to the overall matrix element.

No really direct comparison can be made between the theoretical oscillator strength for the pair interaction and the experimental one for solid γ - O_2 because of its extremely complicated crystal structure (Fig. 3).[6] There are eight molecules per unit cell. Each O_2 at (000) and $(\frac{1}{2}\frac{1}{2}\frac{1}{2})$ has twelve nearest neighbors at a separation of 3.81 Å between molecular centers, and eight next-nearest neighbors at 6.08 Å. The six other molecules in the unit cell each have two neighbors at 3.42 Å, four neighbors at 3.81 Å and eight at 4.17 Å. Since the two oxygen molecules at the van der Waals' distance 3.42 Å are in a fixed orientation with such high symmetry that the matrix elements vanish, they do not contribute to the intensity enhancement. Neglecting interactions between more than two molecules at a time and interactions for molecules with an intermolecular separation larger than 3.81 Å, we can take the average pairwise interaction at 3.81 Å for solid γ - O_2 to be identical to the calculated one. Since three such interactions per molecule are involved, the calculated oscillator strength for the 0, 0 band in solid γ - O_2 should be 7.8×10^{-8}, which is about $1\frac{1}{2}$ times the experimental value. The error is in the right direction considering the nature of the approximate B $^3\Sigma_u^-$ orbitals used. The agreement between theory and experiment is therefore satisfactory when one takes into account this and other approximations employed in the calculations, and indicates the essential validity of the overall approach to this intensity enhancement problem.

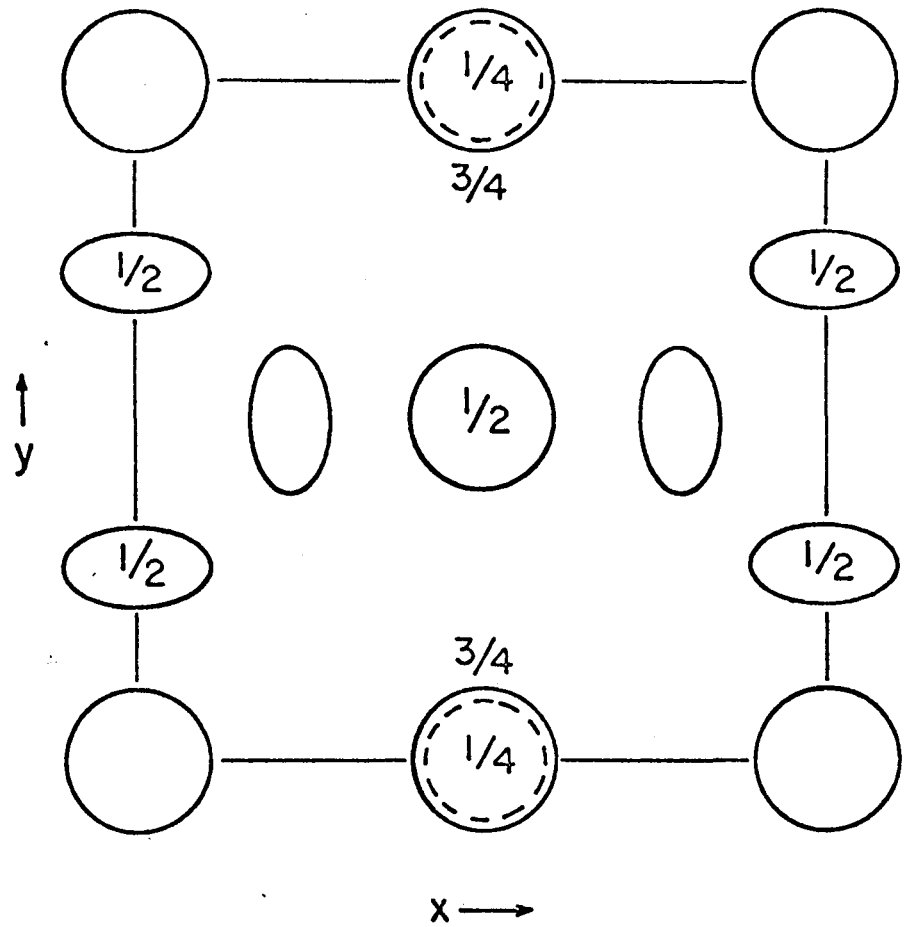

FIG. 3. Crystal structure of γ-O_2. Out-of-plane coordinates are indicated for each molecular center, except for those at z = 0, which are unlabeled. The two molecules at 000 and $\frac{1}{2}\frac{1}{2}\frac{1}{2}$ are approximately spherically disordered. The other six molecules, at $\frac{1}{4}\frac{1}{2}0$, $0\frac{1}{4}\frac{1}{2}$, $\frac{1}{2}0\frac{1}{4}$, $\frac{3}{4}\frac{1}{2}0$, $0\frac{3}{4}\frac{1}{2}$ and $\frac{1}{2}0\frac{3}{4}$, show an oblate spheroidal distribution of electron density such that the ratio of major to minor axis is about two. Minor axes are aligned along the shortest intermolecular contacts (3.4 Å in O_2) along x($y = \frac{1}{2}$, $z = 0$), along y($x = 0$, $z = \frac{1}{2}$) and along z($x = \frac{1}{2}$, $y = 0$). A bond distance of 1.21 Å for O_2 was assumed.

REFERENCES

1. H. Salow and W. Steiner, Z. Physik 99, 137 (1936).
2. V.I. Dianov-Klokov, Opt. Spectrosc. 16, 224 (1964).
3. L.W. Bader and E.A. Ogryzlo, Discussions Faraday Soc. 37, 46 (1964).
4. J.S. Arnold, R.J. Browne, and E.A. Ogryzlo, Photochem. Photobiol. 4, 963 (1965).
5. G.W. Robinson, J. Chem. Phys. 46, 572 (1967).
6. T.H. Jordan, W.E. Streib, H.W. Smith, and W.N. Lipscomb, Acta Cryst. 17, 777 (1964).
7. At certain orientations, the interactions are identically zero because of symmetry.
8. G.R. Cook and B.K. Ching, Air Force Report No. TDR-469 (9260-01)-4 (1965); Y. Tanaka, J. Chem. Phys. 20, 1728 (1952).
9. T. Itoh and K. Ohno, J. Chem. Phys. 25, 1098 (1956).
10. E.U. Condon and G.H. Shortley, The Theory of Atomic Spectra (Cambridge University Press, London, England, 1967), p. 79.
11. A subscript designates the molecule in the specified state, while no subscript means that both molecules can be in the state and both should be considered.
12. Subscripts of a certain matrix element differentiate the symmetry of the different states involved. For example, the subscript of C^{BX}_{++} corresponds to the "++" of the state $(a\ ^1\Delta_g^+)(a\ ^1\Delta_g^+)$. No subscript represents any one of the whole set "++, --, +-, -+."
13. P.E. Cade, private communication.

14. R.P. Frosch, Ph.D. thesis, California Institute of Technology, 1965.

15. A. Landan, E.J. Allin, and H.L. Welsh, Spectrochim. Acta 18, 1 (1962).

PROPOSITION I.

To understand the atmospheric processes on Jupiter and the origin of life, knowledge about primary and secondary processes in the photolyses of methane and ammonia is very important. In these respects, the following investigations are proposed.

(1) Existence of NH ($a\,^1\Delta$) state in the vacuum ultraviolet photodissociation of NH_3 excited with 1470 Å Xe-resonance line and 1633 Å Br-line:

First of all, the threshold energies for the photodissociation of NH_3 are depicted as follows:

(1)	$NH_3 \longrightarrow NH(X\,^3\Sigma^-) + H_2$	4. lev.	2990 Å
(2)	$NH_3 \longrightarrow NH_2(^2B_1) + H$	4.5	2750 Å
(3)	$NH_3 \longrightarrow NH(a\,^1\Delta) + H_2$	~5.1	2420 Å
(4)	$NH_3 \longrightarrow NH_2(^2A_1\,\Pi) + H$	~5.8	2130 Å
(5)	$NH_3 \longrightarrow NH(b\,^1\Sigma^+) + H_2$	~6.3	1960 Å
(6)	$NH_3 \longrightarrow NH(A\,^3\Pi) + H_2$	7.8	1590 Å
(7)	$NH_3 \longrightarrow NH(X\,^3\Sigma^-) + 2H$	8.7	1420 Å
(8)	$NH_3 \longrightarrow NH(c\,^1\Pi) + H_2$	~9.1	1360 Å

Reactions (1) and (6) are ruled out because of spin conservation. Reactions (2) and (4) are confirmed from the absorption[1, 2] and emission spectra[3] of NH_2 in the photolysis of NH_3 below or above 1600 Å. Reaction (7) is rationalized from the 3360 Å absorption band of NH ($A\,^3\Pi \leftarrow X\,^3\Sigma^-$) when the photodissociating wavelength was below (shorter than) 1600Å. Reaction (8) is established by Becker and Welge.[4] They observed the 3240 Å emission band of

NH ($c\ ^1\Pi \rightarrow a\ ^1\Delta$) in the vacuum ultraviolet photolysis of gaseous ammonia excited with Kr-resonance lines (1165 Å and 1236 Å) and Xe-line 1295 Å. The intensity of the emission increases with the pressure of NH_3 in the range of 6×10^{-3} to 5 Torr. Neither emission nor absorption due to NH($a\ ^1\Delta$) and NH($b\ ^1\Sigma^+$) have been confirmed. However, from the reactions (3) and (5), the two singlet states can be populated as well in the photodissociation for NH_3 at the 1470 Å Xe-line or 1633 Å Br-line. The state NH($a\ ^1\Delta$) is expected furthermore to have a long lifetime, because the mixing of states in simple diatomic molecules is small.

To verify the existence of the two states when NH_3 is photolyzed at 1470 Å and 1633 Å, it is proposed to examine the emission spectra from these states in the wavelength region, 4000 Å to 10,000 Å. The experiment can be carried out in the low pressure ammonia gas with or without Kr (rare gas). If the intensity is not strong enough, dilute solid solution of NH_3 in Kr is suggested. To confirm the existence of NH($a\ ^1\Delta$), it is also proposed to investigate the 3324 Å absorption band, which might be masked in the 3360 Å band of NH($A\ ^3\Pi \rightarrow X\ ^3\Sigma^-$). A high resolution spectrometer will be useful in this investigation.

(2) Spectroscopic observation of radicals CH, CH_2, and CH_3 frozen in a Kr-matrix at 4.2 °K from the photodissociation of CH_4 excited at wavelengths 1236 Å, 1470 Å, 1630 Å and 2537 Å.

(3) Gas-phase photolysis of a mixture of NH_3 and CH_4 excited with intense light of wavelength 1236 Å, 1470 Å and 1633 Å:

In the vacuum ultraviolet, photolysis of $NH_3 + CH_4 + H_2O$, hydrogen cyanide was thought to be the major intermediate for the formation of amino acids and other biological materials. Cyanides were formed when ethylene was added to the glowing gases which were produced when ammonia was pumped at high speed through a discharge and passed into a trap at 93 °K. It seems highly possible to form HCN by the photolysis of $CH_4 + NH_3$. High intensity of excitation and low pressure of the gas mixture will increase the yield of HCN. Based on the spin conservation rule and energy requirements, the following mechanism is proposed:

$$NH(A\ ^3\Pi) + CH_2(X\ ^3\Sigma_g^-) \longrightarrow CH_2{=}NH \longrightarrow CH{\equiv}N + H_2.$$

This mechanism can be justified by study of the photolysis of $CH_4 + NH_3$ and CH_4 at different wavelengths of excitation.

(4) Photochemistry of hydrogen cyanide in the gas phase and in aqueous solution with excitation at Kr-resonance lines (1165 Å and 1236 Å) and at Xe-line 1470 Å.

Hydrogen cyanide was thought[5] to be a major intermediate in synthesis of amino acids from primitive mixtures. It is considered as a major product when the primitive atmosphere is exposed to electric discharges or ionizing radiation. Another reason for using hydrogen cyanide as a starting material is that comets contain a large number of cyanide compounds. It has been suggested that in the first 2 billion years of the earth's existence, about one hundred comets must have struck the earth. The cometary material trapped

by the earth during the strikes may have been an important intermediate in biochemical synthesis. Consequently it is proposed to investigate whether the ionized state or the excited electronic states are responsible in the synthesis of adenine and guanine from hydrogen cyanide. It is also proposed to study the photochemical products of hydrogen cyanide at various experimental conditions as mentioned.

REFERENCES

1. K. H. Becker and K. H. Welge, Z. Naturforsch. 17a, 676 (1962).
2. O. Schnepp and K. Kressler, J. Chem. Phys. 32, 1682 (1960).
3. Lavin and Bates, Proc. Natl. Acad. Sci. Wash. 16, 804 (1930).
4. K. H. Becker and K. H. Welge, Z. Naturforsch. 18a, 600 (1963).
5. S. L. Miller and H. C. Urey, Science 130, 245 (1959); H. C. Urey, Proc. Natl. Acad. Sci. U.S. 28, 351 (1952).

PROPOSITION II

The photosynthetic mechanism can be envisioned as follows. In the photosynthetic unit, light is absorbed by two different pigment systems (chlorophyll a and accessory pigment), which are called S_I and S_{II}. Each system contains a large number of pigment molecules. The excitation energy is transferred to two different reaction centers where it is trapped and the primary photochemical reactions are initiated. Neither primary reaction, however, can efficiently sustain photosynthesis alone since the one associated with S_{II} quickly depletes reactants which are replenished by products derived from the primary photochemical reaction associated with S_I. Therefore the mechanism is a two-quantum process in which the two primary photochemical reactions are linked together by intermediate chemical reactions.

The purpose of this proposal is to investigate the state of the pigments for transfer of the excitation energy. In other words, the excitation is transferred directly via the singlet state (S_1), or it is first relaxed to the triplet state (T_1) and then transferred, or both of these situations take place. It is generally assumed that the singlet energy transfer is the only method. However there is still no conclusive experimental evidence against the triplet energy transfer. The quantum yield of fluorescence and photosynthesis in Chlorella has been reported to be 1.3% and 40 ~80% respectively, making a total yield of 41.3 ~81.3%.[1] The rest can be attributed to

radiationless intersystem crossing and internal conversion. The intersystem crossing $S_1 \overset{k_{IC}}{\rightsquigarrow} T_1$ might be important because of the heavy-atom effect or a paramagnetic environment[2] in the photosynthetic unit. Furthermore, the intrinsically long triplet lifetime and moderate interaction energy cause the triplet energy transfer in many kinds of organic aggregates to be as important as singlet transfer.

First of all, the decay processes of singlet and triplet states are depicted in Fig. 1. The triplet state might participate directly or indirectly (i.e. back to the singlet state by means of triplet-triplet annihilation) in the primary photosynthetic process. The rate constants for these two processes are respectively k_1 and k_2. The rate constants for fluorescence, phosphorescence, intersystem crossing and radiationless decays from T_1 and S_1 to the ground state S_0 are respectively k_F, k_p, k_{IC}, k_n and k'_n. The quenching of S_1 which proceeds to photosynthesis is designated by k_{ps}. The fluorescence quantum yield ϕ_F is given

$$\phi_F = \frac{k_F}{k_F + k_{ps} + k_{IC} + k'_n} .$$

The quantum yields for the photosynthesis in the absence (ϕ^1_{ps}) and the presence ($\phi^{1,3}_{ps}$) of triplet energy transfer are respectively given by

$$\phi^1_{ps} = \frac{k_{ps}}{k_{ps} + k_F + k_{IC} + k'_n}$$

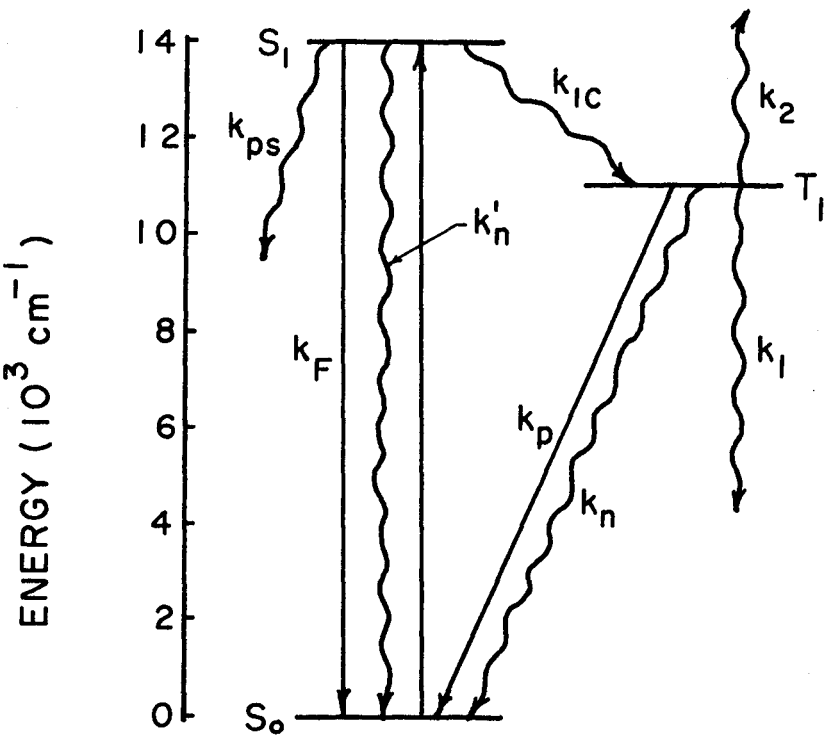

FIG. 1

$$\phi_{ps}^{1,3} = \frac{1}{k_{ps} + k_F + k_{IC} + k'_n} \left\{ k_{ps} + \frac{k_{IC}(k_1 + k_2[T_1]}{k_p + k_n + k_1 + k_2[T_1]} \right\} \quad (1)$$

where $[T_1]$ is the concentration of the triplet state. Assume $k_1 + k_2[T_1] \gg k_p + k_n$, then Eq. (1) can be simplified as follows:

$$\phi_{ps}^{1,3} = \frac{k_{ps} + k_{IC}}{k_F + k_{ps} + k_{IC} + k'_n} .$$

The ratio of fluorescence quantum yield to quantum yield of photosynthesis (ϕ_F / ϕ_{ps}) in the absence and the presence of triplet energy transfer can be written respectively by

$$\phi_F / \phi_{ps}^{1} = \frac{k_F}{k_{ps}}$$

$$\phi_F / \phi_{ps}^{1,3} = \frac{k_F}{k_{ps} + k_{IC}} .$$

From the above two equations, it is obvious that if the singlet transfer is the only method, the quantum yield ratio is independent of k_{IC}. However, if the triplet transfer is also important, the quantum yield ratio will vary when k_{IC} is changed.

The simplest way to change the rate of intersystem crossing but not the primary photosynthetic reaction is the deuteration of the pigments. It is therefore proposed to measure the quantum yields of fluorescence and photosynthesis in protonated and deuterated

Chlorella which are spectroscopically and chemically similar[3] to each other. The quantum yield of photosynthesis can be obtained by measuring manometrically the quantity of oxygen involved.[4, 1b] The method to measure the fluorescence quantum yield is conventional.[5]

Because of the small S_1-T_1 energy gap in chlorophyll a deuterium effect on k_{IC} may not be present. In order first to determine this it is proposed that a preliminary experiment be performed which measures the quantum yield of phosphorescence and the lifetime of the triplet states of protonated and perdeuterated chlorophyll-a in a glassy matrix.

REFERENCES

1. (a) M.D. Kamen, Primary Processes in Photosynthesis (Academic Press, New York and London, 1963), p. 107; (b) W.M. Manning, J.M. Stauffer, and F. Daniel, J. Am. Chem. Soc. 60, 266 (1938).
2. G.W. Robinson and R.P. Frosch, J. Chem. Phys. 37, 1962 (1962).
3. A.K. Ghosh and H.L. Crespi, Biochim. Biophys. Acta 120 19-22 (1966).
4. R. Emerson and C.M. Lewis, Am. J. Botany, 28, 789 (1941).
5. N.R. Murth, C.N. Cederstrand, and E. Rabinowitch, Photochem. Photobiol. 4, 917 (1965).

PROPOSITION III

With very high symmetry, dibenzenechromium is a very interesting compound to theoreticians[1, 2] who use LCAO-MO theory to treat the metal-ring bonding through hybridization of e_{1g}, e_{2g} symmetry orbitals of benzene rings and the 3d, 4s atomic orbitals of Cr. It is also very important in the industry of plating and polymerization.[3]

After the unsuccessful organic reaction experiment on the aromatic characters of ditoluenechromium,[4] very few attempts were tried again.

However, increasing evidences show its aromatic characters: electron scattering data result in a model of D_{6h} symmetry in the gaseous phase.[5] Spectroscopic observations[6, 7] favor D_{6h} symmetry, too. Metallation with butyllithium was unsuccessful in the work of Ref. 4, but successful with amylsodium in boiling hexane.[8] It can be alkylated with alkylhalide without any Lewis acid.[9]

Reinvestigation of the previous experiment[4] on the Friedel-Craft acylation[4] leads to the conclusion that the failure of the experiment[4] might be because the cation formed during the reaction decomposes gradually in the acid solution.

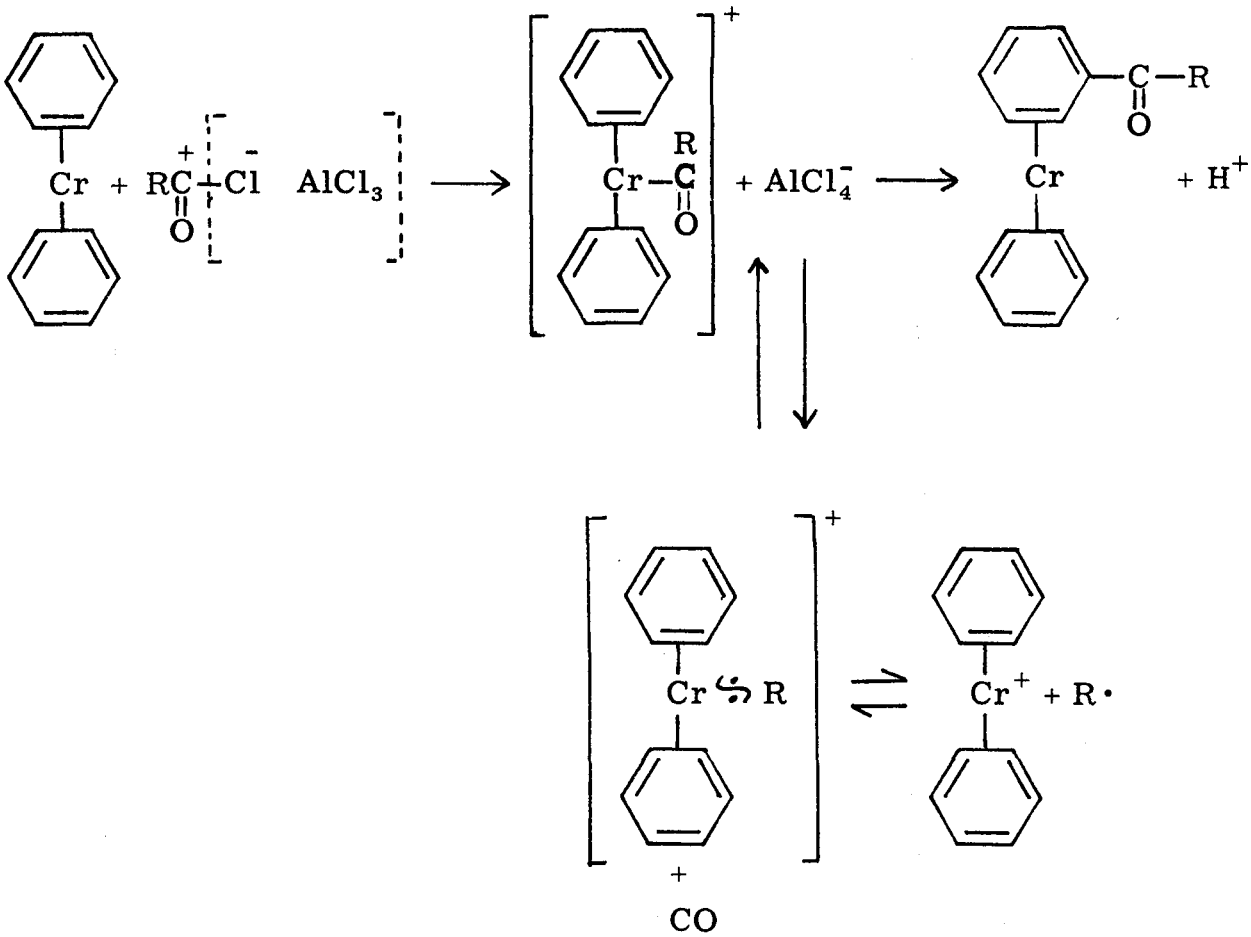

Therefore, it is proposed to change the catalyst for the Friedel-Craft acylation. Use a mild catalyst such as $SbCl_5$, $SnCl_4$, because stronger Lewis acid will decompose dibenzenechromium. Furthermore, the catalyzing rate of $SbCl_5$ in benzoylation is about 1300 faster than the stronger Lewis acid $AlCl_3$.[10] (or try the cation-forming agent $AgSbF_6$, $AgPO_4$).[10]

Use cyclohexane as solvent, acetylchloride as reagent, a crystalline acetyl derivative of dibenzenechromium is expected to be the product that can be identified by chemical analysis.

REFERENCES

1. H.C. Longuet-Higging, Mol. Phys. 5, 387 (1962).
2. R. Dieter Fischer, Theoret. Chim. Acta, 1, 418 (1963).
3. Hiroshi Ramazaki and Nobue Hagihara, Nippon Kagaku Zasshi, 83, 959 (1962).
4. Von Leopoldo José Anghileri, Z. Naturforsch. 12b, 67 (1957).
5. Acta Chem. Scand. 19, 41 (1965).
6. R.D. Feltham, J. Inorg. Nucl. Chem. 16, 197 (1961).
7. R. Stephen Berry, J. Chem. Phys. 35, 2025 (1961).
8. Ernst Otto Fischer and Henri Brunner, Ber. 95, 1999 (1962).
9. G.A. Razuvaev, G.A. Domrachev, and O.N. Druzhkov, Zh. Obshch. Khim. 33, 3084 (1963).
10. G. Olah, Friedel-Craft and Its Related Reactions (Interscience Publishers Inc., New York, 1963), Vols. I and III.

PROPOSITION IV.

Pressure effects on the intensities of wavelengths[1-3] of fluorescence $S_1 \rightarrow S_0$ and phosphorescence $T \rightarrow S_0$ and on the decay rate of the lowest triplet state T_1[2,3] of aromatic hydrocarbons have been examined recently for solutions in rigid media, especially polymethylmethacrylate (PMMA). The spectral shifts of fluorescence and phosphorescence of naphthalene are identical within experimental error. The rate of the red shift of the triplet-triplet absorption maxima with increasing pressure is about twice as great as those of fluorescence and phosphorescence.[4] This can be attributed to the solvent shift under high pressure. However, the apparent large increase of phosphorescence intensity and relatively smaller decrease of the phosphorescence lifetime[3] are still very mysterious.

According to the kinetic analysis the quantum yield of phosphorescence Q_p and of fluorescence Q_F are given by

$$Q_p = k_p \, k_{sT} \, \tau_F \, \tau_p \qquad (1a)$$

$$= k_p (1 - Q_F) \tau_p \qquad (1b)$$

$$Q_F = k_F \cdot \tau_F \qquad (2)$$

where k_F, k_p are the radiative decay rates of S_1 and T_1 respectively; k_{sT} is the non-radiative decay rate of intersystem crossing $S_1 \rightsquigarrow T_1$; $\tau_F \approx \frac{1}{k_F + k_{sT}}$ is the lifetime of S_1; and $\tau_p \equiv \frac{1}{k_p + k_n'}$ is the lifetime of T_1 and k_n is the non-radiative decay rate of $T_1 \rightsquigarrow S_0$. From

Eq. (1a), it is seen that the intrinsic increase of Q_p with increasing pressure can be attributed to an increase of k_p[7] or k_{sT},[2] because the lifetimes are generally shortened by high pressure. From a dynamic measurement[3] of phosphorescence intensity of naphthalene in PMMA at room temperature under 20 Kbar, it was found that the natural lifetime decreases by $\lesssim 30\%$. It was therefore concluded[7] that pressure enhances spin-orbit coupling. However, direct measurement of the pressure effect on k_p, which was obtained from the integrated absorption intensity of the $S_0 \rightarrow T_1$ transition, indicates that such an effect was not observed for α-chloronaphthalene in a solvent without a heavy-atom under a pressure of 7 Kbar.[6]

Pressure effect on the radiationless transition can be explained in terms of Franck-Condon factors. At high pressures, the red shift of the excited states and the change in the relative position of the two potential surfaces result in an increase of vibrational overlap integrals. The effect is larger for vibrations of high quantum number. This is rationalized by the larger pressure effect on the phosphorescence lifetime of perdeuterated compounds as shown in Table 1.[7]

To determine whether the increase of phosphorescence intensity under high pressure is due to the non-radiative intersystem crossing or due to the radiative decay k_p, the following experiments are proposed:

It is proposed to measure the quantum yield of phosphorescence and fluorescence of naphthalene. The experiment can be

TABLE 1. Phosphorescence Lifetimes of Aromatic Hydrocarbons in PMMA (298°K) at Atmospheric Pressure (0 Kbar) and 32 Kbar.

	τ_0	$\tau_{32\ Kbar}$
Triphenylene	8.55	4.16
Diphenyl	2.47	2.14
Diphenyl-d_{10}	6.35	4.32
Phenanthrene	2.46	1.80
Phenanthrene-d_{10}	11.2	7.63
Naphthalene	1.50	1.19
Naphthalene-d_8	14.2	8.45

carried out in well-degassed rigid media under a pressure range of 0 to 30 Kbar by means of singlet excitation. From the integrated absorption intensity of $S_0 \rightarrow S_1$ under various pressures, one can obtain the effect of pressure on k_F. Subtracting this from the pressure effect on the quantum yield of fluorescence, one can learn the effect on k_{ST}. Therefore the pressure effect on k_p can be derived according to Eq. (1b).

It is also proposed to measure the pressure effect on k_p directly. This can be achieved by measuring the change of integrated absorption intensity of singlet-triplet absorption $S_0 \rightarrow T_1$ of naphthalene in rigid media with increasing pressure. If the singlet-triplet transition for naphthalene is too weak, α-chloronaphthalene is suggested.

REFERENCES

1. M. Nicol, J. Chem. Phys. 45, 4753 (1966).
2. H. W. Offen and B. A. Baldwin, J. Chem. Phys. 44, 3642 (1966).
3. B. A. Baldwin and H. W. Offen, J. Chem. Phys. 46, 4509 (1967).
4. M. Nicol and J. Somekh, J. Opt. Soc. Am. 58, 233 (1968).
5. B. A. Baldwin and H. W. Offen, J. Chem. Phys. 48, 5358 (1968).
6. W. W. Robertson and R. E. Reynolds, J. Chem. Phys. 29, (1958).
7. P. F. Jones and S. Siegel, J. Chem. Phys. 45, 4757 (1966).

PROPOSITION V

The superficial resemblance between two sets of phenomena "ordinary dispersion and absorption," and "rotatory dispersion and circular dichroism" is not confined to experimental aspects. On theoretical grounds, too, both sets of phenomena are expressed in terms of similarly defined quantities. From the perturbation theory, the "ordinary dispersion and absorption" is referred to as first-order optical phenomena while the "rotatory dispersion and circular dichroism" is referred to as second-order. Spectroscopists are more interested in the first-order optical phenomena and understand them fairly well both experimentally and theoretically. On the contrary, biologists and biochemists frequently use the optical rotatory dispersion (ORD) and the circular dichroism (CD) to study the structure of macromolecules and molecular aggregates, because they are very sensitive ways to detect the environmental perturbation on chromophoric centers.

The theory of optical activity (rotatory power) is based on the modification of the material equations in optically active media,

$$\begin{aligned} \underset{\sim}{D} &= \epsilon \underset{\sim}{E} - g \frac{\partial}{\partial t} \underset{\sim}{H} \\ \underset{\sim}{B} &= \mu \underset{\sim}{H} + g \frac{\partial}{\partial t} \underset{\sim}{E} \quad , \end{aligned} \tag{1}$$

where $\underset{\sim}{D}$ and $\underset{\sim}{B}$ are the electric and the magnetic induction, $\underset{\sim}{E}$ and $\underset{\sim}{H}$ the field strengths, ϵ the dielectric constant, μ the magnetic permeability, which is approximately one for non-magnetic media, and g a constant. Then the solution of Maxwell's equations incorporated with Eq. (1) gives,

$$n_L = \epsilon^{\frac{1}{2}} + 2\pi\nu g$$
$$n_R = \epsilon^{\frac{1}{2}} - 2\pi\nu g \,, \qquad (2)$$

where ν is the frequency of light (sec^{-1}), n_L and n_R are refractive indices for left- and right-circularly polarized light. Therefore the optical rotation φ per unit length can be written,

$$\varphi = \frac{\pi}{\lambda}(n_L - n_R) = \frac{4\pi^2}{\lambda^2} cg \,, \qquad (3)$$

where c and λ are the velocity and wavelength of light.

In the following we briefly outline two distinct[1,2] theories of optical rotatory power that are not contradictory but complementary to each other.

1. One-electron theory[1]:

The molecule is considered to be divisible into symmetric groups (groups that have elements of symmetry such as plane or center of symmetry). Optical rotation of a given group arises because the chromophoric electron is moving in a suitable asymmetric force field, such as $V = \frac{1}{2}(k_1x^2 + k_2y^2 + k_3z^2) + Axyz$, where k_i is the force constant, (x, y, z) is the coordinate of the chromophoric electron. The asymmetric field is principally due to the atoms of the group to which the chromophoric electron belongs, but secondarily due to the static asymmetric perturbing field of the rest of the molecule. It is the contribution of the neighboring atoms to the force field in which the chromophoric electron moves that is responsible for the optical activity. The optical rotatory parameter g is given by the Rosenfeld treatment,[3]

$$g = \frac{4N_1}{3h} \sum_n \frac{R_n}{\nu_n^2 - \nu^2} . \qquad (4)$$

In this expression, N_1 is the number of molecules in unit volume and h is Planck's constant. The rotational strength R_n is,

$$R_n = I_m \{ \underset{\sim}{\mu}_{on} \cdot \underset{\sim}{m}_{no} \} \quad , \qquad (5)$$

where $\underset{\sim}{\mu}_{on}$ and $\underset{\sim}{m}_{no}$ are the electric and the magnetic dipole transition moments between the ground state $\underline{0}$ and the excited state $\underline{n}$. ν_n is the frequency associated with this transition. The corresponding electric and magnetic dipole operators are

$$\underset{\sim}{\mu} = e \sum_i \underset{\sim}{r}_i$$

$$\underset{\sim}{m} = \frac{e}{2mc} \sum_i (\underset{\sim}{r}_i \times \underset{\sim}{p}_i + 2\underset{\sim}{s}_i) ,$$

the sum being extended over all the electrons in the molecule, $\underset{\sim}{r}_i$ being position, $\underset{\sim}{p}_i$ momentum and $\underset{\sim}{s}_i$ spin angular momentum of the $i^{\underline{th}}$ electron. $I_m\{\ \}$ means "the imaginary part of".

2. The polarizability theory[2]:

The molecule is also divided into several symmetric groups as before. However, in contrast to the model of a single oscillator in an asymmetric field, it is thought that a dynamic coupling between several electronic oscillators gives rise to the optical rotatory power. Electronic motions on different symmetric groups are coupled by interactions of their instantaneous charge distributions to give asymmetric motions of charge that embrace the entire molecule.

For effective coupling one requires either large transition moments or virtual contiguity of two groups. The simplest model is dynamic coupling of the individual electric transition moments of the groups by dipole-dipole interaction. The rotatory parameter g is given by

$$g = \frac{4\pi N_1}{6hc} \sum_{n}{}' \sum_{i\neq k=1}^{N+1} \frac{\nu_n}{\nu_n^2 - \nu^2} (-\underset{\sim}{R}_k \cdot \underset{\sim}{\mu}^i_{on} \times \underset{\sim}{\mu}^k_{no} + \underset{\sim}{R}_k \cdot \underset{\sim}{\mu}^i_{no} \times \underset{\sim}{\mu}^k_{on}) \ . \qquad (6)$$

In Eq. (6) $\underset{\sim}{R}_k$ is the position vector of the center of gravity of group $\underline{k}$. The superscripts in the electric dipole moments ($\underset{\sim}{\mu}^i_{on}$ and $\underset{\sim}{\mu}^k_{no}$) and the polarizability tensor $\underset{\sim}{\alpha}^i$ designate the individual group.

This theory is named because the optical rotatory parameter can be further expressed in terms of the geometrical configuration and the polarizability tensors of its constituent groups as follows,

$$g = -\frac{4\pi N_1}{c} \sum_{i\neq k=1}^{N} [(\underset{\sim}{a}_3 \cdot \underset{\sim}{\alpha}^i \cdot \underset{\sim}{T}_{ik} \cdot \underset{\sim}{\alpha}^k \cdot \underset{\sim}{a}_2)(\underset{\sim}{R}_k \cdot \underset{\sim}{a}_1)]_{AV.} \ , \qquad (7)$$

where $\underset{\sim}{a}_1$, $\underset{\sim}{a}_2$ and $\underset{\sim}{a}_3$ specify the direction of the wave normal, electric vector and magnetic vector of the incident light. The dipole terms in the potential V of the interaction between groups $\underline{i}$ and $\underline{k}$ is

$$V = \sum_{i>k=1} \underset{\sim}{\mu}^i \cdot \underset{\sim}{T}_{ik} \cdot \underset{\sim}{\mu}^k$$

$$\underset{\sim}{T}_{ik} = \frac{1}{|\underset{\sim}{R}_{ik}|^3} \left[\underset{\sim}{1} - 3 \frac{\underset{\sim}{R}_{ik}\underset{\sim}{R}_{ik}}{|\underset{\sim}{R}_{ik}|^2} \right] \ . \qquad (8)$$

In this theory, the retardation of the electromagnetic wave over all parts of each group is approximated by its value at the center of gravity of the group.

Tinoco[4] used this idea to discuss the exciton contribution to the optical rotation. Consider the case of a dimer whose spectrum is split into ν_+ and ν_-. The dipole strength $D_\pm$ and the rotational strength $R_\pm$ are given as follows:

$$D_\pm = |\underset{\sim}{\mu}_1|^2 \pm \underset{\sim}{\mu}_1 \cdot \underset{\sim}{\mu}_2 \tag{9a}$$

$$R_\pm = \pm \left(\frac{\pi \nu_0}{2c}\right) \underset{\sim}{R}_{12} \cdot \underset{\sim}{\mu}_1 \times \underset{\sim}{\mu}_2 \tag{9b}$$

$$\nu_\pm = \nu_0 \pm V_{12} \tag{9c}$$

$$V_{12} = \frac{1}{|\underset{\sim}{R}_{12}|^3} \left[\underset{\sim}{\mu}_1 \cdot \underset{\sim}{\mu}_2 - \frac{3(\underset{\sim}{R}_{12} \cdot \underset{\sim}{\mu}_1)(\underset{\sim}{R}_{12} \cdot \underset{\sim}{\mu}_2)}{|R_{12}|^2} \right] , \tag{9d}$$

where $\underset{\sim}{R}_{12} = \underset{\sim}{R}_2 - \underset{\sim}{R}_1$, ν_0 is the absorption frequency in free molecule, $\underset{\sim}{\mu}_1$ and $\underset{\sim}{\mu}_2$ are electric dipole transition moments in molecule 1 and 2 respectively. Note that $|\underset{\sim}{\mu}_1| = |\underset{\sim}{\mu}_2|$. V_{12} is the dipole interaction potential.

Equations (4) and (6) are derived for the transparent region. In the absorption band, they are modified[5] by introducing a damping factor Γ_n which is equal to the width at half maximum for the absorption line associated with the $n^{\underline{th}}$ transition. Therefore the energy denominators become $(\nu_n^2 - \nu^2 + i\nu\Gamma_n)$.

In the absorption range, there occurs not only the optical rotation but also the elliptical polarization of the original linearly polarized light. The depolarization is due to the difference of the absorption coefficients for left- and right-circularly polarized light, which gives rise to circular dichroism. In general, the depolarization is very small, the optical rotation can still be measured accurately. However, if the elliptical depolarization is very large, it will give better results

to measure the circular dichroism accurately and then to obtain the rotational strength from the integrated intensity of the circular dichroism spectrum. This can be achieved in the same way as one obtains the dipole strength from the integrated intensity of ordinary absorption.

To verify the polarizability theory, it is proposed to measure the optical rotatory dispersion (ORD) or the optical rotation of a naphthalene single crystal in the range of Davydov splittings of the strong transition $^1B_{2u} \leftarrow {}^1A_{1g}$ (~2800 Å).

Although the optical rotation arises as a second-order effect, its magnitude can be very large because of the energy denominator by choosing the light frequency reasonably close to the absorption band. The resolution of the ORD spectrum can be better than that of the ordinary absorption because of the opposite signs for the two Davydov components as shown in Eq. (9b).

Naphthalene is proposed because its crystallographic structure and optical properties[6] are well known, and the nature of electronic transitions have been understood fairly well from ordinary optical spectroscopy. There are two naphthalene molecules in a unit cell. The two molecules are oriented in such a way that no plane or center of symmetry exists, and the low- and high-frequency components of the two Davydov splittings are respectively $\underset{\wedge}{b}$- and $\underset{\wedge}{a}$-polarized ($\underset{\wedge}{a}$ and $\underset{\wedge}{b}$ are crystallographic axes). In order to eliminate depolarization of linearly polarized light due to the anisotropic dielectric tensor of the naphthalene single crystal, it is proposed to carry out

the experiment with incident light propagating along the b-axis, which is the principal optic axis.

It is also proposed to study the number of maxima and minima in the ORD and CD spectra corresponding to the intensity distribution and the splitting of the electronic multiplet structure in the ordinary absorption. The systems proposed are dilute solution of naphthalene in durene and a naphthalene single crystal in the presence and the absence of a magnetic field. The magnitude of the splitting can be varied through the Zeeman effect on the triplet state in various magnetic field strengths. This knowledge is interesting and useful in the structure determination of polymers.

REFERENCES

1. E.U. Condon, W.Altar, and H. Eyring, J. Chem. Phys. 5, 753 (1937).
2. J.G. Kirkwood, J. Chem. Phys. 5, 479 (1937).
3. L. Rosenfeld, Z. Physik 52, 161 (1928).
4. I. Tinoco, Jr., Radiat. Res. 20, 133 (1963).
5. A. Moscowitz, Advan. Chem. Phys. 4, 67 (1962).
6. The principal optic axis coincides with the b-crystallographic axis; the obtuse and acute bisectrices lie 23°25' from the a- and c'- (perpendicular to the ab plane) crystallographic axes, respectively. A.N. Winchell, The Optical Properties of Organic Compounds (University of Wisconsin Press, Madison, Wisconsin, 1943), p.77; E.E. Wahlstrom, Optical Crystallography (John Wiley and Sons, Inc., New York, 1960).